

Analysis of Single Molecule Fluorescence Microscopy Data

Mohamadreza Fazel

Department of Physics and Astronomy, University of New Mexico,
Albuquerque, New Mexico, USA

Abstract

The diffraction of light imposes a fundamental limit on resolution of light microscopes. This limit can be circumvented by creating and exploiting independent behaviors of the sample at length scales below the diffraction limit. In super-resolution microscopy, the independence arises from individual fluorescent labels switching between dark and fluorescence states, which allows the pinpointing of fluorophores either directly during the experiment or post experimentally using a sequence of acquired sparse image frames. Finally, the resulting list of fluorophore coordinates is utilized to produce high resolution images or to gain quantitative insight into the underlying biological structures. Therefore, image processing and post-processing are essential stages of super-resolution microscopy techniques. Here, we review the latest progresses on super-resolution microscopy data processing and post-processing.

1 Introduction

Some ancient Greeks believed that vision was due to light rays originating from the eye and traveling with infinite speed. Ibn al-Haytham, latinized as Alhazen, (965 AD-1040 AD) explained that eyesight was due to light which comes to the eyes from objects. He also described the optical properties of convex glasses in his *Book of Optics* [1]. The works of Alhazen were introduced to European scholars such as Roger Bacon (1219 AD-1292 AD) via Latin translations. The use of convex lenses as eye-glasses dates back as far as the 13th century in Europe. Telescopes and microscopes came into existence in 17th century and the credit is often given to the Dutch scientists, Zacharias Janssen (1585 AD-1638 AD) and Hans Lippershey (1570 AD-1619 AD) [2]. Robert Hooke (1635 AD-1703 AD) was the first person that wrote a book on microscopes, *Micrographia*, and was the first person to see a cell through a microscope [3].

2 Limits of Light Microscopy

The diffraction of light emitted by a point source and collected by a microscope lens (objective) has an intensity pattern called the Airy disk. In general, the actual pattern may differ from the Airy disk due to optical aberrations and other factors and is referred to as a point spread function (PSF). The resolution of a microscope is often defined as the minimum separation between two emitters in which they can still be recognized as individual point sources of light by the microscope user. In 1873, Ernst Abbe defined resolution as the inverse of the maximum spatial frequency passed by the microscope, which gives a resolution distance of [4]

$$d = \frac{\lambda}{2N_a} \quad (1)$$

where λ and N_a are, respectively, the wavelength of light and the numerical aperture of the microscope. For visible light, $\lambda \sim 600$ nm, and a typical objective, $N_a \sim 1.5$, the resolution is

approximately 200 nm. Other significant limiting factors of light microscopy are that only strongly refractive objects can be imaged effectively, and the contribution of unwanted out of focus light from parts of the specimen outside the focal plane.

In the beginning of 20th century, the realization of fluorescence microscopy was a major breakthrough in the examination of living organisms since these organisms are mostly transparent and only reflect a very small portion of light [5]. The advent of fluorescence microscopy was an important step in overcoming the substantial limit of weak refractivity of the sample. Illumination and optical techniques, such as the confocal microscope [6], total internal reflection fluorescence (TIRF) microscope [7], two-photon microscopy [8], 4-pi microscope [9], structured illumination microscopy (SIM) [10], and light-sheet microscopy [11] were developed to reduce the out of focus light and enhance the resolution and contrast of microscope images. These techniques pushed the Abbe diffraction barrier to its very limits, however, it was not until the end of 20th century when scientists were able to overcome this barrier and achieve resolutions better than the diffraction limit [12].

3 Wide-field Microscopy vs Point Scanning Microscopy

The microscopy techniques listed in the previous section can be divided into three main categories, wide-field microscopy, point scanning microscopy and light-sheet microscopy. In the wide-field approach, the entire specimen is exposed to a light source and therefore there is fluorescent light from out-of-focus points/planes, which obscures the underlying structure and reduces the image contrast. Point scanning microscopes only illuminate a single spot of the sample at a time and use pinholes embedded in the optical setup to considerably reduce the out-of-focus light. In light-sheet microscopy, the focal plane is illuminated rather than the focal point.

3.1 Wide-field Microscopy

Total Internal Reflection Microscopy

In TIRF microscopy, a beam of light is incident upon the coverslip at an angle greater than the critical angle of the coverslip. At this angle, light undergoes a total internal reflection and is entirely reflected back from the coverslip. However, an exponentially decaying electromagnetic wave called the evanescent wave penetrates to the sample

$$I = I_0 \exp\left(\frac{-z}{d}\right) \quad (2)$$

where z , I_0 and d are, respectively, depth, the intensity of the evanescent wave at $z = 0$ and the effective depth that the evanescent wave travels within the specimen. d is of order of the wavelength, $d \sim \lambda$, and fluorophores further than that from the coverslip will not be effectively activated and therefore result in extensive reduction of the out-of-focus light. This approach is simple to implement and is usually suitable for imaging structures close to the coverslip, $z \sim 0$, such as the cell membrane [7, 13]. TIRF microscopy is a wide-field approach, but it provides better contrast due to the small penetration of the evanescent wave into the sample, described by (2), and therefore less out-of-focus light.

Structured Illumination Microscopy

One of the barriers of light microscopy is the limited size of the objective, which prevent collection of all the light/information available from the sample. The numerical aperture in the denominator of (1) is related to the ability of the objective in collecting light/information. Structured illumination microscopy (SIM) collects more information by illuminating the sample with a periodic field instead of a uniform field.

A sinusoidal periodic field is usually used in SIM experiment, which has a Fourier transform with three different spatial frequencies. The fact that a sinusoidal field is represented with more than one frequency in the Fourier domain adds more complications to the actual problem. However for the sake of explanation, we presume that one can generate a field with a single spatial frequency and employ it for a SIM experiment.

Assuming that $f(x)$ describes the sample with Fourier transform

$$F(k) = \int f(x)e^{-ikx} dx, \quad (3)$$

the product of $f(x)$ with e^{-ik_0x} , which stands for a periodic field with spatial frequency k_0 , leads to a shift in the frequency domain:

$$F(k + k_0) = \int f(x)e^{-ik_0x}e^{-ikx} dx \quad (4)$$

Taking advantage of this simple math, one can make more information available through the objective lens by shifting the frequency plane illuminating the sample using fields with different spatial frequencies, Fig. 1.

Images acquired by different illumination fields are then combined to obtain an image with enhanced resolution. SIM provides a resolution of ~ 100 nm in the lateral direction [10, 14]. Note that this is still not breaking the diffraction limit but SIM permits reconstruction of images with higher spatial frequencies than allowed by N_a , which pushes the diffraction barrier to its very limits.

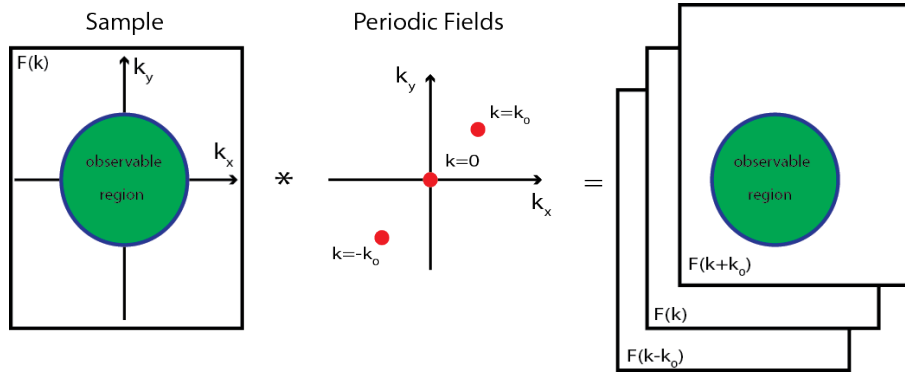


Figure 1: SIM idea explained by illumination with a hypothetical single spatial frequency light. Left: The objective ability to collect all the information available is restricted. Middle: Red dots stand for spatial frequencies of different illumination fields. Right: Illuminating the sample with periodic fields with different spatial frequencies makes more information available via the objective.

3.2 Point Scanning Microscopy

Confocal Microscopy

In the wide-field illumination approach, the entire sample is exposed to a beam of light and out-of-focus fluorophores are activated as well as in-focus fluorophores. The light from the out-of-focus fluorophores interferes with the light from in-focus structures and results in blurry details of in-focus structures. A confocal microscope uses two pinhole apertures after the light source and before the camera to reduce the out-of-focus light, Fig. 2. A single spot of the sample is illuminated at each time and the specimen is scanned point-by-point to obtain an image of the entire sample with improved contrast due to the reduction of out-of-focus fluorescence background [6, 15].

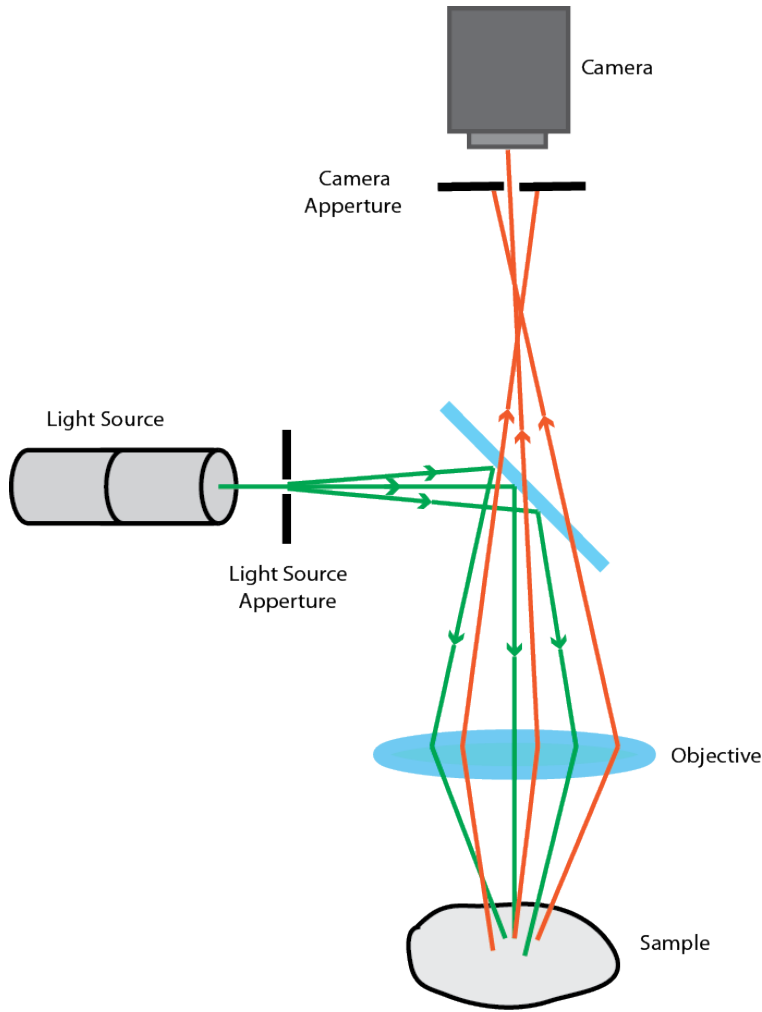


Figure 2: Confocal microscope uses two pinhole apertures to exclude the light from out-of-focus fluorophores.

4- π Microscopy

4- π microscopy was initially developed as a variant of confocal microscopes [9, 16]. When a fluorophore is activated, it emits fluorescent light in all directions (solid angle of 4π), but the light is only collected from one side in a regular microscope. Inefficient light collection causes an increase in the size of the PSF, particularly in the axial direction, which reduces the image resolution. 4- π microscopy makes use of two opposing objectives for either or both of sample illumination and collecting the fluorescent light. Similar to SIM, 4- π microscopy permits collection of more light which yields a larger numerical aperture, N_a , and gives a better resolution (1). Due to isotropic light collection, 4- π microscopy yields an almost symmetric PSF in all directions and hence is of special interest in 3D microscopy [17].

2-photon and Multi-photon Microscopy

Certain fluorophores can be activated by absorbing two or more photons at the same time. Due to the non-linear superposition of the fields from the photons arriving at the focal point simultaneously,

the resulting focal point has a smaller size. Therefore, the out-of-focus fluorophores are less likely to be activated, which reduces the out-of-focus fluorescent light. In this approach, the specimen is scanned point by point to acquire an image of the whole sample with enhanced contrast [8, 18].

3.3 Light-sheet Microscopy

In light-sheet microscopy, a thin sheet laser beam is used to illuminate the in-focus plane and then a wide-field light collection approach is used to collect the fluorescent light from the fluorophores within the focal plane [11, 19]. The illumination and light collection are in perpendicular directions, Fig. 3. Two common approaches to generate a thin layer of light are using a cylindrical lens or rapid movement of the focal point across a plane [19]. Because the out-of-focus fluorophores are not illuminated, the out-of-focus light is at a minimum and also the photo-damaging is less for the fluorophores. This approach has been widely adopted for 3D-imaging of samples by imaging one plane of the sample at a time.

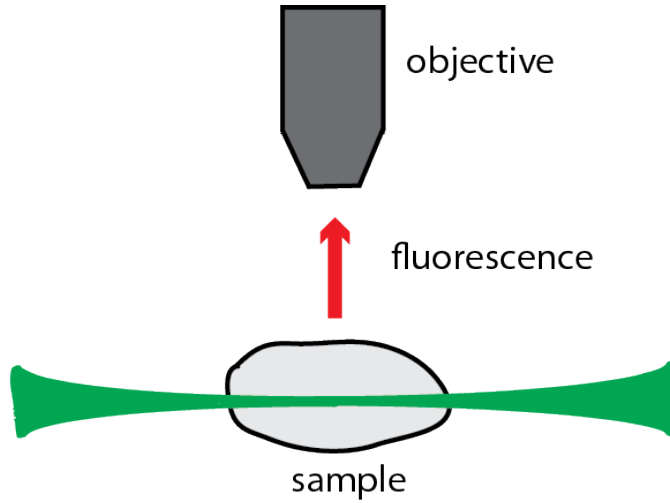


Figure 3: Light-sheet microscopy. The illumination path is perpendicular to the light collection path.

4 Super-resolution Microscopy

The fluorescence microscopy technique along with various illumination and light collection methods pushed the diffraction limit to its extreme. For example, TIRF microscopy, confocal microscopy, 2-photons microscopy and light-sheet microscopy were developed using different illumination techniques to eliminate spurious fluorescent light from out-of-focus fluorophores. SIM and 4-pi microscopy employ light collection techniques to gather more information from the emitted fluorescent light to increase the numerical aperture and obtain better resolutions. However, these techniques do not break the diffraction limit resolution and the resolution still depends on the size of PSF. The microscopy approaches that break the diffraction limit barrier are called super-resolution microscopy or nanoscopy [20, 21, 22, 23, 24, 25, 26]. Super-resolution techniques achieve sub-diffraction resolution by creating independent behavior for individual dyes at scales below the diffraction limit. Many super-resolution procedures use the reversible switching property of some fluorescent probes between a fluorescent state and a dark state to obtain sub-diffraction limit resolution. These approaches can be classified into two different groups based on how they switch the probes between the dark and fluorescent states: targeted switching procedures and stochastic switching procedures. The microscopy

techniques under the first category are STimulated Emission Depletion (STED) microscopy [12, 27], Ground State Depletion (GSD) microscopy [28], REversible Saturable Optically Linear Fluorescence Transition (RSOLFT) microscopy [29] and Saturated Structured Illumination Microscopy (SSIM) [30]. These techniques deterministically switch off the fluorophores in the diffraction limited vicinity of the target fluorophore to accomplish sub-diffraction resolution. Stochastic Optical Reconstruction Microscopy (STORM) [31], direct Stochastic Optical Reconstruction Microscopy (dSTORM) [32], Photoactivated Localization Microscopy (PALM) [33], Fluorescence Photoactivation Localization Microscopy (FPALM) [34], Super-resolution Optical Fluctuation Imaging (SOFI) [35] and DNA-point accumulation for imaging in nanoscale topography (DNA-PAINT) [36, 37] can be categorized as stochastic switching techniques. These approaches activate a small random subset of the probes to avoid simultaneous fluorescent light from more than one probe in a diffraction limited region.

4.1 Targeted Switching Super-resolution Microscopy

Stimulated Emission Depletion Microscopy

In STED, the specimen is simultaneously illuminated by two sources of light. The first source of light is used to excite the fluorophores and the second one restricts the fluorescent emission [12]. When a fluorophore in an excited state encounters a photon with the same energy as the difference between the excited state and ground state, it can emit a photon and returns to the ground state via stimulated emission. The beam profile of the second laser has a donut-like shape where the intensity of light is almost zero in the middle and the chance for stimulated emission is very small. Therefore, fluorophores in the surrounding region will be depleted and fluorescent emission only occurs in the middle. The resolution is given by the size of the middle area with zero intensity. The diameter of this region (resolution) is given by [38, 39]

$$d = \frac{\lambda}{2N_a \sqrt{1 + I_s/I}} \quad (5)$$

where I and I_s are the intensity of the laser used for suppressing the spontaneous fluorescent emission and the saturation intensity. The stimulated emission depletion of the excited state has to compete with the fluorescence decay of this state, and the fluorescence decay is overcome at the saturation intensity, I_s . Higher laser power gives a smaller hole in the center of the donut-like laser profile and thus better resolution. This technique bypasses the diffraction limit and achieves resolution of 20-50 nm [40, 41, 42]. Advantages of STED are computational post-processing is not required, and two channel imaging is easy to implement [43]. Disadvantages of this technique are long image acquisition time and high power lasers, such as pulsed lasers.

Ground State Depletion Microscopy

GSD is another approach that makes use of patterned excitation to achieve sub-diffraction resolution [28]. Fluorophores have singlet and triplet spin excited states with spins of zero and one, in turn [44, 45]. In this technique, a triplet spin state is employed as dark state rather than the ground state, Fig. 4.

A first laser excites the fluorophores to the singlet state, S_1 , and a second laser is then utilized to pump the electrons from S_1 to the triplet state T_1 outside the region of interest (ROI). The lifetime of the triplet state, T_1 , is much longer than that of the singlet state, S_1 , because transition from the triplet state to the ground state, S_0 , with spin zero is prohibited by angular momentum conservation. Therefore, the electrons in the triplet state do not emit fluorescent light. GSD requires lower intensity for depletion and has a smaller threshold intensity I_s (5) than STED [46]. This super-resolution scheme has yielded resolutions better than 20 nm [47].

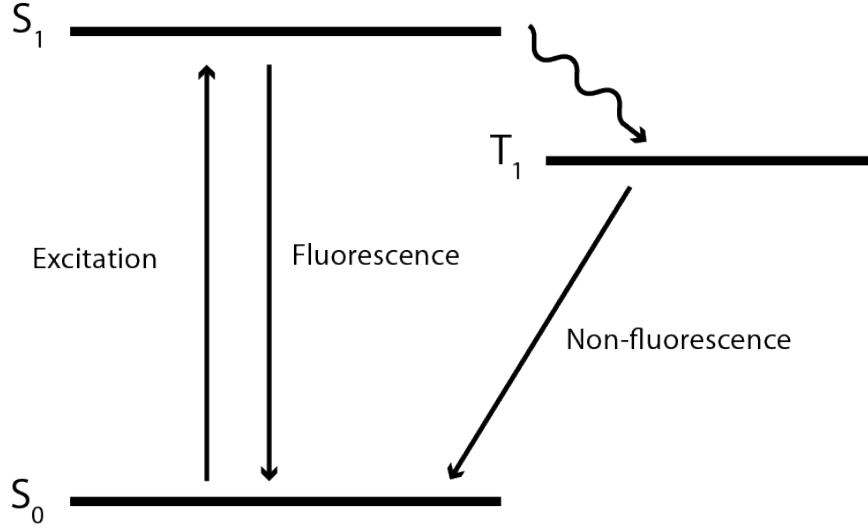


Figure 4: Energy levels in a fluorophore. The ground state, S_0 and the excited state, S_1 are singlet spin states. T_1 is a triplet spin state, which has a long lifetime and is used as dark state in GSD.

Reversible Saturable Optically Linear Fluorescence Transition Microscopy

RESOLFT is a more general approach that uses any fluorophore with a dark state and a bright state with reversible switching between the two states to accomplish super-resolution [29]. STED and GSD are specific cases of RESOLFT where the ground state, S_0 and the triplet state, T_1 , are the bright and dark states, respectively, Fig. 4.

Saturated Structured Illumination Microscopy

SSIM uses a high power laser with a sinusoidal spatial pattern to deplete the ground state of fluorophores. The generated pattern has very narrow line-shaped dark regions with sub-diffraction widths. The dark lines can later be exploited to retrieve features of the sample with sub-diffraction resolution.

4.2 Stochastic Switching Super-resolution Microscopy

4.2.1 Single Molecule Localization Microscopy

A high-resolution image of a structure, for example, a cellular organelle, can be reconstructed from fluorophore positions, Fig. 5. This is the foundation of Single Molecule Localization Microscopy (SMLM) super-resolution approaches, such as STORM [31], PALM [33] and FPALM [34], conceived by different groups around the same time and other variants introduced later [32, 36, 37, 48, 49, 50, 51, 52, 53, 54, 55, 56]. A fluorophore in its fluorescent state emits N photons that form a PSF pattern on the camera. The PSF can be used to localize the fluorophore with localization precision much better than the diffraction limit [57, 58]

$$\sigma = \frac{\sigma_{\text{PSF}}}{\sqrt{N}} \quad (6)$$

where σ and σ_{PSF} are the localization precision and size of the PSF, respectively. However, accurate localizations are not possible for multiple activated fluorophores in close proximity due to overlapping PSFs [59, 60]. SMLM super-resolution approaches were originally demonstrated by making use

of a wide-field illumination method to activate a sparse subset of fluorescent probes that can be stochastically switched between a dark and a fluorescent state. Sparse activation is necessary to prevent activation of more than one fluorophore in a diffraction limited area and avoid overlapping PSFs [31, 32, 33, 34, 48, 49, 50]. Some other SMLM approaches overcome the problem of overlapping PSFs by separating the fluorescent signals from molecules with different emission spectra [51, 52, 53]. Photo-bleaching of fluorophores has also been employed to achieve low density images of PSFs with minimum overlaps [54, 55]. Another promising SMLM technique is based on stochastic binding and unbinding of the diffusing fluorescent emitters to the target [36, 37, 56, 61].

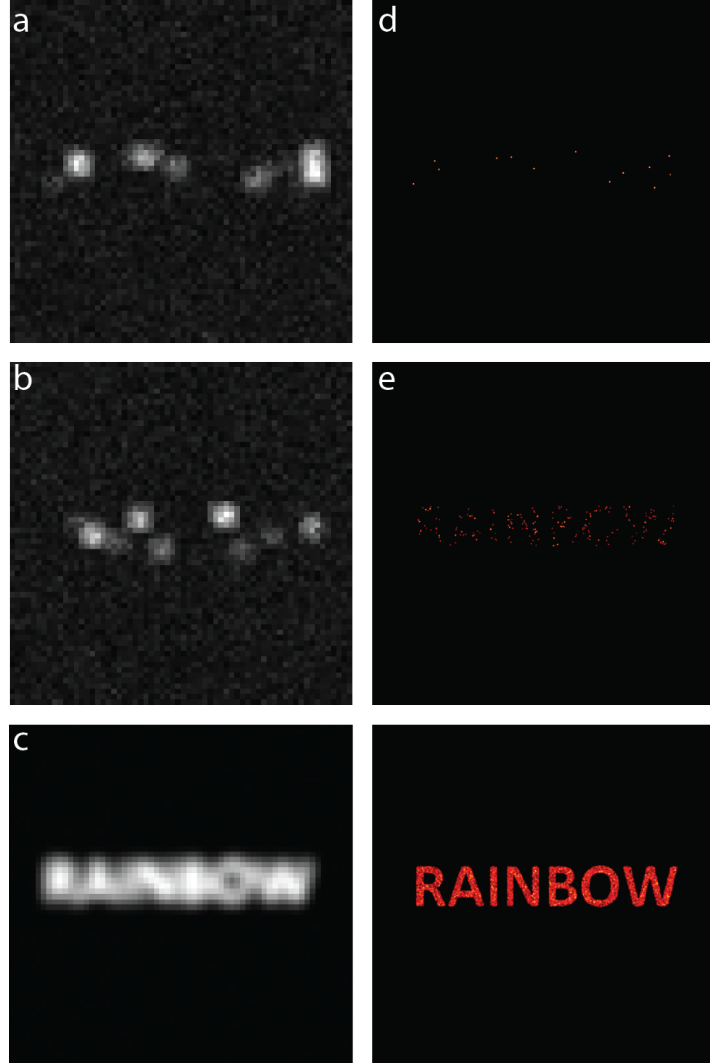


Figure 5: SMLM concept. (a & b) Sample frames of raw super-resolution data. (c) Bright-field image, which is the sum image of 5000 frames of raw super-resolution data. (d) Image reconstructed using localizations from a single frame. (e) Image reconstructed using localizations from 50 frames. (f) Super-resolution image reconstructed using localizations from 5000 frames.

Although wide-field techniques are the most common illumination methods in SMLM techniques, other illumination approaches such as confocal [62], 2-photons [63] and light-sheet [64, 65] approaches have been utilized to demonstrate SMLM super-resolution microscopy.

The major restrictions of SMLM techniques are limited number of photons and long time of data acquisition. For various fluorescent probes, the number of emitted photons per blinking event ranges from a few hundreds to a few thousands with a few blinking events per probe, where more photons and a larger number of blinking events are desired for better image contrast [66]. In order to avoid overlapping PSFs, a small subset of fluorophores is activated each time, but on the other hand enough localizations are required to obtain high-resolution images [67], which demands long data acquisition time [68, 69]. This problem can be alleviated by multiple-emitter fitting methods that are able to localize emitters in denser regions of the data [70, 71, 72].

Cellular organelle are inherently 3D structures and therefore 3D microscopy images are desirable. SMLM super-resolution approaches are able to provide 3D images of cellular structures by exploiting the variance in the PSF shape as a function of axial distance from the focal plane. The variance in the PSF shape can be achieved by different optical techniques. STORM was first implemented in 3D by using an astigmatic PSF [73]. Later approaches use more complex engineered PSFs such as double-helix [74], etc. [75, 76, 77].

4.2.2 Fluctuation Analysis

Super-resolution Optical Fluctuation Imaging (SOFI) is another technique that utilizes stochastic switching of fluorophores to realize sub-diffraction details of cellular structures. However, this approach does not reconstruct super-resolution images using probe locations. It employs temporal fluctuation analysis methods to generate images with resolution beyond the diffraction limit [35, 78, 79]. More recently, Super-Resolution Radial Fluctuations (SRRF) has been introduced that takes advantage of radial and temporal fluctuations in the fluorescent intensity to realize sub-diffraction information from the sample [80, 81].

5 Image Formation

Raw super-resolution data is comprised of a sequence of image frames, where each frame is a two dimensional array of pixels whose values are a function of the number of photons captured by the camera over a fixed exposure time. Photons reaching the camera are often originated from multiple sources of light: the fluorescent light from in-focus fluorophores that label the target structure, the fluorescent light from out of focus fluorophores, which might be fluorophores bound to undesired cellular structures, and the autofluorescence of the specimen or other sources of light that exist in the area. The contribution of the light from sources other than the in focus fluorophores is unwanted and degrades the quality of images [67, 82]. The undesired light reaching the camera gives rise to two types of background noise, an approximately uniform, homogeneous background, and a heterogeneous background called structured background [82, 83, 84, 85].

For each data frame, there is a subset of emitters activated and the image frame is described by

$$\text{Model} = \sum_i I_i \delta(x - x_i) \delta(y - y_i) * \text{PSF}(z_i) + b, \quad (7)$$

which is the convolution of the emitters X and Y locations with the PSF plus a uniform background, Fig. 6. The sum is over the activated emitters. I_i, x_i, y_i, z_i and δ represent the intensity and location of the i th emitter and Dirac delta, respectively. Note that PSF shape is a function of the Z -location (offset from the focal plane) of the emitter [83, 86], and hence the out-of-focus emitters have a different PSF. Some effects like dipole orientation [87, 88], sample movements [89, 90] and optical aberrations [88, 91] also result in distortions of the PSF. The additive term models the homogeneous uniform background while the structured background, usually coming from the out-of-focus emitters, is mixed with the in focus emitters and is given by the convolution term.

The pixel values recorded by the camera are not the same as the photon counts, but they are a function of photon counts. The camera detectors amplify the signal from the detected photons and

multiple photoelectrons are produced per photon, which is used to generate the pixel values [92]. The detector also has Gaussian fluctuations when there is no signal, which is called read-out-noise. To obtain the correct number of photons, therefore, these two effects have to be taken into account [93, 94, 95, 96]. The pixel values are scaled by the camera gain, which gives the amplification factor, and the average of camera offset is subtracted from the given pixel values to get photon counts, where the Gaussian fluctuations are negligible in most cases [93, 94]. Another major source of noise is the shot noise, which comes from the particle nature of photons and can be modeled by a Poisson process [58, 93, 97, 98]. Model (7) yields the expected number of photons for individual pixels but the number of photons captured by the detector over a fixed exposure time have a Poisson distribution, Fig. 6.

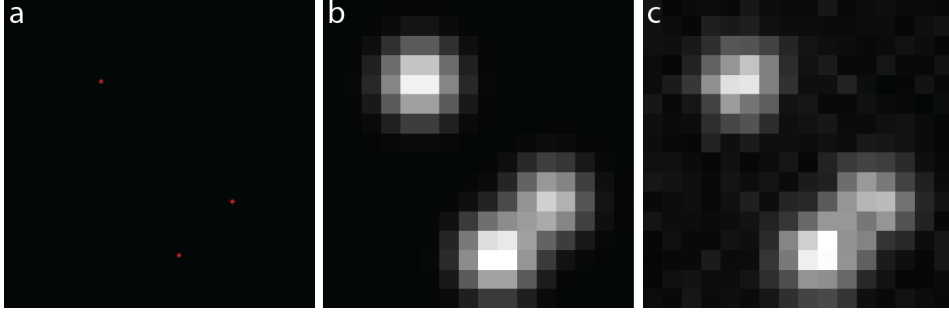


Figure 6: Image Formation. (a) Emitter locations. (b) Model is convolution of emitter locations with PSF. (c) Model corrupted with shot (Poisson) noise. The emitters are assumed to be in focus.

6 Image Processing

Image processing is a key step in SMLM super-resolution approaches. This step is comprised of multiple stages: pre-processing, identification of candidate emitters and localization, filtering and image rendering. The pre-processing step often alleviates the noise introduced during data acquisition, such as camera and background noise.

Estimation of location and/or intensity of emitters using the point spread function predates the advent of SMLM super-resolution approaches and had been employed in other scientific disciplines such as electrical engineering [99, 100, 101], astronomy [84, 102, 97, 103], particle tracking [104, 105], etc. There are two major classes of localization approaches, single-emitter localization algorithms and multiple-emitter localization algorithms. The single-emitter algorithms are only able to localize isolated emitters where there is no overlapping PSFs. Single-emitter candidates are usually identified by applying a threshold to detect local maxima and then ROIs of a certain size including those local maxima are selected for further analysis [57, 98, 106, 107]. Other common detection algorithms employ wavelet transform [108, 109, 110], different types of filters [111, 59] and other detection approaches [112, 113]. The performance of different detection algorithms is highly correlated with the signal to noise ratio (SNR) and signal to background ratio. For a comparison of different detection algorithms see, [114, 115]. The single-emitter localization procedures estimate the locations of the detected emitters employing either a non-iterative or an iterative algorithm.

Dense regions of data with overlapping PSFs from closely spaced activated emitters, Fig. 6, can be generated due to either dense labeling of the sample or fast data collection. Multiple-emitter fitting algorithms localize emitters in the dense regions of the data with overlapping PSFs. Multiple-emitter approaches may be categorized based on their outputs [70] or based on the algorithm itself [71, 72].

After the localization stage, there is often a rejection step that filters out bad localizations to reduce the artifacts in the final reconstructions [116, 117]. A popular filtering criteria is based on

the found parameter values and their uncertainties that removes the localizations with uncertainties larger than given thresholds [31, 116, 85]. An additional filtering approach is based on the nearest neighbor distances where localizations with less than N neighbors within a certain distance are eliminated from the final list of localizations [118, 119].

In single-emitter localization approaches, artifacts may arise due to fitting two or more overlapping PSFs as a single emitter. To reduce this effect, the localization algorithms make use of different criteria for recognizing this type of bad fits, Fig. 8. The filtering of the ROIs, including closely spaced active emitters with overlapping PSFs, can be done before localization. The ROIs with overlapping PSFs are identified with deviation of shape of the bright blob from the given PSF [31]. Another algorithm recognizes the bad fits due to overlapping PSFs by computing the p-value assuming a single PSF as null hypothesis. If the resulting p-values are smaller than a given threshold, the fits are rejected [98]. Finally, the remaining localizations are used to reconstruct a super-resolved image, Fig. 8.

6.1 Background Detection

The ultimate objective of SMLM techniques is reconstructing high resolution images from precise and accurate [83] estimates of the emitter locations from raw super-resolution data. In order to accomplish this goal, a correct measure of background noise is required as incorrect background leads to biased position estimates [70]. The correction of uniform background noise is simple, and various approaches have been conceived to address this issue. These approaches usually select a local ROI and use that to compute uniform background noise as the average of pixel values, median of pixel values, average of pixel values after bleaching of the fluorophore, X th percentile of pixel values or estimating the additive term in (7) using an iterative approach [86, 98, 120, 121, 122, 123].

Structured background is significantly more complicated to remove and its presence results in poor position estimates. A few methods have been put forward to cope with this problem including an approach that uses a temporal median filter to subtract structured background from the signal [124]. This technique inspects the fluctuations of pixel values over time to find the background value. The found background can be overestimated in the dense regions of the data where there is at least one active emitter at each time. An alternative procedure detects all the emitters regardless of being signal or background and then sets a threshold and remove the emitters with intensities below that as structured background [125]. Wavelet decomposition has been employed to subtract structured background as well as uniform background, prior to emitter detection [126]. Recently, a deep learning method has been proposed to detect structured background using the PSF shape [82]. Fazel, et al., used a Bayesian approach to model structured background with a collection of PSF-sized dim emitters [85]. In the field of astronomy, methods such as sigma clipping had been developed to deal with structured background in dense data sets [84]. In sigma clipping procedure, the brightness mean, m and standard deviation, σ , are calculated and those intensities outside the range of $[m - \alpha\sigma, m + \alpha\sigma]$ are considered noise.

6.2 Single Emitter Fitting

The single-emitter localization algorithms can be classified into two major categories: the algorithms that use non-iterative approaches to localize emitters and the algorithms that use an iterative procedure. Studies show that the iterative algorithms are more accurate than the non-iterative algorithms [127]. However, iterative algorithms are computationally more demanding and require a precise PSF model.

6.2.1 Non-iterative Algorithms

Non-iterative algorithms do not need any information about the PSF and are usually fast and easy to implement. However, they are not as accurate as iterative algorithms that utilize the PSF to

make a model of the data. The lack of enough accuracy is often a consequence of different type of noise.

The simplest non-iterative approach takes the center of mass of all the photons in an isolated PSF as the emitter location. Approaches such as QuickPALM [128] and others [74] calculate the emitter locations as center of mass of the ROIs. This gives a good estimation of location, however, failure in correct background correction results in biased localizations towards the center of the ROIs. Virtual Window Center of Mass (VWCM) [129] ameliorates this issue by iteratively adjusting the selected ROI to minimize the separation of the emitter location and the center of the ROI.

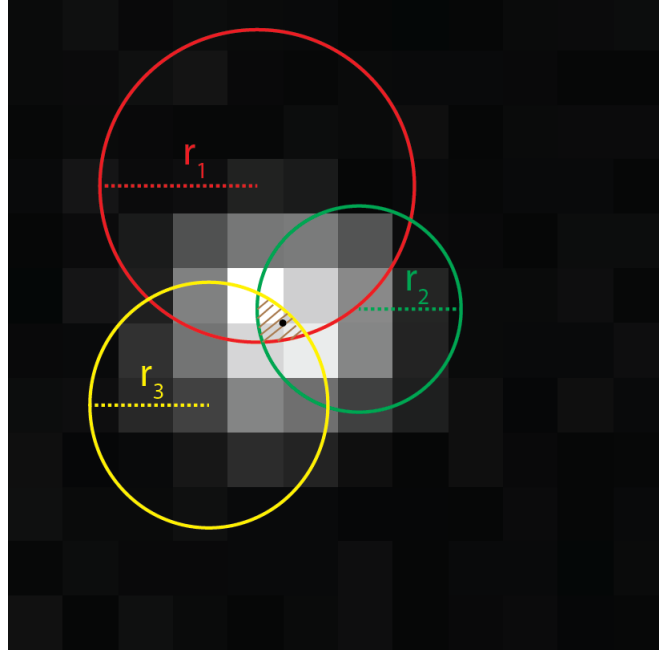


Figure 7: Bancroft algorithm. The emitter sits in the intersection of the three circles where the radii of the circles are calculated based on the values of three selected pixels. The brown lines show the intersection of the circles and the black dot is the emitter location.

FluoroBancroft borrows the Bancroft procedure from the satellite Global Positioning System (GPS) to localize emitters [108, 130]. This approach uses three pixel values within a PSF to draw three circles where the emitter is located within the intersection of these three circles. The size of the intersection region is a measure of localization precision, Fig. 7. A correct measure of background is also of great importance in this approach to calculate accurate radii.

Single emitters can also be localized by finding the gradient of the phase in Fourier domain. For a single emitter, equation (7) reduces to

$$I(m, n) = I_0 \delta(x - x_0) \delta(y - y_0) * \text{PSF}(z_0) + b(m, n) \quad (8)$$

where m and n count rows and columns of pixels in the ROI, and x and y give the centers of those pixels. The Fourier transform of intensity in pixel k and l is given by

$$\tilde{I}(k, l) = H(k, l) \exp \left[-i2\pi \left(\frac{x_0}{M} k + \frac{y_0}{N} l \right) \right] + \tilde{b}(k, l) \quad (9)$$

where M and N are two array dimensions and H is a real function. For data sets with large SNR, the background term is negligible and Fourier Domain Localization Algorithm (FDLA) gives the

emitter position by the average of the gradient of the phase [131]:

$$x_0 = \text{mean} \left(\left(\frac{\partial \phi}{\partial k} \right) \frac{M}{2\pi} \right), \quad y_0 = \text{mean} \left(\left(\frac{\partial \phi}{\partial l} \right) \frac{N}{2\pi} \right) \quad (10)$$

where $\phi = \arctan \frac{\text{Im}(\tilde{I})}{\text{Re}(\tilde{I})}$. The performance of this approach suffers from the presence of the background noise as well. Another approach localizes single emitters by calculating the first Fourier coefficients in both X and Y directions and the phase of these coefficients are then employed to find the emitter location [132].

Radial symmetry of the PSF has also been employed to calculate the emitter locations [111, 133]. Due to the radial symmetry of PSFs, intensity gradient vectors for different pixels converges to the region with maximum intensity where the emitter is located. This approach is robust in the presence of uniform background noise and achieves precision close to the Cramer Rao Lower Bound (CRLB).

6.2.2 Iterative Algorithms

Iterative algorithms are the most rigorous approaches for emitter localization. In these approaches, the parameters in model (8) are adjusted in an iterative manner to fulfill a certain criterion. In the localization problem, the parameters are (x_0, y_0, z_0, I_0, b) , the emitter location, the number of photons from (intensity of) the emitter and a uniform background noise. The criteria that are extensively utilized in emitter fitting literature are the Least Square (LS) difference between data and model and maximizing the likelihood of the problem via a Maximum Likelihood Estimate (MLE).

Cramer Raw Lower Bound (CRLB) states that the fundamental limit of variance for estimating a parameter from a given data is given by the inverse of Fisher Information [57, 58, 134]. Therefore the fundamental limit of precision is given by the inverse of the square root of the Fisher Information. Theoretically, MLE achieves the best localization precision equivalent to CRLB [58, 83, 98, 91, 134, 135, 136, 137, 138]. LS performance is comparable to the MLE under certain conditions described below [91, 136, 137, 138, 139].

The performance of weighted LS at high signal to noise ratio, when the Poisson noise can be well approximated by a Gaussian model, approaches that of MLE as well as when read-out noise is dominant. Note that neither of these scenarios are correct for super-resolution data where the read-out noise is usually negligible in the presence of Poisson noise (shot noise) and the SNR is not too high. In general, MLE yields better localization accuracy and is more robust in the presence of PSF mismatch, but is computationally more complex and requires an accurate model of noise [91, 136].

Least Squares Fitting. The least-squares approaches iteratively vary the parameters of the model to minimize the sum of differences between the pixel values from the data and the model. This difference is given by

$$D = \sum_{\text{pixel}} \frac{(\text{data} - \text{model})^2}{\text{expected variance}} \quad (11)$$

where in weighted LS the differences are scaled by the expected variance of the noise which scales the errors for individual pixels [74, 91, 140, 141, 142, 143]. A pixel with a high signal is expected to have a large noise variance and therefore it is allowed to have a larger error in the weighted LS procedure. However, the scaling factor is replaced by one in the unweighted LS algorithm, which we call LS hereafter [57, 107, 144, 145, 146]. The developed algorithms use the Gaussian PSF [57, 91], theoretical PSFs [142, 143] or experimentally acquired PSFs [140, 145] to make a model of the data. The Levenberg-Marquardt iterative procedure [142, 145, 146] or other procedures [140] are then employed to iteratively adjust the parameters of the model.

The weighted least square algorithms accomplish accuracies close to the CRLB when the photon count is high, but the noise variance needs to be known as well as an accurate PSF model. The

PSF mismatch, particularly in the tail of the PSF, results in large errors when scaled by a small expected noise variance in the pixels far from the emitter [70]. Therefore, the unweighted least square algorithm is more suitable when a reasonable PSF model and/or noise model are not accessible.

Maximum Likelihood Estimator. The photons from a point-like emitter have an approximate spatial Gaussian distribution [59, 91, 98, 106, 141, 147, 148] on the camera which can be employed to calculate the photon counts for different pixels (12). In cases where the Gaussian PSF is not an appropriate approximation, theoretical PSF models [98, 136, 149] can be used or the PSF can be obtained experimentally or by PSF-engineering [150, 151, 152, 153]. The obtained PSF is then utilized to generate a likelihood model of the ROI via either linear or cubic spline numerical interpolation approaches [151, 153]. Using the Gaussian approximation for PSF, the photon counts is given by

$$\Delta_k = \frac{I_0}{2\pi\sigma_{\text{PSF}}(z_0)^2} \int_{x_k-0.5}^{x_k+0.5} \int_{y_k-0.5}^{y_k+0.5} \exp\left[-\frac{(x-x_0)^2 + (y-y_0)^2}{2\sigma_{\text{PSF}}(z_0)^2}\right] dx dy \quad (12)$$

where $\Delta_k, \sigma_{\text{PSF}}, I_0, x_0, y_0, z_0, x_k$ and y_k are, respectively, the number of photons in the k th pixel from the emitter, the half width of the Gaussian PSF, total number of the photons from the emitter, the emitter location and the center of the k th pixel.

The total photon count in the k th pixel is the sum of the photons from the emitter and the uniform background noise

$$\lambda_k = \Delta_k + b \quad (13)$$

Equation (13) yields the expected number of photons for pixel k for a fixed exposure time. Consequently, the number of the photons in pixel k has a Poisson distribution, which gives the likelihood of the k th pixel

$$P_k(D|\theta) = \frac{\lambda_k^{D_k} e^{-\lambda_k}}{D_k!} \quad (14)$$

where θ stands for the set of parameters ($\theta = (x_0, y_0, I_0, b)$). D represent data, which is a two dimensional array of pixels whose values are the number of photons detected by the camera. D_k selects the k th pixel in D . Since the pixels are independent, the likelihood of the ROI can be written as the product of the likelihoods of all the pixels in the ROI.

$$P(D|\theta) = \prod_k P_k(D|\theta) \quad (15)$$

The two main iterative algorithms employed in the literature to find the parameters that optimize the above likelihood are variations of Newton method [91, 98, 147, 148, 149, 151, 152] and a modified version of Levenberg-Marquardt [59, 141, 153, 154] adopted from LS procedures.

The Newton approach is employed to find the root of the derivative of the likelihood function (15) and therefore one needs to calculate the second derivative of the likelihood as well, which is computationally demanding. On the other hand, the Levenberg-Marquardt algorithm only calculates the first derivative of the likelihood, which makes it computationally less demanding in comparison to the Newton approach [141, 153]. Different strategies have been exploited to speed up the Newton optimization algorithm including implementation on Graphical Processing Units (GPUs) which allows parallel analysis of ROIs [98, 147, 148, 152], starting from better initial values [136] and estimating X and Y positions individually utilizing the separability property of the Gaussian function [148]. MLE has also been implemented using a different optimization algorithm on GPUs [106].

6.3 Multiple Emitter Fitting

Raw SMLM super-resolution data is often acquired via a wide-field illumination procedure and the whole sample is exposed to the excitation laser. Emitter activation is a stochastic process and

hence there will always be activated emitters at close proximity. Therefore, overlapping PSFs are unavoidable, even under sparse activation conditions. The overlapping PSFs are eliminated in a filtering step in single-emitter approaches, which results in losing information [135], as well as the appearance of artifacts, for instance, contrast inversion, Fig. 8.

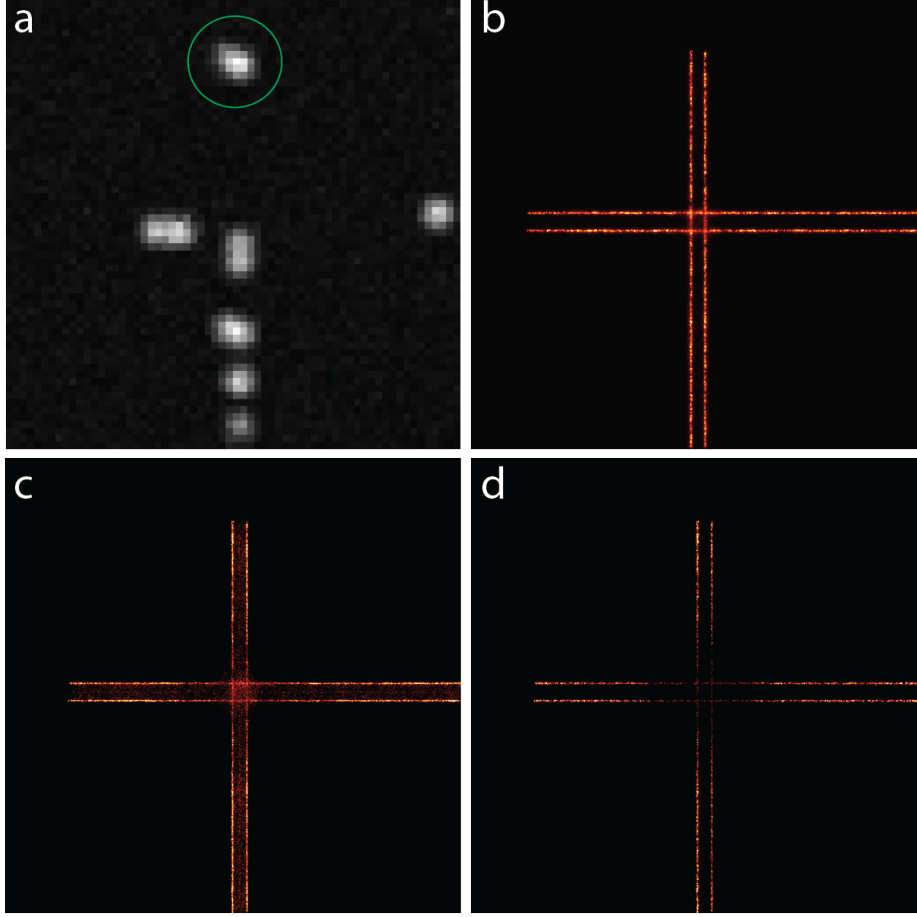


Figure 8: Reconstructions from dense data with overlapping PSFs. (a) A frame of dense raw super-resolution data of a cross with parallel lines. The green circle shows an example of two overlapping PSFs. (b) Reconstruction from multiple-emitter algorithm with no filtering. (c) Reconstruction from single-emitter algorithm with no filtering. The localizations in the area between the lines are the results of fitting overlapping PSFs with a single PSF. (d) Reconstruction from single-emitter algorithm after filtering. The dense regions of data appear sparse when processed with a single-emitter algorithm due to the inability to localize overlapping PSFs, which is called contrast inversion artifact.

The inability of single-emitter algorithms to localize activated emitters in a diffraction limited vicinity enforces the sparse activation of emitters. This is followed by a long acquisition time to build a full list of localizations to reconstruct an image with high resolution. In some experiments, such as studies of live or dynamic samples, fast data acquisition is preferred and hence dense activation of emitters is inevitable. Therefore, proper analysis of dense super-resolution data with overlapping PSFs is necessary to reduce data acquisition time, avoid artifacts, facilitate live sample imaging, etc.

Numerous multiple-emitter fitting algorithms have been devised to fit emitters with overlapping

PSFs, some borrowed from other areas, such as astronomy, statistical analysis, etc. The reported algorithms employ a very wide range of approaches and have a broad spectrum of performances [71, 72]. These procedures are often iterative algorithms or include an iterative training step.

6.3.1 Least Square

The least squares algorithm has been employed to fit multiple-emitters in the field of astronomy [84]. It was modified for SMLM super-resolution microscopy, called DAOSTORM in this context [155]. DAOSTORM uses isolated emitters in the raw data to estimate the PSF and then uses the found PSF to fit emitters in dense data sets. The algorithm starts with an initial number of emitters located at the brightest pixels of the ROI, and then uses least squares fitting to localize them with sub-diffraction precision. Next, the residuum image is calculated by subtracting the model from the data, and is used to detect new emitters in the pixels brighter than a given threshold. The detected emitters are then localized to obtain subdiffraction precision. This step is repeated until there is no pixel with intensity above the threshold in the residuum image.

6.3.2 Maximum Likelihood

The MLE approach that was described before can be modified for multiple-emitter fitting within ROIs with overlapping PSFs. The total photon counts in the k th pixel is given by

$$\lambda_k(N) = b + \sum_{i=1}^N \Delta_{k,i} \quad (16)$$

where $\Delta_{k,i}$ is the number of photons received in the k th pixel from the i th emitter and can be calculated using (12). N and b are the number of emitters and the uniform background. The likelihood of the pixel is then given by

$$P_k(D|\theta) = \frac{\lambda_k(N)^{D_k} e^{-\lambda_k(N)}}{D_k!} \quad (17)$$

The likelihood of the ROI is obtained from the product of the likelihoods of individual pixels (15).

The likelihood (17) has more than one emitter and therefore more parameters to estimate, demanding more iterations and computational time. The MLE approach is implemented in the same manner as single-emitter fitting to estimate the parameters. Nevertheless, there is a new parameter N , the number of emitters, which cannot be directly estimated from the likelihood itself. The approaches that find the number of emitters are called model selection algorithms. Several model selection algorithms have been reported along with the MLE localization procedure, including thresholding of the residuum image [156], p-value of the likelihood ratios [135], Bayesian Information Criteria (BIC) [157, 158], PSF size and nearest neighbor distance [159] and others [160, 161, 162].

The 3D-DAOSTORM [156] is a 3D multiple emitter fitting approach. 3D fitting procedures will be discussed in the next section and here we explain how this procedure deal with overlapping PSFs. 3D-DAOSTORM fits overlapping PSFs by fitting only choices from the brightest emitters in the ROI, at the beginning. It then subtracts the obtained model from the ROI and uses the residuum image to find pixels brighter than a given threshold to detect new emitters. It employs MLE to localize the new emitters. The new emitters are added to the list of detected emitters and this step is repeated until there is no pixel brighter than a given value.

Simultaneous multiple-emitter fitting [135] starts from one emitter, $N = 1$, and goes up to $N = N_{max}$. For each model, this method localizes the emitters employing the MLE approach. The log-likelihood ratio (LLR)

$$\text{LLR} = -2 \log \left[\frac{P(D|\hat{\theta})}{P(D|D)} \right] \quad (18)$$

has an approximate chi-square distribution [135], where $\hat{\theta}$ is the parameters that maximize the likelihood and $P(D|\hat{\theta})$ gives the upper limit of the likelihood. The model with lowest N that meets a threshold p-value is accepted as the best fit.

The MLE approach suffers from overfitting, and adding more parameters (emitters) tends to give larger values for likelihoods. Bayesian Information Criteria is a model selection algorithm that penalizes adding new parameters to an MLE problem. SSM-BIC [157] selects the model that maximizes the following function

$$\text{BIC}(N) = \frac{(\text{Data} - \text{Model})^2}{\text{Data}} + (3N + 1) \log(m) \quad (19)$$

where m is the number of pixels in the given ROI. Note that there are $3N + 1$ parameters in a model with N emitters. This approach has also been implemented on GPUs with ~ 100 times faster computational time [158].

QC-STORM [159] uses a weighted likelihood

$$P_W(D|\theta) = \prod_k W_k P_k(D|\theta) \quad (20)$$

to localize emitters, where W_k is the weight of the k th pixel and is smaller for pixels closer to the edges of the ROI. The weighted likelihood suppresses the signal close to the edges of the ROI and it is therefore an effective method to localize emitters within ROIs with signal contaminations close to their edges. QC-STORM identifies ROIs with more than one emitter based on the ROIs' nearest neighbor distances and the size of the PSF estimated using weighted MLE. This algorithm has been implemented on GPUs and is capable of processing very large fields of view.

Some other approaches use an iterative deconvolution algorithm to accomplish maximum likelihood employing the Richardson and Lucy procedure [163, 164]. These approaches return a grid image with finer pixel sizes than the camera pixel size with non-zero pixel values at the emitter locations rather than returning a list of localizations.

6.3.3 Bayesian Inference

The MLE algorithm suffers from overfitting as discussed above. Bayes' formula (21) provides an elegant way to include prior knowledge into the problem, allowing the problem to be restricted to reasonable number of parameters. It however adds complication to the problem by including more distributions. Moreover, it has been shown that Bayesian approach can achieve localization uncertainties better than those from MLE, by inclusion of reasonable prior knowledge [165]. Bayesian approach is equivalent to MLE when there is no prior knowledge available. The posterior is given by

$$P(\theta|D) = \frac{P(D|\theta)P(\theta)}{P(D)} \quad (21)$$

where $P(\theta)$ and $P(D)$ are, respectively, the prior on θ and the normalization constant,

$$P(D) = \int P(D|\theta)P(\theta)d\theta \quad (22)$$

called the evidence. Another difference of MLE and Bayesian approaches is that MLE returns fixed locations as the emitters' positions, while the Bayesian procedure returns a probability distribution, the posterior, for the emitter parameters.

Two fully Bayesian algorithms have been developed for multiple-emitter fitting, so far [85, 166]. The Bayesian Multiple-emitter fitting (BAMF) algorithm [85] employs Reversible jump Markov chain Monte Carlo (RJMCMC) [167, 168] technique to explore model spaces with different dimensions or equivalently different emitters and returns a posterior distribution which is a weighted average of

different possible models. This technique performs emitter fitting, model selection and structured background modeling simultaneously and therefore takes into account all sources of uncertainties which are often ignored.

3B algorithm [166] analyzes the entire data set at the same time by integrating over all possible positions and blinking events of emitters.

The 3B algorithm keeps track of the emitter locations, intensities, width of the Gaussian PSF and blinking of emitters. The posterior of this problem is given by

$$P(a, b, M|D) = \frac{P(D|a, b, M)P(a)}{P(D)} \quad (23)$$

where a, b and M represent the emitter parameters, blinking events and the number of emitters, in turn. 3B uses a uniform prior for the locations and a log-normal prior for other parameters. The discrete parameter, b , is then integrated out using an MCMC [169] approach to obtain the posterior distribution of a , $P(a, M|D)$. Next, the Maximum A Posteriori (MAP) is computed using the conjugate gradient approach to obtain the emitter locations, intensities and PSF sizes. After that, the parameter a is also marginalized to get the model probability, $P(M|D)$, for model selection.

The 3B algorithm models the entire data set and is able to use all the collected photons from multiple blinking events to achieve better localization precision. The returned image is a probability map of the weighted average of all possible models rather than a selected single model [170]. Moreover, it needs a simple experimental setup for data collection [166]. However, it is reported that 3B suffers from artificial thinning and thickening of the target structures [166]. This technique is very slow because calculating the integrals to marginalize parameters a and b is extremely computationally demanding. There have been several attempts to speed up the algorithm including 3B implementation in cloud computing [171], use of more informative priors [172], and initializing the algorithm with better starting parameter values [173].

6.3.4 Compressed Sensing

A frame of super-resolution data can be considered as a matrix y

$$y = Ax + b \quad (24)$$

where x is the signal, which is an up-sampled discrete grid (image) with non-zero elements at the emitter locations, A is the PSF matrix and b is the uniform background. The objective is to recover the non-zero elements of the signal x where most of the elements are zero due to sparse activation of fluorescent emitters in SMLM microscopy. Compressed Sensing (CS) theory states that a signal x can be recovered from a noisy measurement y if the signal is sufficiently sparse [174]. This mathematically can be expressed as

$$\begin{aligned} &\text{Minimize : } \|x\|_1 \\ &\text{Subject to : } \|y - (Ax + b)\|_2 \leq \epsilon \end{aligned} \quad (25)$$

where $\|x\|_1 = \sum_i |x_i|$ is the L1-norm of the up-sampled image, and $\|y - (Ax + b)\|_2 = \sqrt{\sum_i (y_i - (Ax + b)_i)^2}$ is the L2-norm of the residuum image. The inequality allows fluctuations from the expected model due to different types of noise.

Various mathematical approaches have been utilized to minimize L1-norm in the presence of the given restriction in (25) including convex optimum algorithm [175], L1-Hotomopy [176], gradient descent [126] and others [177, 178]. These algorithms are able to detect and localize the emitters in very dense region of the data. However, due to the large size of the up-sampled image, the CS algorithms are slow and the resolution cannot be better than the grid size of the up-sampled image.

The above mentioned issues have been addressed in later literature using different approaches. FALCON [126] accelerates the algorithm by implementing CS on GPUs. It ameliorates the grid-size

problem by refining the found locations in the subsequent steps after the deconvolution stage. CS has recently been implemented over continuous parameter spaces to remove the limits imposed by the up-sampled grid [179, 180]. To lower the computational cost of the CS algorithm, a recent paper models the entire sequence at the same time rather than by a frame by frame analysis of the data [181]. Another approach implements the CS algorithm in the correlation domain by calculating the frames cross-correlation [182].

Singular Value Decomposition

Assume A is a $n \times n$ square matrix with non-zero determinant, then A can be factorized into

$$A = U\Sigma U^{-1} \quad (26)$$

where U is a $n \times n$ matrix whose columns are the eigenvectors of decomposition and Σ is a diagonal $n \times n$ matrix where the diagonal elements are the eigenvalues. A non-square matrix B can also be decomposed in a similar fashion, called the singular value decomposition (SVD)

$$B_{n \times m} = V_{n \times n} \Lambda_{n \times m} W_{m \times m} \quad (27)$$

where V and W are, respectively, $n \times n$ and $m \times m$ matrices. Λ is a diagonal $n \times m$ matrix with diagonal elements the eigenvalues of B [183].

The Multiple Signal Classification ALgorithm (MUSICAL) for super-resolution fluorescence microscopy [184] takes B as a collection of frames of super-resolution images where each column of B is a frame of the raw data. B is then a non-square matrix that can be factorized into a diagonal matrix and unitary matrices. The eigenvectors are then the eigenimages. The eigenimages are then classified into signal and noise with large and small values, respectively, based on a given threshold. MUSICAL then calculates the projection of the PSF at different locations in the eigenimages to identify and localize the emitters. An alternative method makes use of the SVD in the Fourier domain, analyzing the sequence of raw data frame by frame to localize the emitters [185].

Deep Learning

Deep learning approaches are non-iterative optimization algorithms that perform calculations in a parallel manner and hence are very fast. These approaches are based on Artificial Neural Networks (ANN) that are inspired by animal brains and neural systems. The building blocks of the brain are neurons equivalent to perceptrons or sigmoid neurons in ANNs [186]. Perceptrons takes a few binary inputs and generates a binary output, Fig. 9.

The output of the perceptron is one if the sum of inputs times their weights is larger than a threshold and is zero otherwise, eq. (28).

$$\text{Output} = \begin{cases} 0 & \text{if } \sum_i w_i \text{ input}_i < \text{threshold} \\ 1 & \text{if } \sum_i w_i \text{ input}_i > \text{threshold} \end{cases} \quad (28)$$

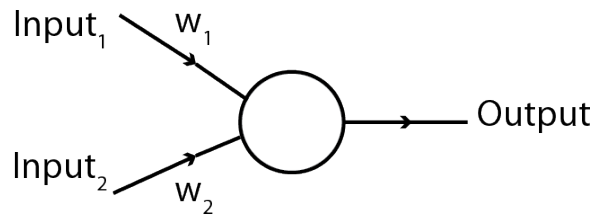


Figure 9: Perceptron takes several binary inputs and gives a binary outcome. w_i s are the weights of the inputs.

It can be shown that certain combinations of perceptrons produce logical operations such as AND, OR and NAND, which are the underlying bases of computation and any mathematical function could be generated using them [186]. Therefore, ANNs are capable of producing any mathematical function using perceptrons. A network of perceptrons can be trained to perform different tasks by adjusting the weights, w_i s. Sigmoid neurons are more sophisticated versions of perceptrons where the output is a value within the interval of $[0, 1]$ rather than a binary output. Sigmoid neurons are more flexible in the training process and are used in neural networks.

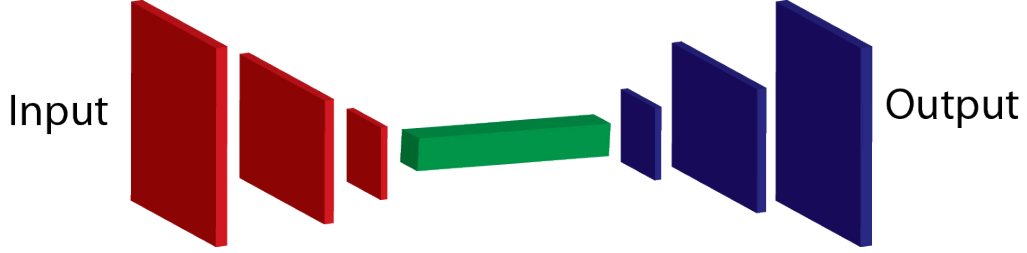


Figure 10: Convolutional neural network. Blocks show layers of neurons. CNNs are comprised of two stages. the first stage is taking the input and encoding the image into a few pixels. The next step decodes the information and upsamples the image into more pixels. The encoding and decoding stages are depicted in red and blue, respectively.

ANNs have been employed to attack various problems in the field of biomedical imaging [187, 188], specifically for SMLM image processing [189]. Convolutional Neural Networks (CNNs) have been employed for super-resolution image processing. CNNs consist of two stages. The first stage of the network receives the input image and then encodes the information into a smaller number of pixels via multiple layers of neurons. This step averages out insignificant details and helps with denoising. Next, the encoded information in the first step is decoded and upsampled to a super-resolved image with a finer pixel size than the input image, Fig. 10, [187].

CNNs designed to localize emitters in super-resolution raw data can be categorized into three different sets based on their training approach:

- 1) ANNs are trained using simulated data where the ground truth is available or using localizations found using a standard iterative algorithm [190, 191, 192]. In the training stage, the ANN learns by minimizing the sum of distances between the found localizations and the given locations. Using synthesized data, there will always be adequate training data.
- 2) ANNs are also trained using two well-registered sets of data acquired from the same sample where one of them is used as ground truth. The ground truth image has high SNR that can be acquired employing different procedures such as confocal microscopy [193, 194], using an objective with high numerical aperture [195], and using a sparse data set to reconstruct a super-resolved image with high SNR [196] to train the network. In the training stage, the network learns by minimizing the difference between the output image and the acquired image with high SNR. The minimization of differences can be implemented via a standard iterative optimization algorithm [193] or by using a sub-network in the training stage called a discriminative network [195, 196]. The discriminative network takes the output of the CNN along with the ground truth images and labels the output as real or fake.
- 3) In an alternative training approach, there is no additional inputs for the training step and the network is trained by reproducing the input data from the list of found emitters and minimizing the difference between the original input and the synthesized image [197]. This training procedure is called unsupervised learning.

The deep learning procedures are very fast during the analysis. There are no required input parameters or thresholds, and their performance is comparable to the MLE algorithm [192, 198].

However, the training process is very sensitive and has to be done very carefully. Some pitfalls of training are the hallucination problem, the generalization problem, etc [187]. Deep learning algorithms might make mistakes in identifying patterns from random inputs when there is not adequate training, which is called the hallucination problem. If there are new patterns that are not seen by the algorithm before it fits these new data by the old patterns, which is called the generalization problem.

Others

WindStorm [199] uses a temporal filter to estimate the background and remove it from the raw data. It then implements deconvolution by dividing the Fourier transform of the clean image with the Fourier transform of the PSF. It next performs frequency truncation. The recovered locations are given by the peaks of the deconvolved image in the spatial domain. This is a fast and non-iterative approach and the found locations can be used as initial values for iterative algorithms.

Wedge Template Matching (WTM) [200] identifies and localizes emitters by matching an entire or partial template of the PSF to the regions of the data with overlapping emitters. The WTM algorithm picks either an entire or partial PSF template based on the degree of overlapping between PSFs. It finds the candidate pixels containing emitters using cross correlation of the template with the image, and then finds the locations of the detected emitters with sub-pixel accuracies.

Other approaches employ machine learning algorithms [201], independent component analysis and a shape matching approach in the frequency domain [202], and other algorithms [203] to identify and localize emitters in dense regions of the data.

6.4 3D fitting

Biological samples are 3D in nature and 3D microscopy approaches are required to gain better insight into biological structures. A standard super-resolution microscope cannot provide precise axial location of an emitter due to slow changes in the 3D PSF as a function of axial position (z) [139]. Super-resolution microscopes can however provide precise axial location of an emitter by some alterations in the optical setup. Several different modifications have been reported in the literature encompassing multi-focal methods [140, 144, 204, 205] which image multiple focal planes at the same time; engineered PSFs [73, 74, 75, 76, 77, 206, 207] where the axial information is encoded into the PSF shape; and other procedures [208, 209, 210, 211].

The multi-focal approaches allow precise axial emitter localization by providing multiple z -slices of the PSF. The PSF engineering approaches attains precise axial localization of emitters by inscribing axial information in the shape of the PSF by simple phase front modifications. The modification in phase front can be achieved by inserting extra optical components [73, 75, 212] or computer controlled phase modulators [74, 76, 207, 213] in the optical path. Several engineered PSFs have been devised for 3D super-resolution microscopy including astigmatic PSF [73], double-helix PSF [74], phase ramp PSF [75], corkscrew PSF [206], self bending PSF [207], and tetrapad PSF [76, 213]. These PSFs have special characteristics, such as relative motions of different parts, width variations in different directions, etc., that quickly changes as a function of axial location. The engineered PSFs cover different ranges of axial locations. It has been shown that the tetrapad PSF accomplishes precise lateral emitter location over the largest axial range compared to the other designed PSFs [76, 139, 72].

Most of the 2D emitter fitting algorithms discussed in the previous sections can be adapted for 3D emitter fitting [72, 214]. These approaches employ either a theoretical 3D PSF [73, 98, 105, 180, 215, 216, 217] or an experimentally acquired numeric PSF to calculate the model [128, 144, 150, 151, 152, 153, 218, 219, 220, 221, 222, 223, 224]. More complicated PSFs such as tetrapad or double-helix have very intricate features that cannot be exactly expressed by an analytical function, so the PSF is generated from empirical data.

The PSF at a z -plane is given by [151]

$$\text{PSF}(x, y, z) = \iint P(k_x, k_y) e^{2\pi i(k_x x + k_y y + k_z(k_x, k_y)z)} dk_x dk_y \quad (29)$$

where $P(k_x, k_y)$ is the pupil function or phase front at the back focal plane of the objective lens and is a characteristic of the optical setup plus the extra phase added for PSF engineering. To obtain the phase front, a stack of images of an isolated emitter at different z -positions is acquired and then employed to retrieve the phase front which is used to calculate the PSF model. The camera records the intensity values, while the phase information is mostly lost, however there are different approaches that can be employed for phase retrieval from the intensity images, such as the Gerchberg-Saxton algorithm [151, 225, 226] and the MLE approach [162]. Substituting the obtained phase front in (29), one is able to obtain the PSF at any given location. However, the integral (29) is computationally expensive and therefore the PSF model is generated at just a few z -slices. The PSF at a desired location can then be numerically produced via either linear or spline interpolation [151, 153]. Deep learning approaches have also been recently employed for 3D emitter fitting by training ANNs with PSFs at different axial locations [191, 192, 197, 198].

6.5 Drift Correction

Drift is a common problem in super-resolution microscopy procedures, in which the sample alters its location overtime, resulting in distortion and degradation in the quality of final images. SMLM microscopy reconstructs high-quality images from a list of localizations collected over the course of experiment, where even slight disturbances in the experiment lead to serious defects in the results. For instance, mechanical vibrations of the microscope stage or fluctuations in temperature result in rotational or translational movements of the sample during data acquisition. Since such disturbances are unavoidable, algorithms are required to measure and correct for drift in the image processing step.

Multiple drift correction algorithms have been employed in super-resolution microscopy, such as use of fixed fiducial markers during the experiment [33, 227, 228, 229, 230, 231, 232], image cross-correlation between frames at different times [233, 234, 235, 236, 237, 238, 239, 240], computing drift directly from the list of found emitter-coordinates [241, 242, 243, 244] and other procedures [245, 246, 247].

Fiducial markers are fixed point sources of light or structures during data acquisition that are used as reference points for drift correction. Since fiducial markers are fixed, their movements can be measured in the localization step and used to eliminate drift errors. Fiducial markers can introduce light corruption to the sample and some fiducial markers emit photons for a limited time, which restricts the data acquisition time. Cross-correlation approaches are the most common procedure for removal of drift error and different variants of that have been reported in the literature. Image noises deteriorate performance of the cross-correlation approaches to calculate drift errors. One algorithm maximizes the cross-correlation of the first frame with the rest of the sequence to calculate drift [235, 238]. A fast implementation of cross-correlation is achieved in Fourier domain [236, 237, 240], and some other approaches employ the cross-correlation of the sum images to reduce the effect of noise [234, 239]. Some approaches have been developed using the list of found localizations to estimate sample drifts, such as nearest neighbor distribution of locations [243, 244].

Wester, et al. [244] made use of a combination of the image registration approach and nearest neighbor distribution of localizations to measure drift in the sample. The algorithm employs periodic 3D registration of the sample using brightfield images to remove drift errors. However, brightfield registration is only accurate to around 10 nm and there might be still residual drift remaining. This approach next uses post-processing of the localizations to extract residual drift from the nearest neighbor distribution of emitter coordinates. This procedure is robust and also capable of calculating axial drift.

6.6 Fitting Quality and Image Quality

The quality of a fit is defined as how close the recovered location of an emitter is to its true location. The fitting quality depends on the emitter detection, emitter fitting and thresholding algorithms. Each of these steps were discussed in previous sections. There are a few metrics to assess the fitting quality including the Jaccard index (JAC), root mean square errors (RMSE) or accuracy, precision [71, 72] and a vectorial model for localization uncertainties [248]. Image resolution is often used as a reporter of image quality. However, there is no widely accepted definition for resolution in super-resolution microscopy literature [83, 138, 249]. There are however a few common metrics that are used to assess microscopy image resolution such as the Abbe/Rayleigh resolution criteria, localization precision [83], signal to noise ratio (SNR), Fourier ring correlation (FRC) [67].

Fitting Quality

The uncertainty in the location of an isolated emitter are characterized by precision and accuracy. Assuming that an emitter with location x_e blinks multiple times, there are then multiple found locations, x_f , of this emitter. The found locations are different and are spread over a small region around the emitter location, x_e , for a perfect fitting algorithm. The localization precision, σ_x , is the standard deviation of the distribution of x_f s. This is a fundamental limit for localization precision imposed by the random nature of photons and is not a result of instrument imperfections or flaws in the experiment design [57, 58, 83]. Due to the random nature of photons, each time that the emitter turns on, the number of photons going to in each direction deviates by a small amount, which is called shot noise, resulting in a small deviation in the found location of the emitter, Fig. 11. The fundamental limit of precision for a perfect localization algorithm is given by the square root of inverse of diagonal elements of the Fisher information matrix

$$\sigma_\theta = \frac{1}{\sqrt{N \int_{-\infty}^{+\infty} \frac{1}{L(D|\theta)} \left(\frac{\partial L(D|\theta)}{\partial \theta} \right)^2 d\theta}} \quad (30)$$

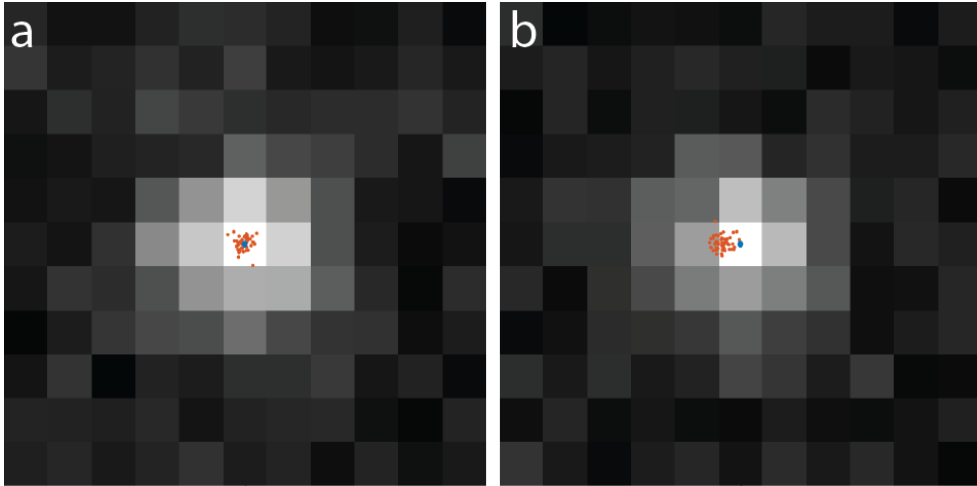


Figure 11: Precision and accuracy concepts. Blue dots are the true emitter position and the orange dots stand for found locations. (a) Distribution of the found locations from a perfect fitting algorithm. Precision is proportional to the size of the distribution of the found locations. (b) Distribution of the found locations from a biased fitting algorithm. Accuracy is described as the deviation of the center of the distribution of found locations from the true position.

where $L(D|\theta)$ is the likelihood given in (14), θ and N stand for the collection of all the parameters and number of photons, respectively. The fundamental limit of localization precision for lateral coordinates due to shot noise is given by (6). The localization precision in the axial direction is usually worse due to larger size of the PSF out of the focal plane and therefore result in a lower SNR and other factors.

Accuracy describes the deviation of the average of the found locations from the true emitter location, Fig. 11. Unlike localization precision, localization accuracy does not have a fundamental limit and can be zero [83]. However, due to instrument imperfections, optical aberrations, etc., the resulted localizations are often a little biased [250, 251, 252, 253]. Acceptable localizations have similar spreads of precisions and accuracies.

In practice, it is often challenging to achieve unbiased localizations and localization precisions close to the square root of CRLB variance derived from a too simplistic model that only takes into account Poisson noise. This is due to other existing factors in super-resolution experiments such as limitations in equipment, experiment and fitting algorithms, such as camera, PSF mismatch, drift, background noise, etc.

Camera. Several properties of cameras, such as camera noise, pixelation, etc., affect the localization precision and accuracy. A major source of noise in cameras is read-out-noise that can affect localization uncertainty. Read-out-noise is particularly important in sCMOS cameras where each pixel has a unique amount of read-out-noise [92, 94]. Model (14) only takes into account shot-noise and ignores the read-out-noise. This model is suitable for EMCCD cameras where the read-out-noise is negligible in comparison to the homogeneous background and has an approximately uniform value over the field of view. However, read-out-noise has a unique value in each pixel for sCMOS cameras and therefore can result in degradation in localization uncertainty. It is shown that read-out-noise can be modeled by an additional source of light in sCMOS cameras to improve the localization uncertainty [94].

Scientific cameras are not able to record the exact location of photons reaching them. However, they report the number of photons reached on a region within a certain area called a pixel. This causes loss of accurate locations of photons from an isolated emitter and therefore results in localization uncertainty. This effect is called pixelation. Moreover, sensitivity of cameras can be nonuniform over the field of view, which is another potential source of deterioration of localization precision [83].

PSF mismatch. Error-free PSF input to the iterative approaches is of key importance for accurate and precise emitter localization [88]. There are several factors that lead to major deviations between the expected PSF and the resultant PSF, including dipole orientation, emitter motions, changes in the optical properties of the environment, like refractive index, etc. [70, 83, 91, 136, 253, 254]. Fluorophore emitters are electric dipoles in nature and do not emit photons in an isotropic manner, despite the assumption of spatial uniform distribution of photons. A rigid emitter therefore has a nonuniform photon distribution which degrades the fitting quality when using an isotropic approximation of the PSF [87, 88, 255]. However, these emitters usually are free to rotate randomly which gives an isotropic distribution of photons. Emitter movements exist in some experiments due to the nature of samples, like live cell imaging or particle tracking, or due to bad fixation of the sample. This can result in an smearing pattern in the PSF, specifically for large exposure times, when the emitter emits photons while moving [89, 90]. Imaging cellular structures within their native environment often requires light traveling through thick tissues of the specimen. The optical properties of the sample, such as refractive index, changes as a function of location which leads to phase front disturbance of light and therefore distortion of the PSF [253, 254].

Background. Another limiting factor for precision and accuracy in localization microscopy is the background noise. Failure in correct background estimation can lead to biased localization estimates as was discussed extensively above. The homogeneous background is usually modeled by

an additive offset to the intensity (13). The situation is worse in the presence of inhomogeneous background which is more difficult to model and can give rise to more uncertainty in localizations.

Fitting algorithm. The limits of the fitting algorithm itself is also an important factor in localization uncertainty. For example, a crude peak finder algorithm that finds the pixels with the maximum intensities has an accuracy comparable to the pixel size. Better localization precision and accuracy come with more computationally expensive algorithms, such as iterative fitting procedures. It was shown that the MLE approach attains the localization precisions comparable to CRLB in the absence of other limiting factors [58, 136].

Analytical calculation of localization precision considering all the important factors is a difficult task, however statistical and experimental techniques have been proposed to calculate localization uncertainties taking into account all those factors [118, 256, 257]. An approach based on nearest neighbor distribution of localizations has been proposed that prescribes a simple way to compute localization precision from nearest neighbor distribution (NND) distances of found localizations [118]. Lee, et al. used well isolated emitters in sparsely labeled biological samples to experimentally measure localization precision under realistic experimental conditions [256].

JAC is another standard metric to measure the quality of fitting for a group of emitters rather than an isolated emitter [71, 72, 85]. JAC evaluates the rate of emitter detection versus the density of emitters. This is particularly important for multiple-emitter fitting algorithms as they are supposed to detect and localize emitters in dense regions of the data. To perform this test, sets of super-resolution data with different emitter densities are simulated and processed with the given fitting algorithm. Next, the pairs of matching emitters within the sets of found and true locations are found by minimizing the cost metric between the two sets. Finally, JAC is defined as the ratio of the number of matched emitters to total number of localizations within both sets

$$\text{JAC} = \frac{\text{ME}}{\text{FE} + \text{TE}} \quad (31)$$

where ME, FE and TE refer to the number of matched emitters, found emitters and true emitters, respectively.

Image Quality

After conducting the experiment and performing the image analysis, the final result is a super-resolved image reconstructed from list of the found localizations. What a scientist eventually cares about is the quality/resolution of this image and the amount of details that it reveals. The metric to evaluate the two-point resolution of conventional microscopy techniques is either Abbe’s resolution or Rayleigh’s resolution criteria. Ram, et al. provided an alternative for Rayleigh’s resolution in localization microscopy employing Fisher information theory for two nearby emitters activated simultaneously [258]. It can be shown that the Rayleigh two-point resolution criterion is equivalent to localization precision for SMLM super-resolution techniques. There are a few metrics to examine the resolution of reconstructed images of localization microscopy, including localization precision [134] and labeling density [116, 259]. To obtain a desired resolution, the localization precisions must be smaller than the desired resolution and there should be at least two localized emitters within a distance equal to the desired resolution [83].

Although precision and labeling density are essential parameters in evaluating the resolution of the SMLM reconstructed images, they do not account for all the factors that contribute to deterioration of resolution. For example, resolution also depends highly on the type of structure being examined and differs from experiment to experiment [83, 138, 260]. For instance, visualization of fine actin filaments requires uniform labeling density as well as high labeling density [61, 261] while in imaging nuclear pore complexes (NPCs), the localization precision is of more importance since the sample itself has a discrete structure [262]. Therefore, more advanced theoretical methods

for estimation of resolution in localization microscopy have been devised such as the information transfer function (ITF) [263], Fourier ring correlation (FRC) [67, 264], super-resolution quantitative image rating and reporting of error locations (SQUIRREL) [265], and algorithmic resolution [266].

Experimental approaches for characterization of resolution have also been reported in the literature, for instance, the use of DNA-rulers, DNA-origami structures or standard biological structures such as NPCs with known spacing between emitters as references to benchmark the ability of microscopy techniques in resolving closely spaced emitters [262, 267, 268]. Some other well characterized biological structures such as microtubules and synthesized raw super-resolution data for different structures such as the Siemens star, crossing lines, have also been employed to inspect the resolution of SMLM reconstructed images [71, 72, 85, 135, 269]. In the following, it will be shown that Rayleigh's two-points resolution criterion is related to localization precision in SMLM techniques and some selected image resolution metrics developed for SMLM techniques will be presented in more details.

Two-points resolution. Rayleigh's resolution criterion was originally developed for observations with human eye. It is defined as the ability of the eye to distinguish two closely spaced objects. In conventional microscopy, the resolving power of a lens is given by the smallest distance, d , between two point-like emitters that can be distinguished under a microscope [4]. Rayleigh's resolution distance is

$$D = 0.61 \frac{\lambda}{N_a} \quad (32)$$

where λ and N_a are the wavelength of the light and the numerical aperture of the lens, in turn.

The diffraction of light from a circular aperture/lens is given by the Airy pattern [4]

$$I(\theta) = I_0 \left[\frac{2J_1\left(\frac{2\pi}{\lambda}na \sin \theta\right)}{\frac{2\pi}{\lambda}na \sin \theta} \right]^2 \quad (33)$$

where J_1, a, n, I_0, λ and θ are, respectively, the Bessel function of the first kind of order one, the radius of the aperture/lens, refractive index of the medium, intensity, wavelength of light and the half angle of observation, Fig. 12. The first zero of this intensity pattern occurs at $\frac{2\pi}{\lambda}na \sin \theta = 3.83$ which yields $D = 0.61 \frac{\lambda}{N_a}$ where $N_a = n \frac{a}{f}$ and $\sin \theta = \frac{D}{R} \sim \frac{D}{f}$. D and f are, respectively, the distance between the main maximum with the first minimum of intensity in the Airy pattern and the focal distance of the lens. Rayleigh's resolution criterion expresses that two noncoherent sources of light can be resolved when at least separated by a distance D .

The Rayleigh resolution, D , is proportional to the size of the diffraction pattern/PSF, on the camera, $D \propto \sigma_{\text{PSF}}$, in conventional microscopy. In super-resolution microscopy, an isolated emitter is represented by a blob with a size equal to the localization precision. Therefore the Rayleigh's resolution in SMLM microscopy is related to the localization precision

$$D \propto \frac{\sigma_{\text{PSF}}}{\sqrt{N}} \quad (34)$$

which is better than resolution in conventional microscopy by an order of \sqrt{N} , where N is the number of photons from the emitter.

Image resolution. While localization precision is a key parameter in evaluating the two-points resolution of super-resolution microscopy, it does not provide a comprehensive assessment of resolution for images of complex biological structures, reconstructed from millions of found emitter locations. Another essential metric to evaluate the resolution of SMLM images is the density of localizations. It describes how many localizations were observed within a unit of area of an image. Nyquist-Shannon sampling theorem states that the minimum sampling frequency of a signal that it will not distort its underlying information, should be double the frequency of its highest frequency components [270, 271]. In the field of SMLM, the Nyquist-Shannon theorem can be interpreted as obtaining a desired resolution the nearest neighbor distance between localized emitters should be

at least half of the desired resolution [272]. However, it has been observed that the real number of localizations required to accomplish such a resolution is higher than the minimum specified by Nyquist-Shannon criterion due to random nature of sampling with low precisions in SMLM procedures [138, 273, 274, 275].

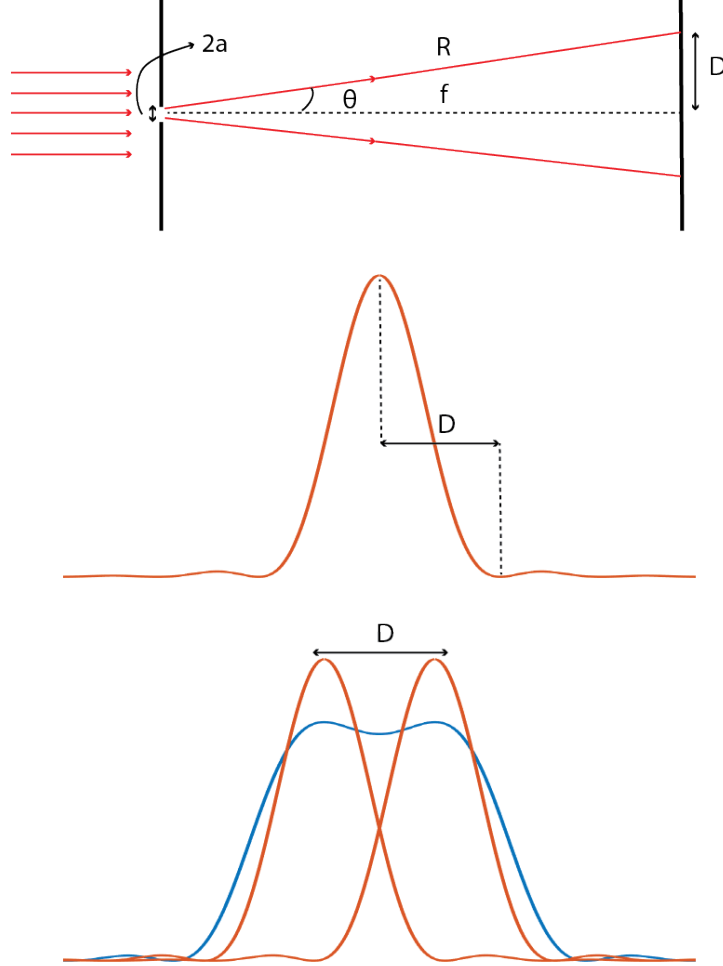


Figure 12: Airy pattern and Rayleigh's resolution. The top diagram shows the diffraction of light from a circular aperture/lens with the radius of a . D and f are the space between the first minimum and the principal maximum of the intensity, where the maximum always overlaps with the central axis, and the distance of the observation point from the aperture or the focal distance of the lens. The middle plot represents the diffraction pattern from a circular aperture (Airy pattern). In the bottom plot, the red plots are two Airy patterns where their maxima are separated by D . The blue curve is the intensity pattern of light from two noncoherent point sources of light with separation D .

Low localization density can be due to several problems in super-resolution microscopy, such as insufficient labeling, broken labels or filtering localizations in the thresholding stage because of inadequate fitting quality, etc. For some cases, such as experiments where there are multiple identical structures, this problem can be overcome by aligning and fusing the images of similar structures [276, 277, 278]. Several alignment and fusion algorithms have been reported in the literature, including a

few that require a template or structural assumptions in the alignment step [279, 280, 281, 282, 283] as well as template-free particle fusion algorithms [119, 284, 285].

ITF formalism gives image resolution bounds by providing a minimum on precision for image frequency estimations

$$\Delta_{I(k)} \leq F^{-1}(k) \quad (35)$$

where Δ_I , k and F stand for uncertainties, spatial frequency, and Fourier transform of ITF, respectively. This idea of resolution equally applies to both conventional and stochastic microscopy and unifies the concept of resolution [263]. Although ITF provides a generalized concept of resolution, it requires models of the target structure which makes it limited in practice [83].

The FRC algorithm was adopted from electron microscopy [286] and adapted for resolution measurement in stochastic fluorescent microscopy [67, 264]. This approach uses two images from two identical structures or reconstruction of two images of the same structure by splitting the list of localization into two halves. It then calculates the cross-correlations of the two images at different image frequencies, where components with frequency k are given by a ring with radius $|k|$ in the Fourier domain. The larger frequencies represent finer details in the image and it is where the two images start to deviate and hence their cross-correlation rapidly decline. The frequency at which the cross-correlation falls below a given threshold can be utilized to calculate the image resolution. The method takes into account both localization precision and labeling density. It however has to be used with care for structures with more complicated geometries and discontinuous boundaries [83, 138].

SQUIRREL compares diffraction-limited images and super-resolution equivalents of the same acquisition to identify artifacts and disappearance of details in the reconstructed images [265]. SQUIRREL does not require any prior knowledge of the sample and is able to identify common super-resolution artifacts. However, out-of-focus light affects the performance of SQUIRREL and, moreover, it cannot recognize small-scale artifacts. This approach returns a quantitative map of image anomalies and artifacts rather than reporting a resolution measure. The returned map can be used to optimize the experiment and image analysis, and improve the reconstructed image qualities. SQUIRREL was used to show that high image resolution does not necessarily correlate with artifact-free reconstructions [265].

As it was discussed, resolution depends on multiple experimental and image analysis factors. A proper choice of labels, buffers, fixation protocols, and other experimental factors can lead to better localization uncertainties and less artifacts and therefore better image resolution. The choice of localization algorithm also helps in optimizing both localization precision and localization density, and reducing the image artifacts. The image rendering and visualization techniques also influence the image resolution. It has been demonstrated that different visualization procedures yield different resolutions for images reconstructed from the same list of emitter coordinates [287].

7 Applications of Single Molecule Localization Microscopy

Super-resolution microscopy has had significant contributions in shedding light on numerous biological problems since its advent in the 1990s. The major improvement in resolution of microscopy images helped with unraveling details of many biological structures and processes, such as nuclear pore complexes [262, 285, 288], actin structures [61], cell membrane [289, 290], cell division [291], neurons [292, 293], plant cell biology [294, 295], live cell imaging [272, 296, 297], and many more [21, 24, 25, 26, 298].

In addition to visualization of intricate structures, a tremendous quantitative insight into cell biology can be gained through post-processing of resulting localizations from SMLM techniques. These post-processing algorithms include single particle tracking (SPT) [139, 299, 300], cluster analysis [301, 302], molecule counting [303, 304, 305, 306, 307, 308, 309, 310, 311], particle fusion [119, 276, 277, 285, 283, 278, 279, 281, 282, 280, 284], etc. In the following, SPT and clustering

approaches are described in more details.

7.1 Single Particle Tracking

While super-resolution microscopy only deals with spatial resolution, SPT is concerned with spatial as well as temporal resolution of dynamic samples. The microscopic world of biology is a live and vibrant place where many phenomena and interactive processes take place over time. An effective examination of these types of processes and interactions requires a comprehensive knowledge of dynamics and the motion of particles in those environments.

SPT was first demonstrated by optical visualization of gold nano-particles on cell membranes [312, 313], which paved the path for use of SPT in the study of cell membranes [314, 315]. Since the first demonstration of SPT in cell biology, there have been a burst of cell membrane research using SPT that have revolutionized our understanding of the cell membrane [316, 317, 318, 319]. An example of such research is the use of SPT in shedding light on the confined motion of receptors on cell membrane imposed by the actin cytoskeleton [317, 320]. SPT has also been employed to explore intracellular environments, including influenza and HIV virus internalization [321, 322, 323], and cargo transport along microtubules [324].

SPT is comprised of three main steps: detection and localization, linking, and post processing. The detection and localization of probes in SPT is similar to emitter localization in SMLM techniques and most of the fitting approaches discussed before can be employed for this stage of SPT. As described previously, more photons from the probes lead to more precise localizations. On the other hand, to increase the temporal resolution, a higher frame rate is desired during data acquisition. Higher frame rate means shorter exposure time and less photons and hence worse localization uncertainties. Therefore, bright probes are necessary for both high temporal resolution and precise localizations. Other important elements are photo-stability and size of the probes [325]. Probes with long-lasting photo-stability and small size are desired for getting longer trajectories and less perturbation in mobility and dynamics of the particles under study. There are three major categories of probes used in SPT: nano-particles, organic dyes and quantum dots (QDs) [300]. Nano-particles reflect light rather than emitting fluorescent light and have high photo-stability but their size is rather large compared to typical proteins. Organic dyes are very small compared to typical proteins but they are really dim and bleach rapidly [300]. The size of QDs are in between organic dyes and nano-particles. They are relatively bright and photo-stable, which make them a perfect probe for most SPT experiments. QDs are manufactured with different emission wavelengths and are also suitable for multi-color SPT [326, 327, 328].

After detection and localization, the detected probes are linked together across consecutive frames to construct particle trajectories. Linking is a non-trivial problem, even in the presence of only a few probes, Fig. 1.13. This is yet the case where there is an equal number of probes in every given frame and in the absence of blinking, bleaching, probes entering or leaving the field of view, and missed probes in the detection stage. The reported linking algorithms in SPT can be categorized in two classes: deterministic approaches and probabilistic approaches. Deterministic approaches give the same results every time, but probabilistic procedures uses a random number generator at some point in the analysis and depending in the sequence of random number produced, they give slightly different answers each time.

Given a set of localizations, deterministic approaches construct trajectories by linking the localizations so that the resulting trajectories minimize a certain cost function [329]. The reported cost functions include distance [330, 331, 332, 333, 334], as well as concepts such as minimal energy path [335, 336, 337] or inertia [338] borrowed from classical mechanics, and ad hoc cost functions that can be a function of parameters like probe location, intensity, motion direction, etc. [339, 340, 341, 342]. A range of different optimization algorithms have been employed to minimize the aforementioned cost functions, including the Hungarian algorithm [333, 340, 343] and the greedy algorithm [338, 339, 342].

Probabilistic SPT approaches make use of a Bayesian algorithm to obtain the most probable

tracks in the linking problem. SPT algorithms that implement a Bayesian procedure have demonstrated better performances compared to deterministic approaches due to inclusion of prior information [344]. Assume a system with state x_t at time t , which leads to an observation z_t , where $x_t \neq z_t$, due to noise. The state at time t is a function of the state at time $t - 1$ and noise as follows

$$x_t = f_t(x_{t-1}, u_t) \quad (36)$$

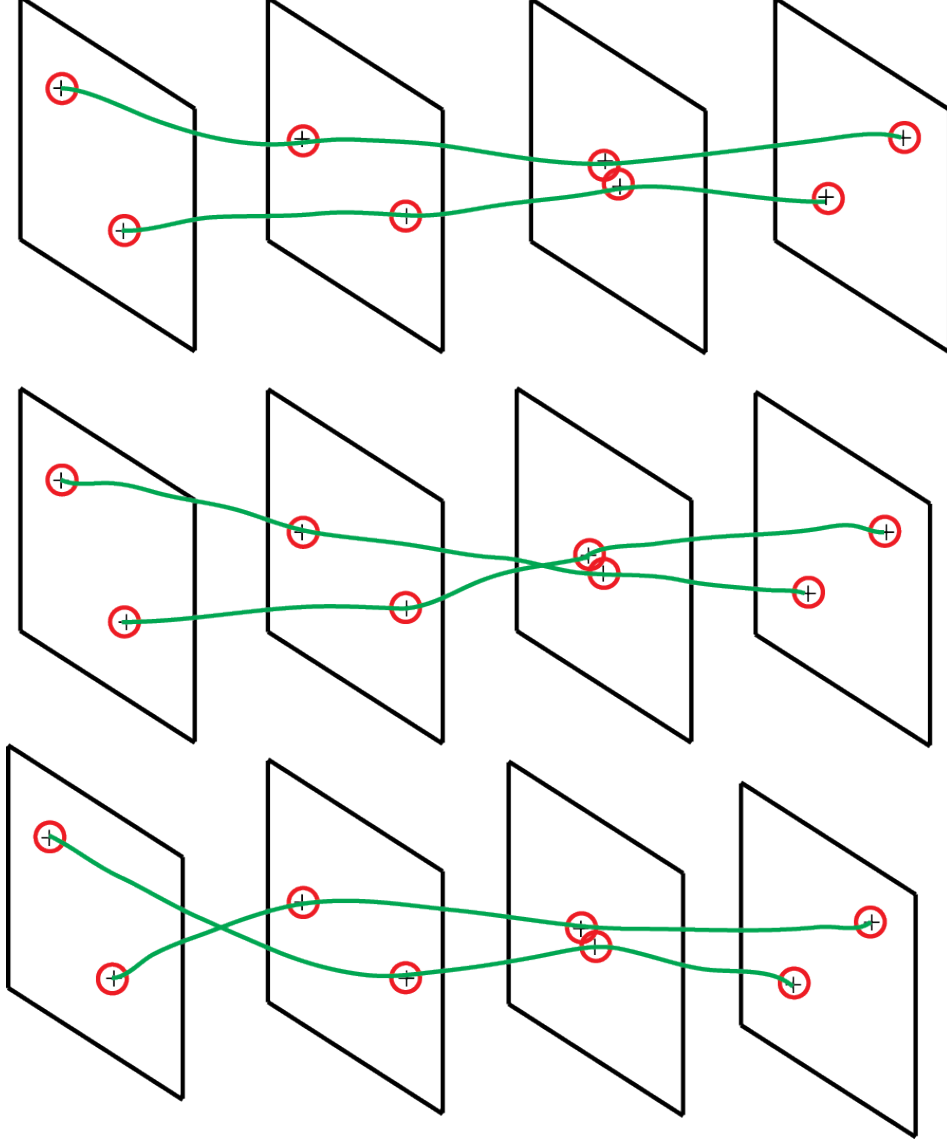


Figure 13: Three possible links in the presence of two probes. The black boxes, red circles and green curves, respectively, represent frames, detected probes and possible trajectories.

where f_t and u_t are, respectively, a function that characterizes the system and a variance. The observation also deviates from the state of the system due to noise and is given by

$$z_t = g(x_t, v_t) \quad (37)$$

where v_t is the noise variance. The objective is finding the state of the system at time t , x_t , given the list of observations up to this time, $z_{1:t}$. Using Bayes theorem, it can be shown that [345]

$$P(x_t|z_{1:t}) = \frac{P(z_t|x_t)P(x_t|z_{1:t-1})}{P(z_t|z_{1:t-1})} \quad (38)$$

where $P(z_t|x_t)$ is the likelihood, and the prior is given by

$$P(x_t|z_{1:t-1}) = \int P(x_t|x_{t-1})P(x_{t-1}|z_{1:t-1})dx_{t-1} \quad (39)$$

Equations (38) and (39) provide a recursive formula to obtain the current state of the system from the list of observations up to this time along with the previous state of the system. However, the form of P , the posterior, as a function is still unknown. One approach takes P to be a Gaussian function, which is called the Kalman filter [346, 347, 348, 349, 350, 351, 352]. The Kalman filter describes a linear system where the system is characterized by a linear function f_t and Gaussian noise g . For example, diffusion is a linear process and can be characterized by a Kalman filter. Another common filter is the particle filter [112, 345, 353, 354, 355, 356, 357]. This filter is suitable for non-linear processes with non-Gaussian noise. For particle filters, a Monte Carlo procedure is often utilized to take some samples from the system, which are then used to compute the posterior probabilities. Other filters such as Gaussian Mixture Probability Hypothesis Density (GM-PHD) filter, Bayesian random set filter, etc. have been employed for probe linking purpose [358, 359, 360].

Biological samples usually exhibit a combination of different motion types such as Brownian motion, directed motion, confined motion, etc. Interacting Multiple Models (IMM) allows modeling the kinetics of the probes as a combination of different motions employing different filters [361, 362, 363, 364]. IMM filter is usually implemented employing a Bayesian approach where a weight is associated to each filter and the algorithm switches between models by updating the weights.

The recursive method described above provides an approach that links new probes to the trajectories on a frame by frame basis. The Multiple Hypothesis Tracking (MHT) algorithm evaluates the possibility of different tracks taking into account localized probes over either the entire data set or over a time window [365, 366, 367, 368, 369, 370]. While this procedure accomplishes the most optimal solution to the linking problem, it is computationally extremely expensive and impractical. Greedy algorithms accomplish approximations to the MHT optimal solution with tremendously less computational cost [367, 371].

Jaqaman et. al. [367] proposed a relatively computationally inexpensive approximate to MHT using a greedy algorithm. This procedure uses a cost matrix approach to incorporate appearance (birth) and disappearance (death) of the probes to the model. They introduced ghost probes to consider three different linking scenarios, when there is not equal number of detected probes in consecutive frames. The real probes are connected together where the cost is calculated from the localization precisions and kinetics of the probes.

$$P(x_2, t_2|x_1, t_1) = \mathcal{N}(x_1, x_2, \sigma^2) \quad (40)$$

where x stand for the locations of the probes and σ^2 is the variance due to diffusion and localization precisions, σ_x , defined as

$$\sigma^2 = 2D\Delta t + \sum_{i=1}^2 \sigma_{x_i}^2 \quad (41)$$

where D and Δt are the diffusion constant and exposure time, in turn. A real probe can be connected to a ghost probe when a probe goes either off or on and the penalty is computed from the blinking statistics of the probes. The blinking process is assumed to be memoryless with k_{on} and k_{off} being the rate of probes, respectively, going from off to on or on to off.

$$\begin{aligned} P(\text{off} \rightarrow \text{on}|k_{\text{on}}, \Delta t) &= k_{\text{on}}\Delta t \\ P(\text{on} \rightarrow \text{off}|k_{\text{off}}, \Delta t) &= k_{\text{off}}\Delta t \end{aligned} \quad (42)$$

Additionally, the probabilities for a probe staying on or off for N frames is given as

$$\begin{aligned} P(\text{Stay off}|N\Delta t) &= P(\text{Not going on}|N\Delta t) = (1 - k_{\text{on}}\Delta t)^N \\ P(\text{Stay on}|N\Delta t) &= P(\text{Not going off}|N\Delta t) = (1 - k_{\text{off}}\Delta t)^N \end{aligned} \quad (43)$$

Eventually, ghost probes can also be linked together where the costs are given by the transpose cost matrix of the real probes. The Hungarian procedure is then utilized to find the connections with the least cost.

The first step only connects probes across consecutive frames and produces short trajectories. In a second stage, the resulting short trajectories are connected together to obtain probe trajectories across the entire given sequence of the frames, which is called gap-closing. The gap-closing cost function is also a function of blinking statistics and localization precisions, except this time the probes are allowed to be linked together in non-consecutive frames.

Recently, deep learning approaches have been employed to implement SPT [372, 373, 374, 375].

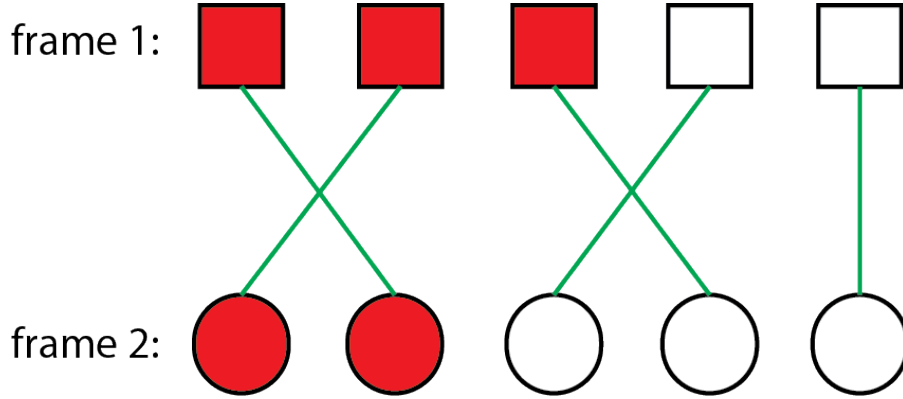


Figure 14: An instance of probe linking in two consecutive frames in the presence of ghost probes. The blank boxes and circles stand for ghost probes.

Once the trajectories are constructed, they can be employed to extract information about the underlying dynamics of the biological sample under study [300, 376, 377, 299]. Mean Square Displacement (MSD) is the most common post-analysis of trajectories employed for this purpose. It is defined as the average of spatial distances between all pairs of localizations that are temporally separated by certain times, called the time lag. Given a trajectory comprised of N localizations, the MSD can be calculated as follows:

$$\text{MSD}(t_{\text{lag}} = m\Delta t) = \frac{1}{N - m} \sum_{i=1}^{N-m} [x(t_i + m\Delta t) - x(t_i)]^2 \quad (44)$$

where $x(t_i)$ is the location of the probe at time t_i and $x(t_i + m\Delta t)$ is the probe location at $t_{\text{lag}} = m\Delta t$ later. The MSD is a function of the time lag, t_{lag} , and this function is extensively investigated and well characterized for different motion types. By comparing the resulting MSD function from the obtained trajectories and the theoretical MSD forms, one is able to determine the underlying dynamic of the system under study. For diffusion or Brownian motion, the MSD is proportional to the time lag

$$\text{MSD}(t_{\text{lag}}) = 2dDt_{\text{lag}} \quad (45)$$

where d is spatial dimensionality of the motion.

7.2 Clustering

Clustering is the task of classifying a given set of data points into subsets in such a way that data points in a subset are more similar to each other than those in other subsets, based on a given property [378]. Clustering has been employed in many scientific spheres, including localization microscopy, recognizing patterns, detecting communities, etc. There are different levels of clustering in a list of localizations resulting from a SMLM experiment [301, 302]. In SMLM techniques, there are multiple observed localizations from an emitter over the course of data acquisition that form a cluster, which I will call an intra-cluster. A higher level of clustering is clustering between emitters/molecules that signifies interactions between the molecules in a cluster at the biological level. I call this type of clusters inter-clusters. There is also co-clustering that takes place among different types of molecules imaged via multi-color super-resolution microscopy [379, 380, 381, 382].

Multiple algorithms have been developed or adapted to identify all sorts of clusters within SMLM localizations, including algorithms that inspect the extent of clustering within a data set [383, 384, 385, 386, 387, 388], density based clustering algorithms [389, 390, 391, 392, 393] and Bayesian clustering approaches [301, 168, 394, 395, 396]. These approaches have specifically been popular in post-processing of SMLM results of cell membrane samples, where it is conjectured that molecular clusters indicate underlying membrane structure or cell signaling [397, 398, 399, 400, 401, 402].

Some methods examine the degree of clustering or examine some properties of clusters, such as the shape or average density of clusters, within a data set rather than inspecting individual clusters, Fig. 15. A few of these approaches are nearest neighbor distances (NND) [383], Hopkins statistics [384], Ripley’s function and pair correlation [385, 386, 387, 388]. The NND distribution for uniform randomly distributed data is given by

$$f(r) = 2\pi\rho e^{-\pi\rho r^2} \quad (46)$$

where ρ is the density of the data points. The deviation of the NND distribution for a given data set from (46) indicates either clustering or a more regularly spaced data set, Fig. 15. Hopkins statistics (H) tests for spatial randomness of a point pattern by comparing nearest neighbor distances between a given data set and a uniform randomly distributed data set. Values of H near 0.5 imply randomly distributed data, while values near 1 indicate highly clustered data, and values near zero signify more regularly spaced data, Fig 15.

Ripley’s K-function, $K(r)$, is another statistical test that explores the extent of clustering within a given data set. Defining $k_i(r)$ as the number of points within distance r from the i th point, $K(r)$ is given by the average of the k_i for all data points divided by the mean density over all data points. The clustering behavior of the given data set is then given by

$$\begin{aligned} K(r) &< \pi r^2 && \text{regularly spaced} \\ K(r) &= \pi r^2 && \text{random} \\ K(r) &> \pi r^2 && \text{clustering} \end{aligned} \quad (47)$$

Pair correlation analysis is the same idea as Ripley’s K-function extended to images rather than a set of points.

A range of clustering algorithms have been developed that take advantage of density fluctuations within a data set to identify clusters. DBSCAN and Voronoi tessellation algorithms are among the most popular density based approaches in SMLM data post-analysis. DBSCAN has two inputs where one of them is the maximum distance between the points within a cluster and the other one is the minimum number of data points within a cluster. The algorithm starts from a random point and adds points to the set until there is no more points within the given maximum distance. If the number of points inside the set is more than the given threshold it will be returned as a cluster, otherwise it is considered as outlier. Voronoi tessellation draws boundary line segments between every pair of data points in the given data set so that the distance from every point of the line between a pair is

equal from both data points in the pair. The final geometry is comprised of polygons where each polygon contains only one data point, called a Voronoi diagram. This algorithm identifies clusters by inspecting the number of vertices and the area of the polygons at different neighboring levels.

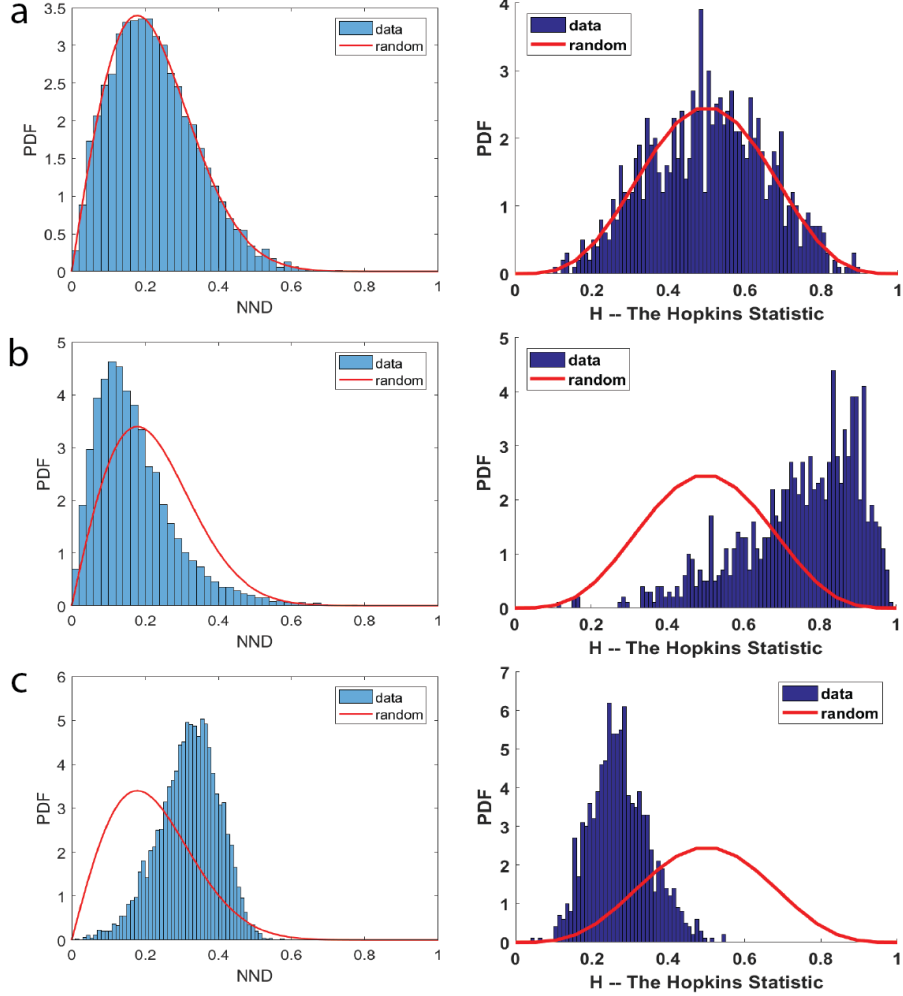


Figure 15: Nearest neighbor distribution and Hopkins statistics. First column and second column represent nearest neighbor distribution and Hopkins statistics, respectively. (a) randomly distributed, (b) clustered, (c) more regularly spaced data.

Bayesian clustering algorithms are superior to density based approaches because they take advantage of prior knowledge. Prior information can be included in the Bayesian algorithms via prior distributions. Rubin-Delanchy, et al. developed an algorithm to identify inter-clusters within SMLM localizations, called Bayesian cluster identification [301, 394]. This algorithm classifies the localizations into either background or signal by means of a binomial distribution. A large number of clustering proposals are then put forward using a procedure similar to Ripley's K-function. Scores for different clustering proposals are calculated using the posterior where the Dirichlet distribution is the prior on different arrangements. At the end, the configuration with the highest score is returned as the solution.

Post, et al. proposed a Bayesian clustering algorithm to identify intra-clusters (emitters) on

the surface of spherical nano-particles [395]. Their algorithm takes full advantage of localization precisions but it does not return the number of emitters on the surface of every individual nano-particle. Otherwise, they find the mean number of emitters on the surface of nano-particles by fitting a log-normal distribution to the number of localizations per nano-particle. They next employ this piece of information to localize those emitters and then inspect their inter-clustering behavior using the NND distribution.

Fazel et al. developed a Bayesian Grouping of Localizations (BaGoL) that takes advantage of localization precisions as well as mean number of blinking/binding events per emitter to identify and localize emitters with sub-nanometer precision in dense regions [396]. This algorithm uses nearest neighbor distribution and an intensity filter to recognize and remove the outliers.

Lin, et al. developed a non-Bayesian clustering algorithm based on hierarchical clustering paradigm, which allows exploitation of localization precisions [400]. This algorithm proposed different clustering configurations for a given set of localizations similar to the hierarchical procedure and then performs a hypothesis test to pick one of the proposed clustering models.

Acknowledgement

I thank Michael J. Wester and Keith A. Lidke for useful comments.

References

- [1] Seyyed Hossein Nasr and Giorgio De Santillana. *Science and civilization in Islam*, volume 16. Harvard University Press Cambridge, MA, 1968.
- [2] David Bardell. The invention of the microscope. *Bios*, 75(2):78–84, 2004.
- [3] Howard Gest. The discovery of microorganisms by robert hooke and antoni van leeuwenhoek, fellows of the royal society. *Notes and records of the Royal Society of London*, 58(2):187–201, 2004.
- [4] Max Born and Emil Wolf. *Principles of optics: electromagnetic theory of propagation, interference and diffraction of light*. Elsevier, 2013.
- [5] Malte Renz. Fluorescence microscopy – a historical and technical perspective. *Cytometry Part A*, 83(9):767–779, 2013.
- [6] Minsky Marvin. Microscopy apparatus, December 19 1961. US Patent 3,013,467.
- [7] Daniel Axelrod. Cell-substrate contacts illuminated by total internal reflection fluorescence. *The Journal of cell biology*, 89(1):141–145, 1981.
- [8] Winfried Denk, James H Strickler, and Watt W Webb. Two-photon laser scanning fluorescence microscopy. *Science*, 248(4951):73–76, 1990.
- [9] Stefan Hell and Ernst HK Stelzer. Fundamental improvement of resolution with a 4pi-confocal fluorescence microscope using two-photon excitation. *Optics Communications*, 93(5-6):277–282, 1992.
- [10] Brent Bailey, Daniel L Farkas, D Lansing Taylor, and Frederick Lanni. Enhancement of axial resolution in fluorescence microscopy by standing-wave excitation. *Nature*, 366(6450):44, 1993.
- [11] Arne H Voie, DH Burns, and FA Spelman. Orthogonal-plane fluorescence optical sectioning: three-dimensional imaging of macroscopic biological specimens. *Journal of microscopy*, 170(3):229–236, 1993.
- [12] Stefan W Hell and Jan Wichmann. Breaking the diffraction resolution limit by stimulated emission: stimulated-emission-depletion fluorescence microscopy. *Optics letters*, 19(11):780–782, 1994.
- [13] Daniel Axelrod. Total internal reflection fluorescence microscopy in cell biology. *Traffic*, 2(11):764–774, 2001.
- [14] Mats GL Gustafsson. Surpassing the lateral resolution limit by a factor of two using structured illumination microscopy. *Journal of microscopy*, 198(2):82–87, 2000.
- [15] James Pawley. *Handbook of biological confocal microscopy*. Springer Science & Business Media, 2010.
- [16] Stefan Hell and Ernst HK Stelzer. Properties of a 4pi confocal fluorescence microscope. *JOSA A*, 9(12):2159–2166, 1992.
- [17] Diane S Lidke and Keith A Lidke. Advances in high-resolution imaging–techniques for three-dimensional imaging of cellular structures. *J Cell Sci*, 125(11):2571–2580, 2012.
- [18] Warren R Zipfel, Rebecca M Williams, and Watt W Webb. Nonlinear magic: multiphoton microscopy in the biosciences. *Nature biotechnology*, 21(11):1369, 2003.

- [19] Omar E Olarte, Jordi Andilla, Emilio J Gualda, and Pablo Loza-Alvarez. Light-sheet microscopy: a tutorial. *Advances in Optics and Photonics*, 10(1):111–179, 2018.
- [20] Bo Huang, Mark Bates, and Xiaowei Zhuang. Super-resolution fluorescence microscopy. *Annual review of biochemistry*, 78:993–1016, 2009.
- [21] Eugenio F Fornasiero and Felipe Opazo. Super-resolution imaging for cell biologists: Concepts, applications, current challenges and developments. *Bioessays*, 37(4):436–451, 2015.
- [22] Christian Eggeling, Katrin I Willig, Steffen J Sahl, and Stefan W Hell. Lens-based fluorescence nanoscopy. *Quarterly reviews of biophysics*, 48(2):178–243, 2015.
- [23] Bartosz Turkowyd, David Virant, and Ulrike Endesfelder. From single molecules to life: microscopy at the nanoscale. *Analytical and bioanalytical chemistry*, 408(25):6885–6911, 2016.
- [24] Steffen J Sahl, Stefan W Hell, and Stefan Jakobs. Fluorescence nanoscopy in cell biology. *Nature reviews Molecular cell biology*, 18(11):685, 2017.
- [25] Lothar Schermelleh, Alexia Ferrand, Thomas Huser, Christian Eggeling, Markus Sauer, Oliver Biehlmaier, and Gregor PC Drummen. Super-resolution microscopy demystified. *Nature cell biology*, 21(1):72, 2019.
- [26] Jeroen Vangindertael, R Camacho, W Sempels, H Mizuno, P Dedeker, and KPF Janssen. An introduction to optical super-resolution microscopy for the adventurous biologist. *Methods and applications in fluorescence*, 6(2):022003, 2018.
- [27] Thomas A Klar and Stefan W Hell. Subdiffraction resolution in far-field fluorescence microscopy. *Optics letters*, 24(14):954–956, 1999.
- [28] Stefan W Hell and Matthias Kroug. Ground-state-depletion fluorescence microscopy: A concept for breaking the diffraction resolution limit. *Applied Physics B*, 60(5):495–497, 1995.
- [29] Stefan W Hell. Far-field optical nanoscopy. *science*, 316(5828):1153–1158, 2007.
- [30] Mats GL Gustafsson. Nonlinear structured-illumination microscopy: wide-field fluorescence imaging with theoretically unlimited resolution. *Proceedings of the National Academy of Sciences*, 102(37):13081–13086, 2005.
- [31] Michael J Rust, Mark Bates, and Xiaowei Zhuang. Sub-diffraction-limit imaging by stochastic optical reconstruction microscopy (storm). *Nature methods*, 3(10):793, 2006.
- [32] Sebastian Van de Linde, Anna Löschberger, Teresa Klein, Meike Heidebreder, Steve Wolter, Mike Heilemann, and Markus Sauer. Direct stochastic optical reconstruction microscopy with standard fluorescent probes. *Nature protocols*, 6(7):991, 2011.
- [33] Eric Betzig, George H Patterson, Rachid Sougrat, O Wolf Lindwasser, Scott Olenych, Juan S Bonifacino, Michael W Davidson, Jennifer Lippincott-Schwartz, and Harald F Hess. Imaging intracellular fluorescent proteins at nanometer resolution. *Science*, 313(5793):1642–1645, 2006.
- [34] Samuel T Hess, Thanu PK Girirajan, and Michael D Mason. Ultra-high resolution imaging by fluorescence photoactivation localization microscopy. *Biophysical journal*, 91(11):4258–4272, 2006.
- [35] Thomas Dertinger, Ryan Colyer, Gopal Iyer, Shimon Weiss, and Jörg Enderlein. Fast, background-free, 3d super-resolution optical fluctuation imaging (sofi). *Proceedings of the National Academy of Sciences*, 106(52):22287–22292, 2009.

- [36] Joerg Schnitzbauer, Maximilian T Strauss, Thomas Schlichthaerle, Florian Schueder, and Ralf Jungmann. Super-resolution microscopy with dna-paint. *Nature protocols*, 12(6):1198, 2017.
- [37] Sandeep Pallikkuth, Cheyenne Martin, Farzin Farzam, Jeremy S Edwards, Matthew R Lakin, Diane S Lidke, and Keith A Lidke. Sequential super-resolution imaging using dna strand displacement. *PloS one*, 13(8):e0203291, 2018.
- [38] Stefan W Hell. Toward fluorescence nanoscopy. *Nature biotechnology*, 21(11):1347, 2003.
- [39] Stefan W Hell, Marcus Dyba, and Stefan Jakobs. Concepts for nanoscale resolution in fluorescence microscopy. *Current opinion in neurobiology*, 14(5):599–609, 2004.
- [40] Gerald Donnert, Jan Keller, Rebecca Medda, M Alexandra Andrei, Silvio O Rizzoli, Reinhard Lührmann, Reinhard Jahn, Christian Eggeling, and Stefan W Hell. Macromolecular-scale resolution in biological fluorescence microscopy. *Proceedings of the National Academy of Sciences*, 103(31):11440–11445, 2006.
- [41] Volker Westphal and Stefan W Hell. Nanoscale resolution in the focal plane of an optical microscope. *Physical review letters*, 94(14):143903, 2005.
- [42] Eva Wegel, Antonia Göhler, B Christoffer Lagerholm, Alan Wainman, Stephan Uphoff, Rainer Kaufmann, and Ian M Dobbie. Imaging cellular structures in super-resolution with sim, sted and localisation microscopy: A practical comparison. *Scientific reports*, 6:27290, 2016.
- [43] Fabian Göttfert, Christian A Wurm, Veronika Mueller, Sebastian Berning, Volker C Cordes, Alf Honigsmann, and Stefan W Hell. Coaligned dual-channel sted nanoscopy and molecular diffusion analysis at 20 nm resolution. *Biophysical journal*, 105(1):L01–L03, 2013.
- [44] Michael Kasha. Characterization of electronic transitions in complex molecules. *Discussions of the Faraday society*, 9:14–19, 1950.
- [45] Taekjip Ha and Philip Tinnefeld. Photophysics of fluorescent probes for single-molecule biophysics and super-resolution imaging. *Annual review of physical chemistry*, 63, 2012.
- [46] Stefan Bretschneider, Christian Eggeling, and Stefan W Hell. Breaking the diffraction barrier in fluorescence microscopy by optical shelving. *Physical review letters*, 98(21):218103, 2007.
- [47] Kyu Young Han, Seong Keun Kim, Christian Eggeling, and Stefan W Hell. Metastable dark states enable ground state depletion microscopy of nitrogen vacancy centers in diamond with diffraction-unlimited resolution. *Nano letters*, 10(8):3199–3203, 2010.
- [48] Keith A Lidke, Bernd Rieger, Thomas M Jovin, and Rainer Heintzmann. Superresolution by localization of quantum dots using blinking statistics. *Optics express*, 13(18):7052–7062, 2005.
- [49] B Christoffer Lagerholm, Laurel Averett, Gabriel E Weinreb, Ken Jacobson, and Nancy L Thompson. Analysis method for measuring submicroscopic distances with blinking quantum dots. *Biophysical Journal*, 91(8):3050–3060, 2006.
- [50] Alexander Egner, Claudia Geisler, Claas Von Middendorff, Hannes Bock, Dirk Wenzel, Rebecca Medda, Martin Andresen, Andre C Stiel, Stefan Jakobs, Christian Eggeling, et al. Fluorescence nanoscopy in whole cells by asynchronous localization of photoswitching emitters. *Biophysical journal*, 93(9):3285–3290, 2007.
- [51] L Stirling Churchman, Zeynep Ökten, Ronald S Rock, John F Dawson, and James A Spudich. Single molecule high-resolution colocalization of cy3 and cy5 attached to macromolecules measures intramolecular distances through time. *Proceedings of the National Academy of Sciences*, 102(5):1419–1423, 2005.

- [52] Mark Bates, Bo Huang, Graham T Dempsey, and Xiaowei Zhuang. Multicolor super-resolution imaging with photo-switchable fluorescent probes. *Science*, 317(5845):1749–1753, 2007.
- [53] Shalini T Low-Nam, Keith A Lidke, Patrick J Cutler, Rob C Roovers, Paul MP van Bergen en Henegouwen, Bridget S Wilson, and Diane S Lidke. Erbb1 dimerization is promoted by domain co-confinement and stabilized by ligand binding. *Nature structural & molecular biology*, 18(11):1244, 2011.
- [54] Matthew P Gordon, Taekjip Ha, and Paul R Selvin. Single-molecule high-resolution imaging with photobleaching. *Proceedings of the National Academy of Sciences*, 101(17):6462–6465, 2004.
- [55] Xiaohui Qu, David Wu, Laurens Mets, and Norbert F Scherer. Nanometer-localized multiple single-molecule fluorescence microscopy. *Proceedings of the National Academy of Sciences*, 101(31):11298–11303, 2004.
- [56] Alexey Sharonov and Robin M Hochstrasser. Wide-field subdiffraction imaging by accumulated binding of diffusing probes. *Proceedings of the National Academy of Sciences*, 103(50):18911–18916, 2006.
- [57] Russell E Thompson, Daniel R Larson, and Watt W Webb. Precise nanometer localization analysis for individual fluorescent probes. *Biophysical journal*, 82(5):2775–2783, 2002.
- [58] Raimund J Ober, Sripad Ram, and E Sally Ward. Localization accuracy in single-molecule microscopy. *Biophysical journal*, 86(2):1185–1200, 2004.
- [59] Steve Wolter, Ulrike Endesfelder, Sebastian van de Linde, Mike Heilemann, and Markus Sauer. Measuring localization performance of super-resolution algorithms on very active samples. *Optics express*, 19(8):7020–7033, 2011.
- [60] Alex Small. Multifluorophore localization as a percolation problem: limits to density and precision. *JOSA A*, 33(7):B21–B30, 2016.
- [61] Julia Riedl, Alvaro H Crevenna, Kai Kessenbrock, Jerry Haochen Yu, Dorothee Neukirchen, Michal Bista, Frank Bradke, Dieter Jenne, Tad A Holak, Zena Werb, et al. Lifeact: a versatile marker to visualize f-actin. *Nature methods*, 5(7):605, 2008.
- [62] Andrew G York, Alireza Ghitani, Alipasha Vaziri, Michael W Davidson, and Hari Shroff. Confined activation and subdiffractive localization enables whole-cell palm with genetically expressed probes. *Nature methods*, 8(4):327, 2011.
- [63] Jeroen Vangindertael, Isabel Beets, Susana Rocha, Peter Dedecker, Liliane Schoofs, Karen Vanhoorelbeke, Johan Hofkens, and Hideaki Mizuno. Super-resolution mapping of glutamate receptors in *c. elegans* by confocal correlated palm. *Scientific reports*, 5:13532, 2015.
- [64] Remi Galland, Gianluca Greci, Ajay Aravind, Virgile Viasnoff, Vincent Studer, and Jean-Baptiste Sibarita. 3d high-and super-resolution imaging using single-objective spin. *Nature methods*, 12(7):641, 2015.
- [65] Marjolein BM Meddens, Sheng Liu, Patrick S Finnegan, Thayne L Edwards, Conrad D James, and Keith A Lidke. Single objective light-sheet microscopy for high-speed whole-cell 3d super-resolution. *Biomedical optics express*, 7(6):2219–2236, 2016.
- [66] Graham T Dempsey, Joshua C Vaughan, Kok Hao Chen, Mark Bates, and Xiaowei Zhuang. Evaluation of fluorophores for optimal performance in localization-based super-resolution imaging. *Nature methods*, 8(12):1027, 2011.

- [67] Robert PJ Nieuwenhuizen, Keith A Lidke, Mark Bates, Daniela Leyton Puig, David Grünwald, Sjoerd Stallinga, and Bernd Rieger. Measuring image resolution in optical nanoscopy. *Nature methods*, 10(6):557, 2013.
- [68] Alexander R Small. Theoretical limits on errors and acquisition rates in localizing switchable fluorophores. *Biophysical journal*, 96(2):L16–L18, 2009.
- [69] Patrick Fox-Roberts, Richard Marsh, Karin Pfisterer, Asier Jayo, Maddy Parsons, and Susan Cox. Local dimensionality determines imaging speed in localization microscopy. *Nature communications*, 8:13558, 2017.
- [70] Alex Small and Shane Stahlheber. Fluorophore localization algorithms for super-resolution microscopy. *Nature methods*, 11(3):267, 2014.
- [71] Daniel Sage, Hagai Kirshner, Thomas Pengo, Nico Stuurman, Junhong Min, Suliana Manley, and Michael Unser. Quantitative evaluation of software packages for single-molecule localization microscopy. *Nature methods*, 12(8):717, 2015.
- [72] Daniel Sage, Thanh-An Pham, Hazen Babcock, Tomas Lukes, Thomas Pengo, Jerry Chao, Ramraj Velmurugan, Alex Herbert, Anurag Agrawal, Silvia Colabrese, et al. Super-resolution fight club: assessment of 2d and 3d single-molecule localization microscopy software. *Nature methods*, 16(5):387, 2019.
- [73] Bo Huang, Wenqin Wang, Mark Bates, and Xiaowei Zhuang. Three-dimensional super-resolution imaging by stochastic optical reconstruction microscopy. *Science*, 319(5864):810–813, 2008.
- [74] Sri Rama Prasanna Pavani, Michael A Thompson, Julie S Biteen, Samuel J Lord, Na Liu, Robert J Twieg, Rafael Piestun, and WE Moerner. Three-dimensional, single-molecule fluorescence imaging beyond the diffraction limit by using a double-helix point spread function. *Proceedings of the National Academy of Sciences*, 106(9):2995–2999, 2009.
- [75] David Baddeley, Mark B Cannell, and Christian Soeller. Three-dimensional sub-100 nm super-resolution imaging of biological samples using a phase ramp in the objective pupil. *Nano Research*, 4(6):589–598, 2011.
- [76] Yoav Shechtman, Steffen J Sahl, Adam S Backer, and WE Moerner. Optimal point spread function design for 3d imaging. *Physical review letters*, 113(13):133902, 2014.
- [77] Sudhakar Prasad. Rotating point spread function via pupil-phase engineering. *Optics letters*, 38(4):585–587, 2013.
- [78] Stefan Geissbuehler, Claudio Dellagiacoma, and Theo Lasser. Comparison between sofi and storm. *Biomedical optics express*, 2(3):408–420, 2011.
- [79] Idir Yahiatene, Simon Hennig, Marcel Muller, and Thomas Huser. Entropy-based super-resolution imaging (esi): From disorder to fine detail. *Acs Photonics*, 2(8):1049–1056, 2015.
- [80] Nils Gustafsson, Siân Culley, George Ashdown, Dylan M Owen, Pedro Matos Pereira, and Ricardo Henriques. Fast live-cell conventional fluorophore nanoscopy with imagej through super-resolution radial fluctuations. *Nature communications*, 7:12471, 2016.
- [81] Siân Culley, Kalina L Tosheva, Pedro Matos Pereira, and Ricardo Henriques. Srrf: Universal live-cell super-resolution microscopy. *The international journal of biochemistry & cell biology*, 101:74–79, 2018.

- [82] Leonhard Möckl, Anish R Roy, Petar N Petrov, and WE Moerner. Bgnet: Accurate and rapid background estimation in single-molecule localization microscopy with deep neural nets. *arXiv preprint arXiv:1909.08151*, 2019.
- [83] Hendrik Deschout, Francesca Cella Zanacchi, Michael Mlodzianoski, Alberto Diaspro, Joerg Bewersdorf, Samuel T Hess, and Kevin Braeckmans. Precisely and accurately localizing single emitters in fluorescence microscopy. *Nature methods*, 11(3):253, 2014.
- [84] Peter B Stetson. Daophot: A computer program for crowded-field stellar photometry. *Publications of the Astronomical Society of the Pacific*, 99(613):191, 1987.
- [85] Mohamadreza Fazel, Michael J. Wester, Hanieh Mazloom-Farsibaf, Marjolein B. M. Meddens, Alexandra S. Eklund, Thomas Schlichthaerle, Florian Schueder, Ralf Jungmann, and Keith A. Lidke. Bayesian multiple emitter fitting using reversible jump markov chain monte carlo. *Scientific Reports*, 9:13791, 2019.
- [86] Christian Franke, Markus Sauer, and Sebastian van de Linde. Photometry unlocks 3d information from 2d localization microscopy data. *Nature methods*, 14(1):41, 2017.
- [87] Johann Engelhardt, Jan Keller, Patrick Hoyer, Matthias Reuss, Thorsten Staudt, and Stefan W Hell. Molecular orientation affects localization accuracy in superresolution far-field fluorescence microscopy. *Nano letters*, 11(1):209–213, 2010.
- [88] Sjoerd Stallinga and Bernd Rieger. Accuracy of the gaussian point spread function model in 2d localization microscopy. *Optics express*, 18(24):24461–24476, 2010.
- [89] Yau Wong, Zhiping Lin, and Raimund J Ober. Limit of the accuracy of parameter estimation for moving single molecules imaged by fluorescence microscopy. *IEEE Transactions on Signal Processing*, 59(3):895–911, 2010.
- [90] Hendrik Deschout, Kristiaan Neyts, and Kevin Braeckmans. The influence of movement on the localization precision of sub-resolution particles in fluorescence microscopy. *Journal of biophotonics*, 5(1):97–109, 2012.
- [91] Anish V Abraham, Sripad Ram, Jerry Chao, ES Ward, and Raimund J Ober. Quantitative study of single molecule location estimation techniques. *Optics express*, 17(26):23352–23373, 2009.
- [92] Saumya Saurabh, Suvrajit Maji, and Marcel P Bruchez. Evaluation of scmos cameras for detection and localization of single cy5 molecules. *Optics express*, 20(7):7338–7349, 2012.
- [93] Tingwei Quan, Shaoqun Zeng, and Zhenli Huang. Localization capability and limitation of electron-multiplying charge-coupled, scientific complementary metal-oxide semiconductor, and charge-coupled devices for superresolution imaging. *Journal of biomedical optics*, 15(6):066005, 2010.
- [94] Fang Huang, Tobias MP Hartwich, Felix E Rivera-Molina, Yu Lin, Whitney C Duim, Jane J Long, Pradeep D Uchil, Jordan R Myers, Michelle A Baird, Walther Mothes, et al. Video-rate nanoscopy using scmos camera-specific single-molecule localization algorithms. *Nature methods*, 10(7):653, 2013.
- [95] Jerry Chao, Sripad Ram, E Sally Ward, and Raimund J Ober. Ultrahigh accuracy imaging modality for super-localization microscopy. *nature methods*, 10(4):335, 2013.
- [96] Rainer Heintzmann, Peter K Relich, Robert PJ Nieuwenhuizen, Keith A Lidke, and Bernd Rieger. Calibrating photon counts from a single image. *arXiv preprint arXiv:1611.05654*, 2016.

- [97] Donald L Snyder, Abed M Hammoud, and Richard L White. Image recovery from data acquired with a charge-coupled-device camera. *JOSA A*, 10(5):1014–1023, 1993.
- [98] Carlas S Smith, Nikolai Joseph, Bernd Rieger, and Keith A Lidke. Fast, single-molecule localization that achieves theoretically minimum uncertainty. *Nature methods*, 7(5):373, 2010.
- [99] William Hadley Richardson. Bayesian-based iterative method of image restoration. *JoSA*, 62(1):55–59, 1972.
- [100] SS Reddi. Multiple source location-a digital approach. *IEEE Transactions on Aerospace and Electronic Systems*, (1):95–105, 1979.
- [101] Norman Bobroff. Position measurement with a resolution and noise-limited instrument. *Review of Scientific Instruments*, 57(6):1152–1157, 1986.
- [102] Leon B Lucy. An iterative technique for the rectification of observed distributions. *The astronomical journal*, 79:745, 1974.
- [103] Mohammad Faisal, Aaron D Lanterman, Donald L Snyder, and Richard L White. Implementation of a modified richardson-lucy method for image restoration on a massively parallel computer to compensate for space-variant point spread of a charge-coupled-device camera. *JOSA A*, 12(12):2593–2603, 1995.
- [104] Mark Goulian and Sanford M Simon. Tracking single proteins within cells. *Biophysical journal*, 79(4):2188–2198, 2000.
- [105] D Thomann, DR Rines, PK Sorger, and G Danuser. Automatic fluorescent tag detection in 3d with super-resolution: application to the analysis of chromosome movement. *Journal of microscopy*, 208(1):49–64, 2002.
- [106] Tingwei Quan, Pengcheng Li, Fan Long, Shaoqun Zeng, Qingming Luo, Per Niklas Hedde, Gerd Ulrich Nienhaus, and Zhen-Li Huang. Ultra-fast, high-precision image analysis for localization-based super resolution microscopy. *Optics Express*, 18(11):11867–11876, 2010.
- [107] Steve Wolter, Mark Schüttelpelz, Marko Tscherepanow, Sebastian Van de Linde, Mike Heilemann, and Markus Sauer. Real-time computation of subdiffraction-resolution fluorescence images. *Journal of microscopy*, 237(1):12–22, 2010.
- [108] Sean B Andersson. Localization of a fluorescent source without numerical fitting. *Optics express*, 16(23):18714–18724, 2008.
- [109] Adel Kechkar, Deepak Nair, Mike Heilemann, Daniel Choquet, and Jean-Baptiste Sibarita. Real-time analysis and visualization for single-molecule based super-resolution microscopy. *PLoS One*, 8(4):e62918, 2013.
- [110] I Izeddin, J Boulanger, V Racine, CG Specht, A Kechkar, D Nair, A Triller, D Choquet, M Dahan, and JB Sibarita. Wavelet analysis for single molecule localization microscopy. *Optics express*, 20(3):2081–2095, 2012.
- [111] Hongqiang Ma, Fan Long, Shaoqun Zeng, and Zhen-Li Huang. Fast and precise algorithm based on maximum radial symmetry for single molecule localization. *Optics letters*, 37(13):2481–2483, 2012.
- [112] Ihor Smal, Erik Meijering, Katharina Draegestein, Niels Galjart, Ilya Grigoriev, Anna Akhmanova, ME Van Royen, Adriaan B Houtsmuller, and Wiro Niessen. Multiple object tracking in molecular bioimaging by rao-blackwellized marginal particle filtering. *Medical Image Analysis*, 12(6):764–777, 2008.

- [113] Yiming Li, Yuji Ishitsuka, Per Niklas Hedde, and G Ulrich Nienhaus. Fast and efficient molecule detection in localization-based super-resolution microscopy by parallel adaptive histogram equalization. *ACS nano*, 7(6):5207–5214, 2013.
- [114] Ihor Smal, Marco Loog, Wiro Niessen, and Erik Meijering. Quantitative comparison of spot detection methods in fluorescence microscopy. *IEEE transactions on medical imaging*, 29(2):282–301, 2009.
- [115] Pekka Ruusuvuori, Tarmo Äijö, Sharif Chowdhury, Cecilia Garmendia-Torres, Jyrki Selinummi, Mirko Birbaumer, Aimée M Dudley, Lucas Pelkmans, and Olli Yli-Harja. Evaluation of methods for detection of fluorescence labeled subcellular objects in microscope images. *BMC bioinformatics*, 11(1):248, 2010.
- [116] Anne Burgert, Sebastian Letschert, Sören Doose, and Markus Sauer. Artifacts in single-molecule localization microscopy. *Histochemistry and cell biology*, 144(2):123–131, 2015.
- [117] Jochen Michael Reichel, Thomas Vomhof, and Jens Michaelis. Artifact formation in single molecule localization microscopy. *bioRxiv*, page 700955, 2019.
- [118] Ulrike Endesfelder, Sebastian Malkusch, Franziska Fricke, and Mike Heilemann. A simple method to estimate the average localization precision of a single-molecule localization microscopy experiment. *Histochemistry and cell biology*, 141(6):629–638, 2014.
- [119] Hamidreza Heydarian, Florian Schueder, Maximilian T Strauss, Ben Van Werkhoven, Mohammadreza Fazel, Keith A Lidke, Ralf Jungmann, Sjoerd Stallinga, and Bernd Rieger. Template-free 2d particle fusion in localization microscopy. *Nature methods*, 15(10):781, 2018.
- [120] Taekjip Ha, Thilo Enderle, DF Ogletree, Daniel S Chemla, Paul R Selvin, and Shimon Weiss. Probing the interaction between two single molecules: fluorescence resonance energy transfer between a single donor and a single acceptor. *Proceedings of the National Academy of Sciences*, 93(13):6264–6268, 1996.
- [121] Massimo Piccardi. Background subtraction techniques: a review. In *2004 IEEE International Conference on Systems, Man and Cybernetics (IEEE Cat. No. 04CH37583)*, volume 4, pages 3099–3104. IEEE, 2004.
- [122] Rahul Roy, Sungchul Hohng, and Taekjip Ha. A practical guide to single-molecule fret. *Nature methods*, 5(6):507, 2008.
- [123] Søren Preus, Lasse L Hildebrandt, and Victoria Birkedal. Optimal background estimators in single-molecule fret microscopy. *Biophysical journal*, 111(6):1278–1286, 2016.
- [124] Eelco Hoogendoorn, Kevin C Crosby, Daniela Leyton-Puig, Ronald MP Breedijk, Kees Jalink, Theodorus WJ Gadella, and Marten Postma. The fidelity of stochastic single-molecule super-resolution reconstructions critically depends upon robust background estimation. *Scientific reports*, 4:3854, 2014.
- [125] Yunqing Tang, Johnny Hendriks, Thomas Gensch, Luru Dai, and Junbai Li. Automatic bayesian single molecule identification for localization microscopy. *Scientific reports*, 6:33521, 2016.
- [126] Junhong Min, Cédric Vonesch, Hagai Kirshner, Lina Carlini, Nicolas Olivier, Seamus Holden, Suliana Manley, Jong Chul Ye, and Michael Unser. Falcon: fast and unbiased reconstruction of high-density super-resolution microscopy data. *Scientific reports*, 4:4577, 2014.

- [127] Michael K Cheezum, William F Walker, and William H Guilford. Quantitative comparison of algorithms for tracking single fluorescent particles. *Biophysical journal*, 81(4):2378–2388, 2001.
- [128] Ricardo Henriques, Mickael Lelek, Eugenio F Fornasiero, Flavia Valtorta, Christophe Zimmer, and Musa M Mhlanga. Quickpalm: 3d real-time photoactivation nanoscopy image processing in imagej. *Nature methods*, 7(5):339, 2010.
- [129] Andrew J Berglund, Matthew D McMahon, Jabez J McClelland, and J Alexander Liddle. Fast, bias-free algorithm for tracking single particles with variable size and shape. *Optics express*, 16(18):14064–14075, 2008.
- [130] Per Niklas Hedde, Jochen Fuchs, Franz Oswald, Jörg Wiedenmann, and Gerd Ulrich Nienhaus. Online image analysis software for photoactivation localization microscopy. *Nature Methods*, 6(10):689, 2009.
- [131] Bin Yu, Danni Chen, Junle Qu, and Hanben Niu. Fast fourier domain localization algorithm of a single molecule with nanometer precision. *Optics letters*, 36(22):4317–4319, 2011.
- [132] Koen JA Martens, Arjen N Bader, Sander Baas, Bernd Rieger, and Johannes Hohlbein. Phasor based single-molecule localization microscopy in 3d (psmlm-3d): an algorithm for mhz localization rates using standard cpus. *The Journal of chemical physics*, 148(12):123311, 2018.
- [133] Raghuveer Parthasarathy. Rapid, accurate particle tracking by calculation of radial symmetry centers. *Nature methods*, 9(7):724, 2012.
- [134] Sripad Ram, E Sally Ward, and Raimund J Ober. Beyond rayleigh’s criterion: a resolution measure with application to single-molecule microscopy. *Proceedings of the National Academy of Sciences*, 103(12):4457–4462, 2006.
- [135] Fang Huang, Samantha L Schwartz, Jason M Byars, and Keith A Lidke. Simultaneous multiple-emitter fitting for single molecule super-resolution imaging. *Biomedical optics express*, 2(5):1377–1393, 2011.
- [136] Kim I Mortensen, L Stirling Churchman, James A Spudich, and Henrik Flyvbjerg. Optimized localization analysis for single-molecule tracking and super-resolution microscopy. *Nature methods*, 7(5):377, 2010.
- [137] Bernd Rieger and Sjoerd Stallinga. The lateral and axial localization uncertainty in super-resolution light microscopy. *ChemPhysChem*, 15(4):664–670, 2014.
- [138] David Baddeley and Joerg Bewersdorf. Biological insight from super-resolution microscopy: what we can learn from localization-based images. *Annual review of biochemistry*, 87:965–989, 2018.
- [139] Alex von Diezmann, Yoav Shechtman, and WE Moerner. Three-dimensional localization of single molecules for super-resolution imaging and single-particle tracking. *Chemical reviews*, 117(11):7244–7275, 2017.
- [140] Michael J Mlodzianoski, Manuel F Juetten, Glen L Beane, and Joerg Bewersdorf. Experimental characterization of 3d localization techniques for particle-tracking and super-resolution microscopy. *Optics express*, 17(10):8264–8277, 2009.
- [141] Steve Wolter, Anna Löschberger, Thorge Holm, Sarah Aufmkolk, Marie-Christine Dabauvalle, Sebastian Van De Linde, and Markus Sauer. rapidstorm: accurate, fast open-source software for localization microscopy. *Nature methods*, 9(11):1040, 2012.

- [142] Hagai Kirshner, Francois Aguet, Daniel Sage, and Michael Unser. 3-d psf fitting for fluorescence microscopy: implementation and localization application. *Journal of microscopy*, 249(1):13–25, 2013.
- [143] Martin Ovesný, Pavel Krížek, Josef Borkovec, Zdeněk Švindrych, and Guy M Hagen. Thunderstorm: a comprehensive imagej plug-in for palm and storm data analysis and super-resolution imaging. *Bioinformatics*, 30(16):2389–2390, 2014.
- [144] Manuel F Juetten, Travis J Gould, Mark D Lessard, Michael J Mlodzianoski, Bhupendra S Nagpure, Brian T Bennett, Samuel T Hess, and Joerg Bewersdorf. Three-dimensional sub-100 nm resolution fluorescence microscopy of thick samples. *Nature methods*, 5(6):527, 2008.
- [145] Hagai Kirshner, Cédric Vonesch, and Michael Unser. Can localization microscopy benefit from approximation theory? In *2013 IEEE 10th International Symposium on Biomedical Imaging*, pages 588–591. IEEE, 2013.
- [146] Xiang Zhu and Dianwen Zhang. Efficient parallel levenberg-marquardt model fitting towards real-time automated parametric imaging microscopy. *PloS one*, 8(10):e76665, 2013.
- [147] Norman Brede and Melike Lakadamyali. Graspj: an open source, real-time analysis package for super-resolution imaging. *Optical Nanoscopy*, 1(1):11, 2012.
- [148] Rebecca Starr, Shane Stahlheber, and Alex Small. Fast maximum likelihood algorithm for localization of fluorescent molecules. *Optics letters*, 37(3):413–415, 2012.
- [149] François Aguet, Dimitri Van De Ville, and Michael Unser. A maximum-likelihood formalism for sub-resolution axial localization of fluorescent nanoparticles. *Optics Express*, 13(26):10503–10522, 2005.
- [150] Ginni Grover, Keith DeLuca, Sean Quirin, Jennifer DeLuca, and Rafael Piestun. Super-resolution photon-efficient imaging by nanometric double-helix point spread function localization of emitters (spindle). *Optics express*, 20(24):26681–26695, 2012.
- [151] Sheng Liu, Emil B Kromann, Wesley D Krueger, Joerg Bewersdorf, and Keith A Lidke. Three dimensional single molecule localization using a phase retrieved pupil function. *Optics express*, 21(24):29462–29487, 2013.
- [152] Hazen P Babcock and Xiaowei Zhuang. Analyzing single molecule localization microscopy data using cubic splines. *Scientific reports*, 7(1):552, 2017.
- [153] Yiming Li, Markus Mund, Philipp Hoess, Joran Deschamps, Ulf Matti, Bianca Nijmeijer, Vilma Jimenez Sabinina, Jan Ellenberg, Ingmar Schoen, and Jonas Ries. Real-time 3d single-molecule localization using experimental point spread functions. *Nature methods*, 15(5):367, 2018.
- [154] Ted A Laurence and Brett A Chromy. Efficient maximum likelihood estimator fitting of histograms. *Nature methods*, 7(5):338, 2010.
- [155] Seamus J Holden, Stephan Uphoff, and Achillefs N Kapanidis. Daostorm: an algorithm for high-density super-resolution microscopy. *Nature methods*, 8(4):279, 2011.
- [156] Hazen Babcock, Yaron M Sigal, and Xiaowei Zhuang. A high-density 3d localization algorithm for stochastic optical reconstruction microscopy. *Optical Nanoscopy*, 1(1):6, 2012.
- [157] Tingwei Quan, Hongyu Zhu, Xiaomao Liu, Yongfeng Liu, Jiuping Ding, Shaoqun Zeng, and Zhen-Li Huang. High-density localization of active molecules using structured sparse model and bayesian information criterion. *Optics express*, 19(18):16963–16974, 2011.

- [158] Yina Wang, Tingwei Quan, Shaoqun Zeng, and Zhen-Li Huang. Palmer: a method capable of parallel localization of multiple emitters for high-density localization microscopy. *Optics express*, 20(14):16039–16049, 2012.
- [159] Luchang Li, Bo Xin, Weibing Kuang, Zhiwei Zhou, and Zhen-Li Huang. Divide and conquer: Real-time maximum likelihood fitting of multiple emitters for super-resolution localization microscopy. *bioRxiv*, page 659631, 2019.
- [160] Yuto Ashida and Masahito Ueda. Precise multi-emitter localization method for fast super-resolution imaging. *Optics letters*, 41(1):72–75, 2016.
- [161] Mingzhai Sun, Jiaqing Huang, Filiz Bunyak, Kristyn Gumpfer, Gejing De, Matthew Sermersheim, George Liu, Pei-Hui Lin, Kannappan Palaniappan, and Jianjie Ma. Superresolution microscope image reconstruction by spatiotemporal object decomposition and association: application in resolving t-tubule structure in skeletal muscle. *Optics express*, 22(10):12160–12176, 2014.
- [162] Andrey Aristov, Benoit Lelandais, Elena Rensen, and Christophe Zimmer. Zola-3d allows flexible 3d localization microscopy over an adjustable axial range. *Nature communications*, 9(1):2409, 2018.
- [163] Eran A Mukamel, Hazen Babcock, and Xiaowei Zhuang. Statistical deconvolution for super-resolution fluorescence microscopy. *Biophysical journal*, 102(10):2391–2400, 2012.
- [164] Weisong Zhao, Jian Liu, Chenqi Kong, Yixuan Zhao, Changling Guo, Chenguang Liu, Xi-angyan Ding Xumin Ding, Jiubin Tan, and Haoyu Li. Faster superresolution imaging with auto-correlation twostep deconvolution. *arXiv preprint arXiv:1809.07410*, 2018.
- [165] Martin Lindén, Vladimir Ćurić, Elias Amselem, and Johan Elf. Pointwise error estimates in localization microscopy. *Nature communications*, 8:15115, 2017.
- [166] Susan Cox, Edward Rosten, James Monypenny, Tijana Jovanovic-Taliman, Dylan T Burnette, Jennifer Lippincott-Schwartz, Gareth E Jones, and Rainer Heintzmann. Bayesian localization microscopy reveals nanoscale podosome dynamics. *Nature methods*, 9(2):195, 2012.
- [167] Peter J Green. Reversible jump markov chain monte carlo computation and bayesian model determination. *Biometrika*, 82(4):711–732, 1995.
- [168] Sylvia Richardson and Peter J Green. On bayesian analysis of mixtures with an unknown number of components (with discussion). *Journal of the Royal Statistical Society: series B (statistical methodology)*, 59(4):731–792, 1997.
- [169] W Keith Hastings. Monte carlo sampling methods using markov chains and their applications. 1970.
- [170] Keith A Lidke. Super resolution for common probes and common microscopes. *Nature methods*, 9(2):139, 2012.
- [171] Ying S Hu, Xiaolin Nan, Prabuddha Sengupta, Jennifer Lippincott-Schwartz, and Hu Cang. Accelerating 3b single-molecule super-resolution microscopy with cloud computing. *Nature methods*, 10(2):96, 2013.
- [172] Fan Xu, Mingshu Zhang, Zhiyong Liu, Pingyong Xu, and Fa Zhang. Bayesian localization microscopy based on intensity distribution of fluorophores. *Protein & cell*, 6(3):211–220, 2015.

- [173] Fan Xu, Mingshu Zhang, Wenting He, Renmin Han, Fudong Xue, Zhiyong Liu, Fa Zhang, Jennifer Lippincott-Schwartz, and Pingyong Xu. Live cell single molecule-guided bayesian localization super resolution microscopy. *Cell research*, 27(5):713, 2017.
- [174] Emmanuel J Candes, Justin K Romberg, and Terence Tao. Stable signal recovery from incomplete and inaccurate measurements. *Communications on Pure and Applied Mathematics: A Journal Issued by the Courant Institute of Mathematical Sciences*, 59(8):1207–1223, 2006.
- [175] Lei Zhu, Wei Zhang, Daniel Elnatan, and Bo Huang. Faster storm using compressed sensing. *Nature methods*, 9(7):721, 2012.
- [176] Hazen P Babcock, Jeffrey R Moffitt, Yunlong Cao, and Xiaowei Zhuang. Fast compressed sensing analysis for super-resolution imaging using l1-homotopy. *Optics express*, 21(23):28583–28596, 2013.
- [177] Siewert Hugelier, Johan J De Rooi, Romain Bernex, Sam Duwé, Olivier Devos, Michel Sliwa, Peter Dedecker, Paul HC Eilers, and Cyril Ruckebusch. Sparse deconvolution of high-density super-resolution images. *Scientific reports*, 6:21413, 2016.
- [178] Simon Gazagnes, Emmanuel Soubies, and Laure Blanc-Féraud. High density molecule localization for super-resolution microscopy using cel0 based sparse approximation. In *2017 IEEE 14th International Symposium on Biomedical Imaging (ISBI 2017)*, pages 28–31. IEEE, 2017.
- [179] Nicholas Boyd, Geoffrey Schiebinger, and Benjamin Recht. The alternating descent conditional gradient method for sparse inverse problems. *SIAM Journal on Optimization*, 27(2):616–639, 2017.
- [180] Jiaqing Huang, Mingzhai Sun, Jianjie Ma, and Yuejie Chi. Super-resolution image reconstruction for high-density three-dimensional single-molecule microscopy. *IEEE Transactions on Computational Imaging*, 3(4):763–773, 2017.
- [181] Jingjing Wu, Siwei Li, Saiwen Zhang, Danying Lin, Bin Yu, and Junle Qu. Fast analysis method for stochastic optical reconstruction microscopy using multiple measurement vector model sparse bayesian learning. *Optics letters*, 43(16):3977–3980, 2018.
- [182] Oren Solomon, Maor Mutzafi, Mordechai Segev, and Yonina C Eldar. Sparsity-based super-resolution microscopy from correlation information. *Optics express*, 26(14):18238–18269, 2018.
- [183] Michael A Nielsen and Isaac Chuang. Quantum computation and quantum information, 2002.
- [184] Krishna Agarwal and Radek Machán. Multiple signal classification algorithm for super-resolution fluorescence microscopy. *Nature communications*, 7:13752, 2016.
- [185] Jiaqing Huang, Kristyn Gummer, Yuejie Chi, Mingzhai Sun, and Jianjie Ma. Fast two-dimensional super-resolution image reconstruction algorithm for ultra-high emitter density. *Optics letters*, 40(13):2989–2992, 2015.
- [186] Michael A Nielsen. *Neural networks and deep learning*, volume 25. Determination press San Francisco, CA, USA, 2015.
- [187] Chinmay Belthangady and Loic A Royer. Applications, promises, and pitfalls of deep learning for fluorescence image reconstruction. *Nature methods*, pages 1–11, 2019.
- [188] Leonhard Möckl, Anish R Roy, and WE Moerner. Deep learning in single-molecule microscopy: fundamentals, caveats, and recent developments. *Biomedical optics express*, 11(3):1633–1661, 2020.

- [189] Rita Strack. Deep learning advances super-resolution imaging. *Nature methods*, 15(6):403, 2018.
- [190] Elias Nehme, Lucien E Weiss, Tomer Michaeli, and Yoav Shechtman. Deep-storm: super-resolution single-molecule microscopy by deep learning. *Optica*, 5(4):458–464, 2018.
- [191] Elias Nehme, Daniel Freedman, Racheli Gordon, Boris Ferdman, Tomer Michaeli, and Yoav Shechtman. Dense three dimensional localization microscopy by deep learning. *arXiv preprint arXiv:1906.09957*, 2019.
- [192] P Zelger, K Kaser, B Rossboth, L Velas, GJ Schütz, and A Jesacher. Three-dimensional localization microscopy using deep learning. *Optics express*, 26(25):33166–33179, 2018.
- [193] Martin Weigert, Uwe Schmidt, Tobias Boothe, Andreas Müller, Alexandr Dibrov, Akanksha Jain, Benjamin Wilhelm, Deborah Schmidt, Coleman Broaddus, Siân Culley, et al. Content-aware image restoration: pushing the limits of fluorescence microscopy. *Nature methods*, 15(12):1090, 2018.
- [194] Zhaoqiang Wang, Hao Zhang, Yicong Yang, Yi Li, and Peng Fei. Deep learning light field microscopy for rapid four-dimensional imaging of behaving animals. *bioRxiv*, page 432807, 2018.
- [195] Hongda Wang, Yair Rivenson, Yiyin Jin, Zhensong Wei, Ronald Gao, Harun Günaydin, Laurent A Bentolila, Comert Kural, and Aydogan Ozcan. Deep learning enables cross-modality super-resolution in fluorescence microscopy. *Nat. Methods*, 16:103–110, 2019.
- [196] Wei Ouyang, Andrey Aristov, Mickaël Lelek, Xian Hao, and Christophe Zimmer. Deep learning massively accelerates super-resolution localization microscopy. *Nature biotechnology*, 36(5):460, 2018.
- [197] Artur Speiser, Srinivas C Turaga, and Jakob H Macke. Teaching deep neural networks to localize sources in super-resolution microscopy by combining simulation-based learning and unsupervised learning. *arXiv preprint arXiv:1907.00770*, 2019.
- [198] Taehwan Kim, Seonah Moon, and Ke Xu. Information-rich localization microscopy through machine learning. *Nature communications*, 10(1):1996, 2019.
- [199] Hongqiang Ma, Jianquan Xu, and Yang Liu. Windstorm: Robust online image processing for high-throughput nanoscopy. *Science advances*, 5(4):eaaw0683, 2019.
- [200] T Takeshima, T Takahashi, J Yamashita, Y Okada, and S Watanabe. A multi-emitter fitting algorithm for potential live cell super-resolution imaging over a wide range of molecular densities. *Journal of microscopy*, 271(3):266–281, 2018.
- [201] Silvia Colabrese, Marco Castello, Giuseppe Vicidomini, and Alessio Del Bue. Machine learning approach for single molecule localisation microscopy. *Biomedical optics express*, 9(4):1680–1691, 2018.
- [202] Anthony Barsic and Rafael Piestun. Super-resolution of dense nanoscale emitters beyond the diffraction limit using spatial and temporal information. *Applied Physics Letters*, 102(23):231103, 2013.
- [203] Paul D Simonson, Eli Rothenberg, and Paul R Selvin. Single-molecule-based super-resolution images in the presence of multiple fluorophores. *Nano letters*, 11(11):5090–5096, 2011.

- [204] Prashant Prabhat, Sripad Ram, E Sally Ward, and Raimund J Ober. Simultaneous imaging of different focal planes in fluorescence microscopy for the study of cellular dynamics in three dimensions. *IEEE transactions on nanobioscience*, 3(4):237–242, 2004.
- [205] Amir Tahmasbi, Sripad Ram, Jerry Chao, Anish V Abraham, Felix W Tang, E Sally Ward, and Raimund J Ober. Designing the focal plane spacing for multifocal plane microscopy. *Optics express*, 22(14):16706–16721, 2014.
- [206] Matthew D Lew, Steven F Lee, Majid Badieirostami, and WE Moerner. Corkscrew point spread function for far-field three-dimensional nanoscale localization of pointlike objects. *Optics letters*, 36(2):202–204, 2011.
- [207] Shu Jia, Joshua C Vaughan, and Xiaowei Zhuang. Isotropic three-dimensional super-resolution imaging with a self-bending point spread function. *Nature photonics*, 8(4):302, 2014.
- [208] WE Moerner, Taras Plakhotnik, Thomas Irngartinger, Urs P Wild, Dieter W Pohl, and Bert Hecht. Near-field optical spectroscopy of individual molecules in solids. *Physical review letters*, 73(20):2764, 1994.
- [209] Thomas Ruckstuhl and Dorinel Verdes. Supercritical angle fluorescence (saf) microscopy. *Optics express*, 12(18):4246–4254, 2004.
- [210] Yunmin Jung, Inbal Riven, Sara W Feigelson, Elena Kartvelishvily, Kazuo Tohya, Masayuki Miyasaka, Ronen Alon, and Gilad Haran. Three-dimensional localization of t-cell receptors in relation to microvilli using a combination of superresolution microscopies. *Proceedings of the National Academy of Sciences*, 113(40):E5916–E5924, 2016.
- [211] Yan Fu, Peter W Winter, Raul Rojas, Victor Wang, Matthew McAuliffe, and George H Patterson. Axial superresolution via multiangle tirf microscopy with sequential imaging and photobleaching. *Proceedings of the National Academy of Sciences*, 113(16):4368–4373, 2016.
- [212] Ignacio Izeddin, Mohamed El Beheiry, Jordi Andilla, Daniel Ciepiewski, Xavier Darzacq, and Maxime Dahan. Psf shaping using adaptive optics for three-dimensional single-molecule super-resolution imaging and tracking. *Optics express*, 20(5):4957–4967, 2012.
- [213] Yoav Shechtman, Lucien E Weiss, Adam S Backer, Steffen J Sahl, and WE Moerner. Precise three-dimensional scan-free multiple-particle tracking over large axial ranges with tetrapod point spread functions. *Nano letters*, 15(6):4194–4199, 2015.
- [214] Yongzhuang Zhou, Michael Handley, Guillem Carles, and Andrew R Harvey. Advances in 3d single particle localization microscopy. *APL Photonics*, 4(6):060901, 2019.
- [215] Saiwen Zhang, Danni Chen, and Hanben Niu. 3d localization of high particle density images using sparse recovery. *Applied optics*, 54(26):7859–7864, 2015.
- [216] Jiaqing Huang, Mingzhai Sun, Kristyn Gumpfer, Yuejie Chi, and Jianjie Ma. 3d multifocus astigmatism and compressed sensing (3d macs) based superresolution reconstruction. *Biomedical optics express*, 6(3):902–917, 2015.
- [217] Partha P Mondal, Nikki M Curthoys, and Samuel T Hess. Clean localization super-resolution microscopy for 3d biological imaging. *AIP Advances*, 6(1):015017, 2016.
- [218] Sean Quirin, Sri Rama Prasanna Pavani, and Rafael Piestun. Optimal 3d single-molecule localization for superresolution microscopy with aberrations and engineered point spread functions. *Proceedings of the National Academy of Sciences*, 109(3):675–679, 2012.

- [219] Junhong Min, Seamus J Holden, Lina Carlini, Michael Unser, Suliana Manley, and Jong Chul Ye. 3d high-density localization microscopy using hybrid astigmatic/biplane imaging and sparse image reconstruction. *Biomedical optics express*, 5(11):3935–3948, 2014.
- [220] Yiming Li, Yu-Le Wu, Philipp Hoess, Markus Mund, and Jonas Ries. Depth-dependent psf calibration and aberration correction for 3d single-molecule localization. *Biomedical Optics Express*, 10(6):2708–2718, 2019.
- [221] Christopher H Bohrer, Xinxing Yang, Zhixin Lyu, Shih-Chin Wang, and Jie Xiao. Improved single-molecule localization precision in astigmatism-based 3d superresolution imaging using weighted likelihood estimation. *BioRxiv*, page 304816, 2018.
- [222] Martin Ovesný, Pavel Krížek, Zdeněk Švindrych, and Guy M Hagen. High density 3d localization microscopy using sparse support recovery. *Optics express*, 22(25):31263–31276, 2014.
- [223] Bo Shuang, Wenxiao Wang, Hao Shen, Lawrence J Tauzin, Charlotte Flatebo, Jianbo Chen, Nicholas A Moringo, Logan DC Bishop, Kevin F Kelly, and Christy F Landes. Generalized recovery algorithm for 3d super-resolution microscopy using rotating point spread functions. *Scientific reports*, 6:30826, 2016.
- [224] Xiyu Yi, Rafael Piestun, and Shimon Weiss. 3d super-resolution imaging using a generalized and scalable progressive refinement method on sparse recovery (pris). In *Single Molecule Spectroscopy and Superresolution Imaging XII*, volume 10884, page 1088406. International Society for Optics and Photonics, 2019.
- [225] Bridget M Hanser, Mats GL Gustafsson, DA Agard, and John W Sedat. Phase-retrieved pupil functions in wide-field fluorescence microscopy. *Journal of microscopy*, 216(1):32–48, 2004.
- [226] Ralph W Gerchberg. A practical algorithm for the determination of phase from image and diffraction plane pictures. *Optik*, 35:237–246, 1972.
- [227] Alexandros Pertsinidis, Yunxiang Zhang, and Steven Chu. Subnanometre single-molecule localization, registration and distance measurements. *Nature*, 466(7306):647, 2010.
- [228] Sang Hak Lee, Murat Baday, Marco Tjioe, Paul D Simonson, Ruobing Zhang, En Cai, and Paul R Selvin. Using fixed fiducial markers for stage drift correction. *Optics express*, 20(11):12177–12183, 2012.
- [229] Hongqiang Ma, Jianquan Xu, Jingyi Jin, Yi Huang, and Yang Liu. A simple marker-assisted 3d nanometer drift correction method for superresolution microscopy. *Biophysical journal*, 112(10):2196–2208, 2017.
- [230] Warren Colomb, John Czerski, JD Sau, and Susanta K Sarkar. Estimation of microscope drift using fluorescent nanodiamonds as fiducial markers. *Journal of microscopy*, 266(3):298–306, 2017.
- [231] Yeoan Youn, Yuji Ishitsuka, Chaoyi Jin, and Paul R Selvin. Thermal nanoimprint lithography for drift correction in super-resolution fluorescence microscopy. *Optics express*, 26(2):1670–1680, 2018.
- [232] Alexander Balinovic, David Albrecht, and Ulrike Endesfelder. Spectrally red-shifted fluorescent fiducial markers for optimal drift correction in localization microscopy. *Journal of Physics D: Applied Physics*, 52(20):204002, 2019.
- [233] BA Mantooth, ZJ Donhauser, KF Kelly, and PS Weiss. Cross-correlation image tracking for drift correction and adsorbate analysis. *Review of Scientific Instruments*, 73(2):313–317, 2002.

- [234] Petr Cizmar, András E Vladár, and Michael T Postek. Real-time scanning charged-particle microscope image composition with correction of drift. *Microscopy and Microanalysis*, 17(2):302–308, 2011.
- [235] Michael J Mlodzianoski, John M Schreiner, Steven P Callahan, Katarina Smolková, Andrea Dlasková, Jitka Šantorová, Petr Ježek, and Joerg Bewersdorf. Sample drift correction in 3d fluorescence photoactivation localization microscopy. *Optics express*, 19(16):15009–15019, 2011.
- [236] Adam Parslow, Albert Cardona, and Robert J Bryson-Richardson. Sample drift correction following 4d confocal time-lapse imaging. *JoVE (Journal of Visualized Experiments)*, (86):e51086, 2014.
- [237] Joshua D Sugar, Aron W Cummings, Benjamin W Jacobs, and David B Robinson. A free matlab script for spatial drift correction. *Microscopy Today*, 22(5):40–47, 2014.
- [238] Y Tang, X Wang, X Zhang, J Li, and L Dai. Sub-nanometer drift correction for super-resolution imaging. *Optics letters*, 39(19):5685–5688, 2014.
- [239] Yina Wang, Joerg Schnitzbauer, Zhe Hu, Xueming Li, Yifan Cheng, Zhen-Li Huang, and Bo Huang. Localization events-based sample drift correction for localization microscopy with redundant cross-correlation algorithm. *Optics express*, 22(13):15982–15991, 2014.
- [240] Michael S Smirnov, Paul R Evans, Tavita R Garrett, Long Yan, and Ryohei Yasuda. Automated remote focusing, drift correction, and photostimulation to evaluate structural plasticity in dendritic spines. *PloS one*, 12(1):e0170586, 2017.
- [241] Claudia Geisler, Thomas Hotz, Andreas Schönle, Stefan W Hell, Axel Munk, and Alexander Egner. Drift estimation for single marker switching based imaging schemes. *Optics express*, 20(7):7274–7289, 2012.
- [242] Ahmed Elmokadem and Ji Yu. Optimal drift correction for superresolution localization microscopy with bayesian inference. *Biophysical journal*, 109(9):1772–1780, 2015.
- [243] Mitchell P Yothers, Aaron E Browder, and Lloyd A Bumm. Real-space post-processing correction of thermal drift and piezoelectric actuator nonlinearities in scanning tunneling microscope images. *Review of Scientific Instruments*, 88(1):013708, 2017.
- [244] Michael J Wester, Sandeep Pallikkuth, Hanieh Mazloom-Farsibaf, Mohamadreza Fazel, and Keith A Lidke. Simple and fiducial-free drift correction for super-resolution imaging of cellular structures. *Biophysical Journal*, 116(3):279a, 2019.
- [245] Steffen B Petersen, Thiagarajan Viruthachalam, Isabel Coutinho, Gnana Prakash Gajula, and Maria Teresa Neves-Petersen. Image processing for drift compensation in fluorescence microscopy. In *Imaging, Manipulation, and Analysis of Biomolecules, Cells, and Tissues XI*, volume 8587, page 85871H. International Society for Optics and Photonics, 2013.
- [246] Naresh Marturi, Soukalo Dembélé, and Nadine Piat. Fast image drift compensation in scanning electron microscope using image registration. In *2013 IEEE International Conference on Automation Science and Engineering (CASE)*, pages 807–812. IEEE, 2013.
- [247] Minhua Qiu and Ge Yang. Drift correction for fluorescence live cell imaging through correlated motion identification. In *2013 IEEE 10th International Symposium on Biomedical Imaging*, pages 452–455. IEEE, 2013.

- [248] Hesam Mazidi, Jin Lu, Arye Nehorai, and Matthew D Lew. Minimizing structural bias in single-molecule super-resolution microscopy. *Scientific reports*, 8(1):13133, 2018.
- [249] Justin Demmerle, Eva Wegel, Lothar Schermelleh, and Ian M Dobbie. Assessing resolution in super-resolution imaging. *Methods*, 88:3–10, 2015.
- [250] Yi Deng and Joshua W Shaevitz. Effect of aberration on height calibration in three-dimensional localization-based microscopy and particle tracking. *Applied optics*, 48(10):1886–1890, 2009.
- [251] Ryan McGorty, Joerg Schnitzbauer, Wei Zhang, and Bo Huang. Correction of depth-dependent aberrations in 3d single-molecule localization and super-resolution microscopy. *Optics letters*, 39(2):275–278, 2014.
- [252] Benjamin C Coles, Stephen ED Webb, Noah Schwartz, Daniel J Rolfe, Marisa Martin-Fernandez, and Valentina Lo Schiavo. Characterisation of the effects of optical aberrations in single molecule techniques. *Biomedical optics express*, 7(5):1755–1767, 2016.
- [253] Tsung-li Liu, Srigokul Upadhyayula, Daniel E Milkie, Ved Singh, Kai Wang, Ian A Swinburne, Kishore R Mosaliganti, Zach M Collins, Tom W Hiscock, Jamien Shea, et al. Observing the cell in its native state: Imaging subcellular dynamics in multicellular organisms. *Science*, 360(6386):eaq1392, 2018.
- [254] Sheng Liu, Hyun Huh, Sang-Hyuk Lee, and Fang Huang. Three-dimensional single-molecule localization microscopy in whole-cell and tissue specimens. *Annual review of biomedical engineering*, 22:155–184, 2020.
- [255] Jörg Enderlein, Erdal Toprak, and Paul R Selvin. Polarization effect on position accuracy of fluorophore localization. *Optics express*, 14(18):8111–8120, 2006.
- [256] Hsiao-lu D Lee, Steffen J Sahl, Matthew D Lew, and WE Moerner. The double-helix microscope super-resolves extended biological structures by localizing single blinking molecules in three dimensions with nanoscale precision. *Applied physics letters*, 100(15):153701, 2012.
- [257] Amir Tahmasbi, E Sally Ward, and Raimund J Ober. Determination of localization accuracy based on experimentally acquired image sets: applications to single molecule microscopy. *Optics express*, 23(6):7630–7652, 2015.
- [258] Sripad Ram, E Sally Ward, and Raimund J Ober. A stochastic analysis of distance estimation approaches in single molecule microscopy: quantifying the resolution limits of photon-limited imaging systems. *Multidimensional systems and signal processing*, 24(3):503–542, 2013.
- [259] Travis J Gould, Samuel T Hess, and Joerg Bewersdorf. Optical nanoscopy: from acquisition to analysis. *Annual review of biomedical engineering*, 14:231–254, 2012.
- [260] Varun Venkataramani, Frank Herrmannsdörfer, Mike Heilemann, and Thomas Kuner. Suresim: simulating localization microscopy experiments from ground truth models. *Nature methods*, 13(4):319, 2016.
- [261] Vera DesMarais, Robert J Eddy, Ved P Sharma, Orrin Stone, and John S Condeelis. Optimizing leading edge f-actin labeling using multiple actin probes, fixation methods and imaging modalities. *BioTechniques*, 66(3):113–119, 2019.
- [262] Jervis Vermal Thevathasan, Maurice Kahnwald, Konstanty Cieřliński, Philipp Hoess, Sudheer Kumar Peneti, Manuel Reitberger, Daniel Heid, Krishna Chaitanya Kasuba, Sarah Janice Hoerner, Yiming Li, et al. Nuclear pores as versatile reference standards for quantitative superresolution microscopy. *BioRxiv*, page 582668, 2019.

- [263] Eran A Mukamel and Mark J Schnitzer. Unified resolution bounds for conventional and stochastic localization fluorescence microscopy. *Physical review letters*, 109(16):168102, 2012.
- [264] Niccolò Banterle, Khanh Huy Bui, Edward A Lemke, and Martin Beck. Fourier ring correlation as a resolution criterion for super-resolution microscopy. *Journal of structural biology*, 183(3):363–367, 2013.
- [265] Siân Culley, David Albrecht, Caron Jacobs, Pedro Matos Pereira, Christophe Leterrier, Jason Mercer, and Ricardo Henriques. Quantitative mapping and minimization of super-resolution optical imaging artifacts. *Nature methods*, 15(4):263, 2018.
- [266] Edward AK Cohen, Anish V Abraham, Sreevidhya Ramakrishnan, and Raimund J Ober. Resolution limit of image analysis algorithms. *Nature communications*, 10(1):793, 2019.
- [267] Christian Steinhauer, Ralf Jungmann, Thomas L Sobey, Friedrich C Simmel, and Philip Tinnefeld. Dna origami as a nanoscopic ruler for super-resolution microscopy. *Angewandte Chemie International Edition*, 48(47):8870–8873, 2009.
- [268] Mario Raab, Ija Jusuk, Julia Molle, Egbert Buhr, Bernd Bodermann, Detlef Bergmann, Harald Bosse, and Philip Tinnefeld. Using dna origami nanorulers as traceable distance measurement standards and nanoscopic benchmark structures. *Scientific reports*, 8(1):1780, 2018.
- [269] Richard J Marsh, Karin Pfisterer, Pauline Bennett, Liisa M Hirvonen, Mathias Gautel, Gareth E Jones, and Susan Cox. Artifact-free high-density localization microscopy analysis. *Nature methods*, 15(9):689, 2018.
- [270] Harry Nyquist. Certain topics in telegraph transmission theory. *Transactions of the American Institute of Electrical Engineers*, 47(2):617–644, 1928.
- [271] Claude Elwood Shannon. Communication in the presence of noise. *Proceedings of the IRE*, 37(1):10–21, 1949.
- [272] Hari Shroff, Catherine G Galbraith, James A Galbraith, and Eric Betzig. Live-cell photoactivated localization microscopy of nanoscale adhesion dynamics. *Nature methods*, 5(5):417, 2008.
- [273] Wesley R Legant, Lin Shao, Jonathan B Grimm, Timothy A Brown, Daniel E Milkie, Brian B Avants, Luke D Lavis, and Eric Betzig. High-density three-dimensional localization microscopy across large volumes. *Nature methods*, 13(4):359, 2016.
- [274] Sara A Jones, Sang-Hee Shim, Jiang He, and Xiaowei Zhuang. Fast, three-dimensional super-resolution imaging of live cells. *Nature methods*, 8(6):499, 2011.
- [275] James E Fitzgerald, Ju Lu, and Mark J Schnitzer. Estimation theoretic measure of resolution for stochastic localization microscopy. *Physical review letters*, 109(4):048102, 2012.
- [276] Tania Stathaki. *Image fusion: algorithms and applications*. Elsevier, 2011.
- [277] Mark Bates. Single-particle analysis for fluorescence nanoscopy. *Nature methods*, 15(10):771, 2018.
- [278] Richard Henderson. Avoiding the pitfalls of single particle cryo-electron microscopy: Einstein from noise. *Proceedings of the National Academy of Sciences*, 110(45):18037–18041, 2013.
- [279] Anna Löschberger, Sebastian van de Linde, Marie-Christine Dabauvalle, Bernd Rieger, Mike Heilemann, Georg Krohne, and Markus Sauer. Super-resolution imaging visualizes the eight-fold symmetry of gp210 proteins around the nuclear pore complex and resolves the central channel with nanometer resolution. *J Cell Sci*, 125(3):570–575, 2012.

- [280] V Mennella, B Keszthelyi, KL McDonald, B Chhun, F Kan, Gregory C Rogers, B Huang, and DA3767400 Agard. Subdiffraction-resolution fluorescence microscopy reveals a domain of the centrosome critical for pericentriolar material organization. *Nature cell biology*, 14(11):1159–1168, 2012.
- [281] Anna Szymborska, Alex De Marco, Nathalie Daigle, Volker C Cordes, John AG Briggs, and Jan Ellenberg. Nuclear pore scaffold structure analyzed by super-resolution microscopy and particle averaging. *Science*, 341(6146):655–658, 2013.
- [282] Jordi Broeken, Hannah Johnson, Diane S Lidke, Sheng Liu, Robert PJ Nieuwenhuizen, Sjoerd Stallinga, Keith A Lidke, and Bernd Rieger. Resolution improvement by 3d particle averaging in localization microscopy. *Methods and applications in fluorescence*, 3(1):014003, 2015.
- [283] Xiaoyu Shi, Galo Garcia III, Yina Wang, Jeremy F Reiter, and Bo Huang. Deformed alignment of super-resolution images for semi-flexible structures. *PloS one*, 14(3):e0212735, 2019.
- [284] Christian Sieben, Niccolo Banterle, Kyle M Douglass, Pierre Gönczy, and Suliana Manley. Multicolor single-particle reconstruction of protein complexes. *Nature methods*, 15(10):777, 2018.
- [285] Hamidreza Heydarian, Adrian Przybylski, Florian Schueder, Ralf Jungmann, Ben van Werkhoven, Jan Keller-Findeisen, Jonas Ries, Sjoerd Stallinga, Mark Bates, and Bernd Rieger. Three dimensional particle averaging for structural imaging of macromolecular complexes by localization microscopy. *bioRxiv*, page 837575, 2019.
- [286] Marin van Heel, Brent Gowen, Rishi Matadeen, Elena V Orlova, Robert Finn, Tillmann Pape, Dana Cohen, Holger Stark, Ralf Schmidt, Michael Schatz, et al. Single-particle electron cryo-microscopy: towards atomic resolution. *Quarterly reviews of biophysics*, 33(4):307–369, 2000.
- [287] David Baddeley, Mark B Cannell, and Christian Soeller. Visualization of localization microscopy data. *Microscopy and Microanalysis*, 16(1):64–72, 2010.
- [288] Thomas Schlichthaerle, Maximilian T Strauss, Florian Schueder, Alexander Auer, Bianca Nijmeijer, Moritz Kueblbeck, Vilma Jimenez Sabinina, Jervis V Thevathasan, Jonas Ries, Jan Ellenberg, et al. Direct visualization of single nuclear pore complex proteins using genetically-encoded probes for dna-paint. *BioRxiv*, page 579961, 2019.
- [289] Daniel Lingwood and Kai Simons. Lipid rafts as a membrane-organizing principle. *science*, 327(5961):46–50, 2010.
- [290] Alessandra Cambi and Diane S Lidke. *Cell membrane nanodomains: From biochemistry to nanoscopy*. CRC Press, 2014.
- [291] Julie S Biteen, Erin D Goley, Lucy Shapiro, and WE Moerner. Three-dimensional super-resolution imaging of the midplane protein ftsz in live caulobacter crescentus cells using astigmatism. *ChemPhysChem*, 13(4):1007–1012, 2012.
- [292] Adish Dani, Bo Huang, Joseph Bergan, Catherine Dulac, and Xiaowei Zhuang. Superresolution imaging of chemical synapses in the brain. *Neuron*, 68(5):843–856, 2010.
- [293] Michihiro Igarashi, Motohiro Nozumi, Ling-Gang Wu, Francesca Cella Zanacchi, István Kátona, László Barna, Pingyong Xu, Mingshu Zhang, Fudong Xue, and Edward Boyden. New observations in neuroscience using superresolution microscopy. *Journal of Neuroscience*, 38(44):9459–9467, 2018.

- [294] Jessica Fitzgibbon, Karen Bell, Emma King, and Karl Oparka. Super-resolution imaging of plasmodesmata using three-dimensional structured illumination microscopy. *Plant physiology*, 153(4):1453–1463, 2010.
- [295] Veit Schubert. Super-resolution microscopy—applications in plant cell research. *Frontiers in plant science*, 8:531, 2017.
- [296] Volker Westphal, Silvio O Rizzoli, Marcel A Lauterbach, Dirk Kamin, Reinhard Jahn, and Stefan W Hell. Video-rate far-field optical nanoscopy dissects synaptic vesicle movement. *Science*, 320(5873):246–249, 2008.
- [297] Peter Kner, Bryant B Chhun, Eric R Griffis, Lukman Winoto, and Mats GL Gustafsson. Super-resolution video microscopy of live cells by structured illumination. *Nature methods*, 6(5):339, 2009.
- [298] Markus Sauer and Mike Heilemann. Single-molecule localization microscopy in eukaryotes. *Chemical reviews*, 117(11):7478–7509, 2017.
- [299] Hao Shen, Lawrence J Tauzin, Rashad Baiyasi, Wenxiao Wang, Nicholas Moringo, Bo Shuang, and Christy F Landes. Single particle tracking: from theory to biophysical applications. *Chemical reviews*, 117(11):7331–7376, 2017.
- [300] Carlo Manzo and Maria F Garcia-Parajo. A review of progress in single particle tracking: from methods to biophysical insights. *Reports on progress in physics*, 78(12):124601, 2015.
- [301] Juliette Griffié, Michael Shannon, Claire L Bromley, Lies Boelen, Garth L Burn, David J Williamson, Nicholas A Heard, Andrew P Cope, Dylan M Owen, and Patrick Rubin-Delanchy. A bayesian cluster analysis method for single-molecule localization microscopy data. *nature protocols*, 11(12):2499, 2016.
- [302] Philip R Nicovich, Dylan M Owen, and Katharina Gaus. Turning single-molecule localization microscopy into a quantitative bioanalytical tool. *Nature protocols*, 12(3):453, 2017.
- [303] Sarah L Veatch, Benjamin B Machta, Sarah A Shelby, Ethan N Chiang, David A Holowka, and Barbara A Baird. Correlation functions quantify super-resolution images and estimate apparent clustering due to over-counting. *PloS one*, 7(2):e31457, 2012.
- [304] Sang-Hyuk Lee, Jae Yen Shin, Antony Lee, and Carlos Bustamante. Counting single photoactivatable fluorescent molecules by photoactivated localization microscopy (palm). *Proceedings of the National Academy of Sciences*, 109(43):17436–17441, 2012.
- [305] Elias M Puchner, Jessica M Walter, Robert Kasper, Bo Huang, and Wendell A Lim. Counting molecules in single organelles with superresolution microscopy allows tracking of the endosome maturation trajectory. *Proceedings of the National Academy of Sciences*, 110(40):16015–16020, 2013.
- [306] Nela Durisic, Lara Laparra-Cuervo, Ángel Sandoval-Álvarez, Joseph Steven Borbely, and Melike Lakadamyali. Single-molecule evaluation of fluorescent protein photoactivation efficiency using an in vivo nanotemplate. *Nature methods*, 11(2):156, 2014.
- [307] Geoffrey C Rollins, Jae Yen Shin, Carlos Bustamante, and Steve Pressé. Stochastic approach to the molecular counting problem in superresolution microscopy. *Proceedings of the National Academy of Sciences*, 112(2):E110–E118, 2015.
- [308] Franziska Fricke, Joel Beaudouin, Roland Eils, and Mike Heilemann. One, two or three? probing the stoichiometry of membrane proteins by single-molecule localization microscopy. *Scientific reports*, 5:14072, 2015.

- [309] Gerhard Hummer, Franziska Fricke, and Mike Heilemann. Model-independent counting of molecules in single-molecule localization microscopy. *Molecular biology of the cell*, 27(22):3637–3644, 2016.
- [310] Christos Karathanasis, Franziska Fricke, Gerhard Hummer, and Mike Heilemann. Molecule counts in localization microscopy with organic fluorophores. *ChemPhysChem*, 18(8):942–948, 2017.
- [311] Daniel Nino, Nafiseh Rafiei, Yong Wang, Anton Zilman, and Joshua N Milstein. Molecular counting with localization microscopy: a bayesian estimate based on fluorophore statistics. *Biophysical journal*, 112(9):1777–1785, 2017.
- [312] Hugo Geerts, M De Brabander, Ronny Nuydens, Staf Geuens, Mark Moeremans, J De Mey, and Peter Hollenbeck. Nanovid tracking: a new automatic method for the study of mobility in living cells based on colloidal gold and video microscopy. *Biophysical journal*, 52(5):775–782, 1987.
- [313] M De Brabander, R Nuydens, Hm Geerts, and CR Hopkins. Dynamic behavior of the transferrin receptor followed in living epidermoid carcinoma (a431) cells with nanovid microscopy. *Cell motility and the cytoskeleton*, 9(1):30–47, 1988.
- [314] Michael P Sheetz, Stephen Turney, Hong Qian, and Elliot L Elson. Nanometre-level analysis demonstrates that lipid flow does not drive membrane glycoprotein movements. *Nature*, 340(6231):284, 1989.
- [315] Michael J Saxton and Ken Jacobson. Single-particle tracking: applications to membrane dynamics. *Annual review of biophysics and biomolecular structure*, 26(1):373–399, 1997.
- [316] Diane S Lidke, Peter Nagy, Rainer Heintzmann, Donna J Arndt-Jovin, Janine N Post, Hernan E Grecco, Elizabeth A Jares-Erijman, and Thomas M Jovin. Quantum dot ligands provide new insights into erbb/her receptor-mediated signal transduction. *Nature biotechnology*, 22(2):198, 2004.
- [317] Akihiro Kusumi, Chieko Nakada, Ken Ritchie, Kotonu Murase, Kenichi Suzuki, Hideji Murakoshi, Rinshi S Kasai, Junko Kondo, and Takahiro Fujiwara. Paradigm shift of the plasma membrane concept from the two-dimensional continuum fluid to the partitioned fluid: high-speed single-molecule tracking of membrane molecules. *Annu. Rev. Biophys. Biomol. Struct.*, 34:351–378, 2005.
- [318] Damien Alcor, Géraldine Gouzer, and Antoine Triller. Single-particle tracking methods for the study of membrane receptors dynamics. *European Journal of Neuroscience*, 30(6):987–997, 2009.
- [319] Thomas S van Zanten, Alessandra Cambi, and Maria F Garcia-Parajo. A nanometer scale optical view on the compartmentalization of cell membranes. *Biochimica et Biophysica Acta (BBA)-Biomembranes*, 1798(4):777–787, 2010.
- [320] Nicholas L Andrews, Keith A Lidke, Janet R Pfeiffer, Alan R Burns, Bridget S Wilson, Janet M Oliver, and Diane S Lidke. Actin restricts fce ri diffusion and facilitates antigen-induced receptor immobilization. *Nature cell biology*, 10(8):955, 2008.
- [321] Melike Lakadamyali, Michael J Rust, Hazen P Babcock, and Xiaowei Zhuang. Visualizing infection of individual influenza viruses. *Proceedings of the National Academy of Sciences*, 100(16):9280–9285, 2003.

- [322] Boerries Brandenburg and Xiaowei Zhuang. Virus trafficking—learning from single-virus tracking. *Nature Reviews Microbiology*, 5(3):197, 2007.
- [323] Nadia Ruthardt, Don C Lamb, and Christoph Bräuchle. Single-particle tracking as a quantitative microscopy-based approach to unravel cell entry mechanisms of viruses and pharmaceutical nanoparticles. *Molecular therapy*, 19(7):1199–1211, 2011.
- [324] Štefan Bálint, Ione Verdeny Vilanova, Ángel Sandoval Álvarez, and Melike Lakadamyali. Correlative live-cell and superresolution microscopy reveals cargo transport dynamics at microtubule intersections. *Proceedings of the National Academy of Sciences*, 110(9):3375–3380, 2013.
- [325] Mathias P Clausen and B Christoffer Lagerholm. The probe rules in single particle tracking. *Current Protein and Peptide Science*, 12(8):699–713, 2011.
- [326] Marcel Bruchez, Mario Moronne, Peter Gin, Shimon Weiss, and A Paul Alivisatos. Semiconductor nanocrystals as fluorescent biological labels. *science*, 281(5385):2013–2016, 1998.
- [327] Fabien Pinaud, Samuel Clarke, Assa Sittner, and Maxime Dahan. Probing cellular events, one quantum dot at a time. *Nature methods*, 7(4):275, 2010.
- [328] Patrick J Cutler, Michael D Malik, Sheng Liu, Jason M Byars, Diane S Lidke, and Keith A Lidke. Multi-color quantum dot tracking using a high-speed hyperspectral line-scanning microscope. *PloS one*, 8(5):e64320, 2013.
- [329] Yannis Kalaidzidis. Intracellular objects tracking. *European journal of cell biology*, 86(9):569–578, 2007.
- [330] Richik N Ghosh and Watt W Webb. Automated detection and tracking of individual and clustered cell surface low density lipoprotein receptor molecules. *Biophysical journal*, 66(5):1301–1318, 1994.
- [331] Salman S Rogers, Thomas A Waigh, Xiubo Zhao, and Jian R Lu. Precise particle tracking against a complicated background: polynomial fitting with gaussian weight. *Physical Biology*, 4(3):220, 2007.
- [332] Kevin Claytor, Saumyakanti Khatua, Jason M Guerrero, Alexei Tcherniak, James M Tour, and Stephan Link. Accurately determining single molecule trajectories of molecular motion on surfaces. *The Journal of chemical physics*, 130(16):04B624, 2009.
- [333] Kathryn T Applegate, Sebastien Besson, Alexandre Matov, Maria H Bagonis, Khuloud Jaqaman, and Gaudenz Danuser. plustiptracker: Quantitative image analysis software for the measurement of microtubule dynamics. *Journal of structural biology*, 176(2):168–184, 2011.
- [334] Mohak Patel, Susan E Leggett, Alexander K Landauer, Ian Y Wong, and Christian Franck. Rapid, topology-based particle tracking for high-resolution measurements of large complex 3d motion fields. *Scientific reports*, 8(1):5581, 2018.
- [335] Stéphane Bonneau, Maxime Dahan, and Laurent D Cohen. Single quantum dot tracking based on perceptual grouping using minimal paths in a spatiotemporal volume. *IEEE transactions on image processing*, 14(9):1384–1395, 2005.
- [336] Quan Xue and Mark C Leake. A novel multiple particle tracking algorithm for noisy in vivo data by minimal path optimization within the spatio-temporal volume. In *2009 IEEE International Symposium on Biomedical Imaging: From Nano to Macro*, pages 1158–1161. IEEE, 2009.

- [337] Sheng Lu, Tong Chen, Fan Yang, Chenglei Peng, Sidan Du, and Yang Li. Minimal path based particle tracking in low snr fluorescence microscopy images. In *Proceedings of the 2019 4th International Conference on Biomedical Signal and Image Processing (ICBIP 2019)*, pages 93–97, 2019.
- [338] Ishwar K Sethi and Ramesh Jain. Finding trajectories of feature points in a monocular image sequence. *IEEE Transactions on pattern analysis and machine intelligence*, (1):56–73, 1987.
- [339] Daniel Sage, Florence Hediger, Susan M Gasser, and Michael Unser. Automatic tracking of particles in dynamic fluorescence microscopy. In *3rd International Symposium on Image and Signal Processing and Analysis, 2003. ISPA 2003. Proceedings of the*, volume 1, pages 582–586. IEEE, 2003.
- [340] Jochen Rink, Eric Ghigo, Yannis Kalaidzidis, and Marino Zerial. Rab conversion as a mechanism of progression from early to late endosomes. *Cell*, 122(5):735–749, 2005.
- [341] Ivo F Sbalzarini and Petros Koumoutsakos. Feature point tracking and trajectory analysis for video imaging in cell biology. *Journal of structural biology*, 151(2):182–195, 2005.
- [342] Lassi Paavola, P Kankaanpää, Pekka Ruusuvuori, Gregory McNerney, Mikko Karjalainen, and V Marjomäki. Application independent greedy particle tracking method for 3d fluorescence microscopy image series. In *2012 9th IEEE International Symposium on Biomedical Imaging (ISBI)*, pages 672–675. IEEE, 2012.
- [343] Harold W Kuhn. The hungarian method for the assignment problem. *Naval research logistics quarterly*, 2(1-2):83–97, 1955.
- [344] Nicolas Chenouard, Ihor Smal, Fabrice De Chaumont, Martin Maška, Ivo F Sbalzarini, Yuanhao Gong, Janick Cardinale, Craig Carthel, Stefano Coraluppi, Mark Winter, et al. Objective comparison of particle tracking methods. *Nature methods*, 11(3):281, 2014.
- [345] M Sanjeev Arulampalam, Simon Maskell, Neil Gordon, and Tim Clapp. A tutorial on particle filters for online nonlinear/non-gaussian bayesian tracking. *IEEE Transactions on signal processing*, 50(2):174–188, 2002.
- [346] Sébastien Nguyen Ngoc, Frédéric Briquet-Laugier, Christian Boulin, and J-C Olivo. Adaptive detection for tracking moving biological objects in video microscopy sequences. In *Proceedings of International Conference on Image Processing*, volume 3, pages 484–487. IEEE, 1997.
- [347] Auguste Genovesio, Bo Zhang, and J-C Olivo-Marin. Tracking of multiple fluorescent biological objects in three dimensional video microscopy. In *Proceedings 2003 International Conference on Image Processing (Cat. No. 03CH37429)*, volume 1, pages I–1105. IEEE, 2003.
- [348] Ihor Smal, Wiro Niessen, and Erik Meijering. A new detection scheme for multiple object tracking in fluorescence microscopy by joint probabilistic data association filtering. In *2008 5th IEEE International Symposium on Biomedical Imaging: From Nano to Macro*, pages 264–267. IEEE, 2008.
- [349] William J Godinez, Marko Lampe, Stefan Wörz, Barbara Müller, Roland Eils, and Karl Rohr. Deterministic and probabilistic approaches for tracking virus particles in time-lapse fluorescence microscopy image sequences. *Medical image analysis*, 13(2):325–342, 2009.
- [350] William J Godinez, Marko Lampe, Roland Eils, Barbara Müller, and Karl Rohr. Tracking multiple particles in fluorescence microscopy images via probabilistic data association. In *2011 IEEE International Symposium on Biomedical Imaging: From Nano to Macro*, pages 1925–1928. IEEE, 2011.

- [351] William J Godinez and Karl Rohr. Tracking multiple particles in fluorescence time-lapse microscopy images via probabilistic data association. *IEEE transactions on medical imaging*, 34(2):415–432, 2014.
- [352] Astha Jaiswal, William J Godinez, Roland Eils, Maik Jörg Lehmann, and Karl Rohr. Tracking virus particles in fluorescence microscopy images using multi-scale detection and multi-frame association. *IEEE Transactions on Image Processing*, 24(11):4122–4136, 2015.
- [353] Zia Khan, Tucker Balch, and Frank Dellaert. Mcmc-based particle filtering for tracking a variable number of interacting targets. *IEEE transactions on pattern analysis and machine intelligence*, 27(11):1805–1819, 2005.
- [354] Ihor Smal, Wiro Niessen, and Erik Meijering. Bayesian tracking for fluorescence microscopic imaging. In *3rd IEEE International Symposium on Biomedical Imaging: Nano to Macro, 2006.*, pages 550–553. IEEE, 2006.
- [355] William J Godinez, Marko Lampe, S Worz, B Muller, Roland Eils, and Karl Rohr. Tracking of virus particles in time-lapse fluorescence microscopy image sequences. In *2007 4th IEEE International Symposium on Biomedical Imaging: From Nano to Macro*, pages 256–259. IEEE, 2007.
- [356] Ihor Smal, Katharina Draegestein, Niels Galjart, Wiro Niessen, and Erik Meijering. Particle filtering for multiple object tracking in dynamic fluorescence microscopy images: Application to microtubule growth analysis. *IEEE transactions on medical imaging*, 27(6):789–804, 2008.
- [357] Ji Won Yoon, Andreas Bruckbauer, William J Fitzgerald, and David Klennerman. Bayesian inference for improved single molecule fluorescence tracking. *Biophysical journal*, 94(12):4932–4947, 2008.
- [358] Jaco Vermaak, Simon J Godsill, and Patrick Perez. Monte carlo filtering for multi target tracking and data association. *IEEE Transactions on Aerospace and Electronic systems*, 41(1):309–332, 2005.
- [359] Klas EG Magnusson and Joakim Jaldén. Tracking of non-brownian particles using the viterbi algorithm. In *2015 IEEE 12th International Symposium on Biomedical Imaging (ISBI)*, pages 380–384. IEEE, 2015.
- [360] Vasileios Maroulas, Andreas Nebenführ, et al. Tracking rapid intracellular movements: a bayesian random set approach. *The Annals of Applied Statistics*, 9(2):926–949, 2015.
- [361] Henk AP Blom and Yaakov Bar-Shalom. The interacting multiple model algorithm for systems with markovian switching coefficients. *IEEE transactions on Automatic Control*, 33(8):780–783, 1988.
- [362] Auguste Genovesio, Bo Zhang, and J-C Olivo-Marin. Interacting multiple model based method to track moving fluorescent biological spots. In *2004 2nd IEEE International Symposium on Biomedical Imaging: Nano to Macro (IEEE Cat No. 04EX821)*, pages 1239–1242. IEEE, 2004.
- [363] Auguste Genovesio, Tim Liedl, Valentina Emiliani, Wolfgang J Parak, Maité Coppey-Moisán, and J-C Olivo-Marin. Multiple particle tracking in 3-d+ t microscopy: method and application to the tracking of endocytosed quantum dots. *IEEE Transactions on Image Processing*, 15(5):1062–1070, 2006.
- [364] Lei Yang, Zhen Qiu, Alan H Greenaway, and Weiping Lu. A new framework for particle detection in low-snr fluorescence live-cell images and its application for improved particle tracking. *IEEE Transactions on Biomedical Engineering*, 59(7):2040–2050, 2012.

- [365] Donald Reid. An algorithm for tracking multiple targets. *IEEE transactions on Automatic Control*, 24(6):843–854, 1979.
- [366] Ingemar J. Cox and Sunita L. Hingorani. An efficient implementation of reid’s multiple hypothesis tracking algorithm and its evaluation for the purpose of visual tracking. *IEEE Transactions on pattern analysis and machine intelligence*, 18(2):138–150, 1996.
- [367] Khuloud Jaqaman, Dinah Loerke, Marcel Mettlen, Hirotaka Kuwata, Sergio Grinstein, Sandra L Schmid, and Gaudenz Danuser. Robust single-particle tracking in live-cell time-lapse sequences. *Nature methods*, 5(8):695, 2008.
- [368] Nicolas Chenouard, Isabelle Bloch, and Jean-Christophe Olivo-Marin. Multiple hypothesis tracking in microscopy images. In *2009 IEEE International Symposium on Biomedical Imaging: From Nano to Macro*, pages 1346–1349. IEEE, 2009.
- [369] Nicolas Chenouard, Isabelle Bloch, and Jean-Christophe Olivo-Marin. Multiple hypothesis tracking for cluttered biological image sequences. *IEEE transactions on pattern analysis and machine intelligence*, 35(11):2736–2750, 2013.
- [370] Liang Liang, Hongying Shen, Pietro De Camilli, and James S Duncan. A novel multiple hypothesis based particle tracking method for clathrin mediated endocytosis analysis using fluorescence microscopy. *IEEE Transactions on Image Processing*, 23(4):1844–1857, 2014.
- [371] Khurram Shafique and Mubarak Shah. A noniterative greedy algorithm for multiframe point correspondence. *IEEE transactions on pattern analysis and machine intelligence*, 27(1):51–65, 2005.
- [372] Jay M Newby, Alison M Schaefer, Phoebe T Lee, M Gregory Forest, and Samuel K Lai. Convolutional neural networks automate detection for tracking of submicron-scale particles in 2d and 3d. *Proceedings of the National Academy of Sciences*, 115(36):9026–9031, 2018.
- [373] Maximilian Jakobs, Andrea Dimitracopoulos, and Kristian Franze. Kymobutler: A deep learning software for automated kymograph analysis. *bioRxiv*, page 405183, 2019.
- [374] Mariia Dmitrieva, Helen L Zenner, Jennifer Richens, Daniel St Johnston, and Jens Rittscher. Protein tracking by cnn-based candidate pruning and two-step linking with bayesian network. In *2019 IEEE 29th International Workshop on Machine Learning for Signal Processing (MLSP)*, pages 1–6. IEEE, 2019.
- [375] Naor Granik, Lucien E Weiss, Elias Nehme, Maayan Levin, Michael Chein, Eran Perlson, Yael Roichman, and Yoav Shechtman. Single particle diffusion characterization by deep learning. *Biophysical Journal*, 2019.
- [376] Hong Qian, Michael P Sheetz, and Elliot L Elson. Single particle tracking. analysis of diffusion and flow in two-dimensional systems. *Biophysical journal*, 60(4):910–921, 1991.
- [377] Xavier Michalet. Mean square displacement analysis of single-particle trajectories with localization error: Brownian motion in an isotropic medium. *Physical Review E*, 82(4):041914, 2010.
- [378] Naomi Altman and Martin Krzywinski. Points of significance: clustering, 2017.
- [379] Fedor V Subach, George H Patterson, Suliana Manley, Jennifer M Gillette, Jennifer Lippincott-Schwartz, and Vladislav V Verkhusha. Photoactivatable mcherry for high-resolution two-color fluorescence microscopy. *Nature methods*, 6(2):153, 2009.

- [380] Kathrin Spendier, Keith A Lidke, Diane S Lidke, and James L Thomas. Single-particle tracking of immunoglobulin e receptors (fc ϵ ri) in micron-sized clusters and receptor patches. *FEBS letters*, 586(4):416–421, 2012.
- [381] Jérémie Rossy, Edward Cohen, Katharina Gaus, and Dylan M Owen. Method for co-cluster analysis in multichannel single-molecule localisation data. *Histochemistry and cell biology*, 141(6):605–612, 2014.
- [382] Mariya Georgieva, Diego I Cattoni, Jean-Bernard Fiche, Thibaut Mutin, Delphine Chamousset, and Marcelo Nollmann. Nanometer resolved single-molecule colocalization of nuclear factors by two-color super resolution microscopy imaging. *Methods*, 105:44–55, 2016.
- [383] Philip J Clark and Francis C Evans. Distance to nearest neighbor as a measure of spatial relationships in populations. *Ecology*, 35(4):445–453, 1954.
- [384] Jun Zhang, Karin Leiderman, Janet R Pfeiffer, Bridget S Wilson, Janet M Oliver, and Stanly L Steinberg. Characterizing the topography of membrane receptors and signaling molecules from spatial patterns obtained using nanometer-scale electron-dense probes and electron microscopy. *Micron*, 37(1):14–34, 2006.
- [385] Dylan M Owen, Carles Rentero, Jérémie Rossy, Astrid Magenau, David Williamson, Macarena Rodriguez, and Katharina Gaus. Palm imaging and cluster analysis of protein heterogeneity at the cell surface. *Journal of biophotonics*, 3(7):446–454, 2010.
- [386] Maria A Kiskowski, John F Hancock, and Anne K Kenworthy. On the use of ripley’s k-function and its derivatives to analyze domain size. *Biophysical journal*, 97(4):1095–1103, 2009.
- [387] Prabuddha Sengupta, Tijana Jovanovic-Talman, Dunja Skoko, Malte Renz, Sarah L Veatch, and Jennifer Lippincott-Schwartz. Probing protein heterogeneity in the plasma membrane using palm and pair correlation analysis. *Nature methods*, 8(11):969, 2011.
- [388] Prabuddha Sengupta and Jennifer Lippincott-Schwartz. Quantitative analysis of photoactivated localization microscopy (palm) datasets using pair-correlation analysis. *Bioessays*, 34(5):396–405, 2012.
- [389] Martin Ester, Hans-Peter Kriegel, Jörg Sander, Xiaowei Xu, et al. A density-based algorithm for discovering clusters in large spatial databases with noise. In *Kdd*, volume 96, pages 226–231, 1996.
- [390] Barna Dudok, László Barna, Marco Ledri, Szilárd I Szabó, Eszter Szabadits, Balázs Pintér, Stephen G Woodhams, Christopher M Henstridge, Gyula Y Balla, Rita Nyilas, et al. Cell-specific storm super-resolution imaging reveals nanoscale organization of cannabinoid signaling. *Nature neuroscience*, 18(1):75, 2015.
- [391] Troels Rahbek-Clemmensen, Matthew D Lycas, Simon Erlendsson, Jacob Eriksen, Mia Apuschkin, Frederik Vilhardt, Trine N Jørgensen, Freja H Hansen, and Ulrik Gether. Super-resolution microscopy reveals functional organization of dopamine transporters into cholesterol and neuronal activity-dependent nanodomains. *Nature communications*, 8(1):740, 2017.
- [392] Leonid Andronov, Igor Orlov, Yves Lutz, Jean-Luc Vonesch, and Bruno P Klaholz. Cluster-visu, a method for clustering of protein complexes by voronoi tessellation in super-resolution microscopy. *Scientific reports*, 6:24084, 2016.
- [393] Florian Levet, Eric Hosy, Adel Kechkar, Corey Butler, Anne Beghin, Daniel Choquet, and Jean-Baptiste Sibarita. Sr-tesseler: a method to segment and quantify localization-based super-resolution microscopy data. *Nature methods*, 12(11):1065, 2015.

- [394] Patrick Rubin-Delanchy, Garth L Burn, Juliette Griffié, David J Williamson, Nicholas A Heard, Andrew P Cope, and Dylan M Owen. Bayesian cluster identification in single-molecule localization microscopy data. *Nature methods*, 12(11):1072, 2015.
- [395] RAJ Post, D van der Zwaag, G Bet, SPW Wijnands, L Albertazzi, EW Meijer, and RW van der Hofstad. A stochastic view on surface inhomogeneity of nanoparticles. *Nature communications*, 10(1):1663, 2019.
- [396] Mohamadreza Fazel, Michael J Wester, Bernd Rieger, Ralf Jungmann, and Keith A Lidke. Sub-nanometer precision using bayesian grouping of localizations. *bioRxiv*, page 752287, 2019.
- [397] David J Williamson, Dylan M Owen, Jérémie Rossy, Astrid Magenau, Matthias Wehrmann, J Justin Gooding, and Katharina Gaus. Pre-existing clusters of the adaptor lat do not participate in early t cell signaling events. *Nature immunology*, 12(7):655, 2011.
- [398] Dylan M Owen, David J Williamson, Astrid Magenau, and Katharina Gaus. Sub-resolution lipid domains exist in the plasma membrane and regulate protein diffusion and distribution. *Nature communications*, 3:1256, 2012.
- [399] Maria F Garcia-Parajo, Alessandra Cambi, Juan A Torreno-Pina, Nancy Thompson, and Ken Jacobson. Nanoclustering as a dominant feature of plasma membrane organization. *J Cell Sci*, 127(23):4995–5005, 2014.
- [400] Jia Lin, Michael J Wester, Matthew S Graus, Keith A Lidke, and Aaron K Neumann. Nanoscopic cell-wall architecture of an immunogenic ligand in candida albicans during antifungal drug treatment. *Molecular biology of the cell*, 27(6):1002–1014, 2016.
- [401] Ingrid Chamma and Olivier Thoumine. Dynamics, nanoscale organization, and function of synaptic adhesion molecules. *Molecular and Cellular Neuroscience*, 91:95–107, 2018.
- [402] S Roberts, Michael Hirsch, Alexandra McStea, L Zanetti-Domingues, D Clarke, Jeroen Claus, P Parker, Lin Wang, and M Martin-Fernandez. Cluster analysis of endogenous her2 and her3 receptors in skbr3 cells. *Bio-Protocol*, 8:e3096, 2018.